School of Mining Engineering

UNIVERSITY OF THE WITWATERSRAND, JOHANNESBURG

SLOPE STABILITY MANAGEMENT USING 2D ANALYSIS METHODS AT CHINGOLA OPEN PITS F AND D OF KONKOLA COPPER MINES

Shoma Syamusana

I declare that this research report is my own unaided work. It is being submitted for the degree of Master of Science at the University of the Witwatersrand, Johannesburg. It has not been submitted before for any degree or examination to any other university.

Johannesburg, 2025

DECLARATION

I have familiarised myself with the University of the Witwatersrand Student Academic Misconduct Policy (SAMP). I hereby declare that the work I am submitting for assessment is my original work. I affirm that I have not plagiarised, misrepresented, or colluded with any other person or source. I have properly acknowledged, cited, and referenced all the sources that I have used in my work. I also declare that where I have used artificial intelligence (AI) tools it has only been as a means of guidance. The ideas and arguments presented in my work are my original thoughts and interpretations. I acknowledge that any academic misconduct, such as plagiarism or collusion will result in serious consequences. According to the SAMP, these consequences may include a reduced grade, a fail mark, or disciplinary action. The Faculty of Engineering and the University of the Witwatersrand have my consent to investigate any potential academic misconduct in my work. This investigation may include the use of similarity and AI detection software to check the originality of my work. I undertake to abide by the decision of any such investigation.

____

(Signature of Supervisor)

9th day of May, 2025

“The reward of one duty is the power to fulfil another”

George Eliot

ABSTRACT

Chingola Open Pits F and D (COPF/D) is a copper open-cast mine located in the town of Chingola on the Copperbelt in Zambia. It is approximately 330 m deep, 1.3 km wide and 2.1 km long. The mine was opened in 2003. COPF/D comprises a rock mass which is currently classified as poor to fair using the Mining Rock Mass Rating (MRMR) system. Despite the implementation of consultants' recommendations, structural slope failures on the south and east slopes have continued to occur. The research described in this report showed that the recommendations were based on inaccurate strength parameters and discontinuity orientations. The consequence has been an increase in stripping ratios and exposure of both equipment and personnel to dangerous conditions. An effective slope management plan was determined to address the uncertainties. This included site-specific recommendations for the high risk of slope failure, to predict or prevent unexpected slope failures in the next three years. The pit was divided into three distinct domains (Domain 1, Domain 2 and Domain 3) based on the observed failure mechanisms, data analysis and the rock mass strength. The structural and stability analysis showed that the domains susceptible to wedge and planar failures covered an area of 4,892 m^2 and 71,650 m^2, respectively. Domain 3, which was also susceptible to circular failures in the upper and lower stack, covered an area of 1,556,769 m^2 and 20,685 m^2, respectively. To mitigate circular failures, it was recommended that the pore pressure coefficient (Ru) be reduced from 0.23 to less than 0.19 and the lower stack angle be reduced from 51° to 42°. To mitigate structural failures in Domain 2, the slope angle should be reduced from 60° to 50°. The unstable portion of Domain 1 should be supported with cable anchors and fibre-reinforced shotcrete to make it stable. An appropriate slope monitoring strategy was recommended for each domain to ensure proactive detection of ground deformation. New technologies such as drones and data acquisition scanners were also recommended for future developments to improve the quality of data assessments.

ACKNOWLEDGMENTS

Firstly, I thank the Almighty God for giving me the ability to do this research report successfully.

I'm immensely thankful to my supervisor, Professor Bryan Watson (School of Mining Engineering Lecturer – University of the Witwatersrand) for his constant professional advice, effort and support in the course of my MSc study.

I'm grateful for the support and encouragement from my dear wife, Ngoza, throughout my study.

I'm grateful to the management of Konkola Copper Mine for permitting me to carry out this research.

Lastly, I thank friends and family for their assistance and support throughout this research.

TABLE OF CONTENTS

DECLARATION i

ABSTRACT iii

ACKNOWLEDGMENTS iv

LIST OF FIGURES vii

LIST OF TABLES x

LIST OF EQUATIONS xv

LIST OF ABBREVIATIONS AND SYMBOLS xvi

1 INTRODUCTION 1

1.1 Research Background and Context 1

1.2 Problem Statement 6

1.3 Justification for Research 7

1.4 Research Objectives 7

1.5 Research Methods 8

1.6 Sources of Data 8

1.7 Research Validation 8

1.8 Structure of the Research Report 9

2 LITERATURE REVIEW 10

2.1 Introduction 10

2.2 Key Concepts, Theories and Studies 10

2.3 Key Debates and Controversies 38

2.4 Chapter Summary 39

3 RESEARCH APPROACH 40

3.1 Introduction 40

3.2 Research Design 40

3.3 Data Collection 40

3.4 Data Validation Process 41

3.5 Data Analysis Approach 41

3.6 Chapter Summary 41

4 DATA FOR THE STUDY 42

4.1 Introduction 42

4.2 Collected Data 42

4.3 Chapter Summary 54

5 ANALYSIS AND FINDINGS 55

5.1 Introduction 55

5.2 Empirical stability analysis of COPF/D slopes 56

5.3 Structural Analysis 57

5.4 Groundwater Analysis 66

5.5 Numerical Stability Analysis 67

5.6 Slope Monitoring 76

5.7 Comparison Between FOGs and Current Pit Slope Design 77

5.8 Comparison Between Current and Recommended Pit Slope Design 78

5.9 Mitigation Strategies to Cater for a Low FOS 78

5.10 Chapter Summary 78

6 CONCLUSIONS AND RECOMMENDATIONS 80

6.1 Introduction 80

6.2 Summary of Chapters 80

6.3 Research Observations 81

6.4 Research Contributions 84

6.5 Research Limitations 84

6.6 Recommendations for Future Research Work 84

REFERENCE LIST 86

APPENDIX B. Q SYSTEM TABLES 103

APPENDIX C.GSI DATA AND STRENGTH PARAMETERS 108

APPENDIX D. UCS TEST RESULT DATA 110

APPENDIX E. COPF/D STRENGTH PARAMETERS FROM MINE DATABASE 112

APPENDIX F. COPF/D Rock properties 113

APPENDIX G. COPF/D STRUCTURAL/MAPPING DATA 114

APPENDIX H. COPF/D Discontinuity offset measurement data and friction angle (Phi) calculation 117

APPENDIX I. COPF/D GROUNDWATER LEVELS 119

APPENDIX J. COPF/D NUMERICAL STABILITY ANALYSIS RESULTS OF SLIDE AND RS2 SOFTWARE 124

LIST OF FIGURES

Figure 1-1: Cutback sequencing at COPF/D of Nchanga Mine 2

Figure 1-2: Location of COPF/D open pit 3

Figure 1-3: COPF/D stratigraphic column 4

Figure 1-4: Geological structures on the COPF/D open pit footwall and south wall 7

Figure 2-1: Typical open pit slope geometry 11

Figure 2-2: Plane failure showing release surfaces/relief planes at the ends of a plane 12

Figure 2-3: cross-section of planes forming a plane failure 13

Figure 2-4: Isometric or 3D view of a wedge failure 14

Figure 2-5: Cross-section of a wedge failure 14

Figure 2-6: Toppling failure 15

Figure 2-7: Block toppling 16

Figure 2-8: Flexural toppling 16

Figure 2-9:Block-flexure toppling 17

Figure 2-10: Circular failure 18

Figure 2-11: Inter-block frictional behaviour (a–c). 26

Figure 2-12: offset measurement for determining Jr........ 27

Figure 2-13: The relationship between Jr and offset 27

Figure 2-14: Empirical slope design chart 32

Figure 2-15: A guide to “Managing Slope hazards, making the right choice”,..... 35

Figure 2-16: Slope stability radar image at COPF/D 36

Figure 2-17: Typical displacement-time curves for open pit slope failures........ 37

Figure 2-18: Slope width (W) and Slope Height (H) illustration for determining the W/H ratio 39

Figure 3-1: Data collection process chart for COPF/D 40

Figure 3-2: Showing Data analysis approach process for the COPF/D pit 41

Figure 4-1: COPF/D Geotechnical domains 44

Figure 4-2: Piezometer locations and representative sections A-A, B-B and C-C positions 46

Figure 5-1:COPF/D slope stability analysis graphical representation 55

Figure 5-2: Dips software result of a kinematic analysis for planar failure in Domain 1 58

Figure 5-3: Dips software kinematic analysis for wedge failure in Domain 1 59

Figure 5-4: Potentially unstable areas at COPF/D pit 60

Figure 5-5: Dips software result of a simulated kinematic analysis for planar failure in Domain 1 61

Figure 5-6: Dips software result of a simulated kinematic analysis for wedge failure in Domain 1 62

Figure 5-7: Dips software result of a kinematic analysis for wedge failure in Domain 2 63

Figure 5-8: Dips software simulated result of a kinematic analysis for wedge failure in Domain 2 64

Figure 5-9: Dips software result of a kinematic analysis for flexural toppling failure in Domain 3 65

Figure 5-10: Dips software result of a kinematic analysis for wedge failure in Domain 3 65

Figure 5-11: Groundwater level monitoring from piezometers on the hangingwall and south wall at the COPF/D pit. 66

Figure 5-12: Stability analysis results for Domain 1. 68

Figure 5-13: Section C-C stability analysis results for Domain 2 69

Figure 5-14: Section A-A Stability analysis result from Slide2 software for COPF/D Domain 3 on the western wall slope 70

Figure 5-15: Section A-A stability analysis results for Domain 3. 72

Figure 5-16: Section B-B stability analysis results for Domain 3 73

LIST OF TABLES

Table 2-1: Typical acceptance criteria values of PoF and FoS for open-pit slopes at various scales 30

Table 2-2: Summary guide of the suitability of the measure of central tendency 30

Table 4-1: Results of MRMR data from drilled boreholes for COPF/D 43

Table 4-2: Results of the Adjusted MRMR for COPF/D pit 45

Table 4-3: Ru for COPF/D pit domains determined from four piezometers 47

Table 4-4: COPF/D slope geometry 47

Table 4-5: UCS data for all rock formations at COPF/D 48

Table 4-6: Strength parameter results from RSData software 49

Table 4-7: Previous and new strength parameters for COPF/D 50

Table 4-8: COPFD rock mass properties 51

Table 4-9: Domain 1 mapping data 52

Table 4-10: Domain 2 mapping data 53

Table 4-11: Φ for discontinuities determined from offset measurement 53

Table 4-12: Failure register of FOG at COPF/D pit 54

Table 5-1: COPF/D acceptability criterion 56

Table 5-2: Results of empirical stability analysis using adjusted MRMR and Terbrugge chart. The FoS of all results is 1.2. 56

Table 5-3: Results of a deterministic stability analysis from Slide2 software for COPF/D Domain 1 on the eastern wall slope. 67

Table 5-4: Results of a deterministic stability analysis from Slide2 software for COPF/D Domain 2 on the southern wall slope. 68

Table 5-5: Section A-A Results of a deterministic stability analysis from Slide2 software for COPF/D Domain 3 on the western wall slope. 71

Table 5-6: Section B-B Results of a deterministic stability analysis from Slide2 72

Table 5-7: Results of the simulated Domain 3 slope stability analysis................74

Table 5-8: comparison of results from Empirical Analysis,Slide2 and RS2 software..76

Table 5-9: SSM equipment selection results using a guide in Figure 2-15 77

Table 5-10: Current versus recommended pit slope design 78

APPENDIX LIST OF FIGURES

Figure A- 1: MRMR classification table showing rating 90

Figure A- 2: MRMR joint spacing rating 90

Figure J- 1: Slide2 section A-A overall slope analysis result 124

Figure J- 2: Slide2 simulated section A-A Upper stack slope analysis result....124

Figure J- 3: Slide2 simulated section A-A upper stack slope analysis result.....125

Figure J- 4: Slide2 simulated section A-A lower stack slope analysis result 125

Figure J- 5: Slide2 simulated section A-A overall slope analysis result 126

Figure J- 6: Slide2 section B-B Upper stack slope analysis result....................126

Figure J- 7: Slide2 section B-B lower stack slope analysis result 127

Figure J- 8: Slide2 section B-B overall slope analysis result 127

Figure J- 9: RS2 section B-B slope analysis result of Domain 3....................... 128

Figure J- 10: Slide2 simulated section B-B Upper stack slope analysis result... 128

Figure J- 11: Slide2 simulated section B-B lower stack slope analysis result ... 129

Figure J- 12: Slide2 simulated section B-B overall slope analysis result 129

Figure J- 13: Slide2 section B-B Upper stack slope analysis result of Domain 1 130

Figure J- 14: Figure J- 15: Slide2 section B-B lower stack slope analysis result of Domain 1.. 130

Figure J- 16: Figure J- 17: Slide2 section B-B overall slope analysis result of Domain 1 131

Figure J- 18: RS2 section B-B slope analysis result of Domain 1..................... 131

Figure J- 19: Slide2 section C-C Upper stack slope analysis result of Domain 2 132

Figure J- 20: Slide2 section C-C lower stack slope analysis result of Domain 2 132

Figure J- 21: Slide2 section C-C overall slope analysis result of Domain 2 133

Figure J- 22: RS2 section C-C slope analysis result of Domain 2 133

APPENDIX LIST OF TABLES

Table A- 1: MRMR Groundwater and Joint Condition adjustments 91

Table A- 2: Adjustment for Weathering 91

Table A- 3: MRMR joint orientation adjustment 92

Table A- 4: MRMR adjustment for effects of blasting 92

Table A- 5: Adjustments for mining induced stresses 92

Table A- 6: MRMR rock mass classification data from logged bore holes at COPF/D 93

Table A- 7: Calculation of Adjusted MRMR values for the footwall (Domain 1) of COPF/D pit 99

Table A- 8: Calculation of Adjusted MRMR values for the South wall (Domain 2) of COPF/D pit 99

Table A- 9: Calculation of Adjusted MRMR values for the Hangingwall (Domain 3) of COPF/D pit 100

Table A- 10: Rock mass rating system classification table 101

Table A- 11: GSI Chart 102

Table A- 12: GSI Chart 103

Table B- 1: joint roughness number (Jr) 103

Table B- 2: Joint alteration number (Ja) 104

Table B- 3: Joint water reduction factor (Jw) 104

Table B- 4: Strength Reduction Factor (SRF) 104

Table B- 5: Excavation Parameter Category 105

Table B- 6: Mapping data,RQD, joint set number (Jn) ans strength reduction fator 106

Table B- 7: Domain 1 rock mass rating, mine support and mining cost calulations 107

Table C- 1: COPF/D GSI classification data and calculation of strength parameters for the Domain 1 on the Footwall slope 108

Table C- 2: COPF/D GSI classification data and calculation of strength parameters for the Domain 2 on the Southwall slope 108

Table C- 3: COPF/D GSI classification data and calculation of strength parameters for the Domain 3 on the hanging wall slope 109

Table D- 1: UCS data for COPF/D 110

Table E- 1: COPF/D strength parameters from mine database 112

Table F- 1: COPF/D rock properties 113

Table G- 1: COPF/D structural data for Domain 1 on the footwall 114

Table G- 2: COPF/D structural data for Domain 2 on the South wall 115

Table G- 3: COPF/D structural data for the Domain 3 on the Hanging wall 116

Table H- 1: Offset data and Phi calculation for Domain 3 on the Hangingwall 117

Table H- 2: Offset data and Phi calculation for Domain 2 on the Footwall 117

Table H- 3: Offset data and Phi calculation for Domain 3 on the Hangingwall 118

LIST OF EQUATIONS

$N_{90} = N_{\theta}/\sin\theta$ Equation 2-1 18

$Uw = \gamma whw$ Equation 2-2 22

$Ru = Uw/\gamma h$ Equation 2-3 22

$Q = (RQD/Jn) \text{ x } (Jr/Ja) \text{ x } (Jw/SRF)$ Equation *2-4* 24

$FC = \tan^{-1}(Jr/Ja) \text{ x } Jw$ Equation 2-5 25

$\tau = \sigma_n \tan^{-1}(JrJa)$ Equation 2-6 25

$\phi = \tan^{-1}(JrJa)$ Equation 2-7 25

$GSI = RMR'89 - 5 \text{ For GSI } > 18 \text{ or RMR} > 23$ Equation 2-8 28

$9\ln Q' + 44 \text{ For GSI} < 18$ Equation 2-9 28

$Q' = (RQD/Jn) \times (Jr/Ja)$ Equation 2-10 28

Mean= $(x1 + x2 + \cdots + xn)/n$ Equation 2-11 30

LIST OF ABBREVIATIONS AND SYMBOLS

COPF/D	Chingola Open Pits F and D
2D	Two Dimension
3D	Three Dimension
KMRL	Konkola Mineral Resources Limited
GSI	Geological Strength Index
UCS	Uniaxial Compressive Strength
PLT	Point Load Test
RMR	Rock Mass Rating
MRMR	Modified Rock Mass Rating
Q	Q system
FOS	Factor of Safety
POF	Probability of Failure
ARK	Arkose
BSSL	Lower Banded Sandstone
BSSU	Upper Banded sandstone
CDOL	Chingola Dolomite
DOLSCH	Dolomitic Schist

LBS	Lower Banded Shale
UBS	Upper Banded Shale
PQ	Pink Quartzite
SWG	Shale with Grit
TR	Transition Arkose
URD	Upper Roan Dolomite
SSR	Slope Stability Radar
Ru	Pore pressure coefficient
w	water

Symbol	**Description**	**Units**
E_i	Modulus of Elasticity	MPa
g	Gravitational acceleration	m/s^2
γ	Specific Weight	N/m^3
h	Height	m
ϱ	Density	Kg/m^3

1 INTRODUCTION

1.1 Research Background and Context

COPF/D open pit comprises a rock mass currently classified as poor to fair using the Mining Rock Mass Rating (MRMR) method (Laubscher, 1990). Some of the contributing factors include the presence of weathered rock formations, high groundwater levels and discontinuities (joints and bedding planes). The discontinuities on the southern and eastern walls are not favourably oriented to the pit and often pose a risk of structural slope failures. In the recent past, wedge and planar failures have occurred in these locations. The consequence has been the exposure of both equipment and personnel to damage and injuries, respectively. To mitigate the risk, back analyses of previous slope failures, particularly wedge and circular failures, have been done. The results suggested favourably re-orienting the pit walls and reducing the slope angles (Nchanga Open Pit Geotechnical, 2012). The recommendations were successfully executed. However, the failures continued to occur. The problem with the back analyses was that the input geotechnical strength data were averages of data determined from the mine geotechnical database (Geotechnical Database, 2008). Some of the data does not account for the current rock mass conditions, and the face position has changed due to pushbacks. Therefore, an effective slope management plan was needed to address the safety and economic uncertainties. This plan included the use of empirical methods and 2D numerical methods. The 2D analysis method was appropriate for the COPF/D pit due to its favourable dimensions of 2.1 km long, 1.3 km wide and 330 m deep. Cala & Flisiak (2001), Arellano & Stark (2000) and Eid, et al. (2006) found that the difference between the results of 2D and 3D model analyses was minimal where the slope width (pit length) was optimally greater than the slope height.

The slope failures have shown a need to obtain new, relevant geotechnical and geomechanical information for some of the slope walls. More modern analyses/methods were also implemented to evaluate the rock data. One such method is the Geological Strength Index (GSI) (Wyllie & Mah, 2004) for evaluation of circular failures (Marinos, et al., 2005) and kinematic analysis of the structures for evaluation of structural failures which may occur. However, for empirical analysis only, the old MRMR data from borehole cores identified to be in the current face positions were used and adjusted using current rock mass conditions to obtain Adjusted MRMR. The Adjusted MRMR with updated rockmass conditions was used in the empirical analyses. Five cutbacks were planned for COPF/D. The cutbacks were done in a westerly direction to expose and mine the orebody safely. Cutback five is currently being mined. The sequencing of the cutbacks is shown in Figure 1-1.

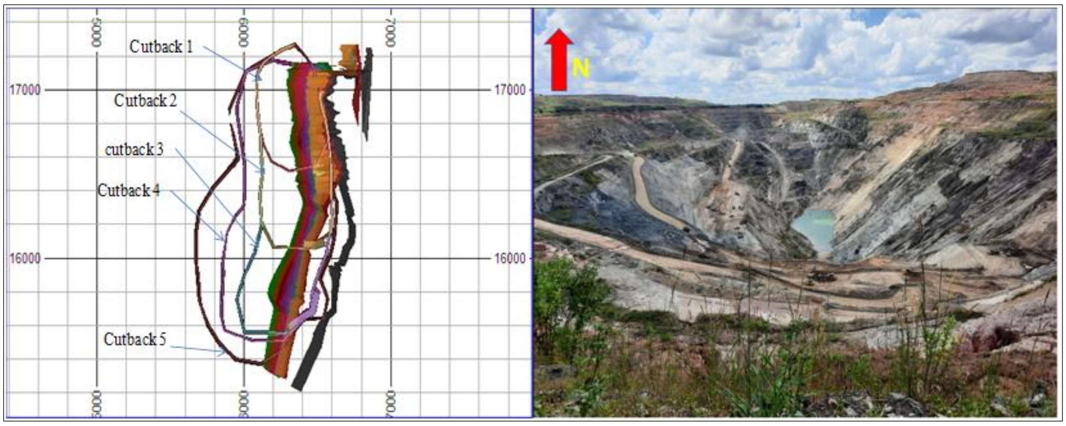

Figure 1-1: Cutback sequencing at COPF/D of Nchanga Mine on the left (Nchanga Open Pit Geotechnical, 2012) and a photograph of the COPF/D open pit mine (right)

1.1.1 Location of Chingola Open Pits F and D

Chingola Open Pits F and D (COPF/D) is located in the town of Chingola on the Zambian Copperbelt. COPF/D is an open-cast copper mine that opened in 2003 and is currently approximately 330 m deep, 1.3 km wide, and 2.1 km long. Figure 1-2 shows the location of the COPF/D open pit mine.

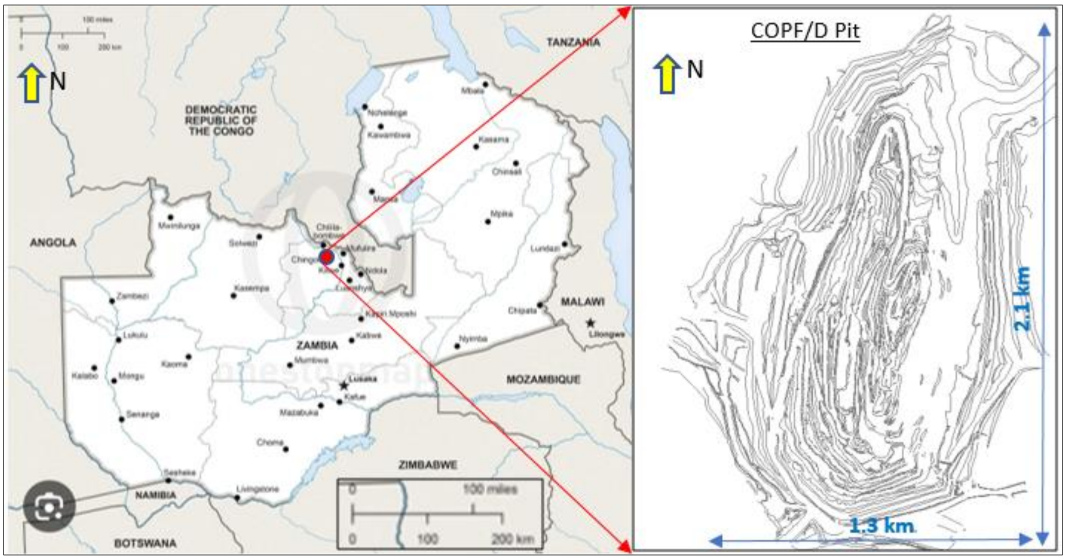

Figure 1-2: Location of COPF/D open pit (Onestopmap, 2023)

1.1.2 Geology of the area

Rocks found in the COPF/D Mining License Area range from the Upper Roan Dolomite (URD) to the Basement rock, which forms the footwall. The ore body is in the Arkose (ARK) rock formation, which overlays the basement rock. Figure 1-3 shows the COPF/D D stratigraphic column. A description of the stratigraphy is provided below (Nchanga Open Pit Geotechnical, 2012):

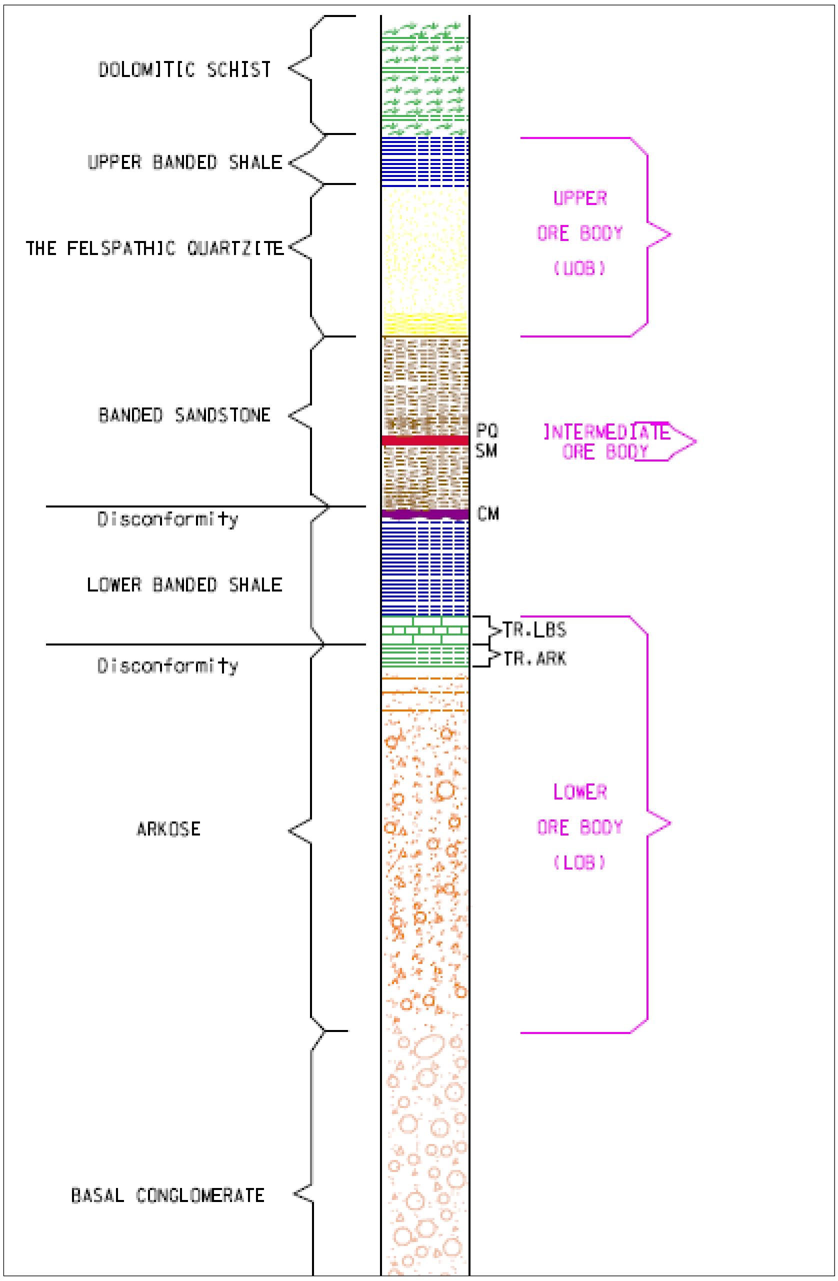

Figure 1-3: COPF/D stratigraphic column (Nchanga Open Pit Geotechnical, 2012)

Dolomitic Schists

The Dolomitic Schists (DOLSCH) are a composition of micaceous, quartzose dolomites and mica-schists, which are overlain by interbedded agillites and dolomites. This formation has a low intact rock strength, and using Laubscher (1990) it is classified as a fair to good rock mass.

Shale with Grit

The Shale with Grit (SWG) unit is a composition of a heterogeneous grouping of thickly-bedded, quartz-micaceous sandstones, siltstones, argillite and grits. It has coarse grains, water-bearing, porous and has a variable weathering profile. Using the graph produced by Laubscher (1990) this rock unit is a poor to fair quality rock mass with low intact rock strength.

Chingola Dolomite

The Chingola dolomite (CDOL) unit is a composition of generally weathered talcose dolomites, micaceous, limonitic, and talc. It has a very low intact rock strength, and using the graph produced by Laubscher (1990) it is classified as a very poor to poor rock

Upper Banded Shale

The Upper Banded Shale (UBS) unit is a micaceous shale rock unit with laminations. The unit has a very low intact rock strength, and using the graph produced by Laubscher (1990) it is classified as poor to fair rock.

The Feldspathic Quartzite and the Feldspathic Quartzite Transitional

The Feldspathic Quartzite (TFQ) unit is composed of medium-grained arkose and quartzite. This unit is a highly jointed rock with high intact rock strength. However, using the graph produced by Laubscher (1990) it is classified as a fair to good rock mass due to its high jointing.

Banded Sandstone

The Banded Sandstone (BSS) unit is composed of siltstones and thinly bedded micaceous sandstones. It is highly weathered, soft and incoherent. This unit is subdivided into three units, which are the Banded Sandstone Lower (BSSL), the Pink Quartzite and the Banded Sandstone Upper (BSSU). The BSSL has a higher content of mica, while BSSU is more dolomitic. PQ is a quartzite and more competent than BSSL and BSSU. Using the graph produced by Laubscher (1990), this unit is a poor rock mass with very low intact rock strength.

Lower banded shale

The Lower Banded Shale (LBS) is composed of carbonaceous and laminated dolomitic shale. The unit has very low intact rock strength, and using the graph produced by Laubscher (1990) it is classified as a poor to fair rock mass.

Arkose and Arkose Transition

The Arkose (ARK) unit is composed of medium to coarse-grained sericite microline and greywacke of quartz. This unit is classified as a fair to good rock mass with medium to high intact rock strength. However, this unit has a sub-rock unit called the ARKTR found between the ARK and LBS, which is micaceous and of low intact strength when classified using the graph produced by Laubscher (1990).

Basement Schist and Gneiss

The Basement Schist and Gneiss (BAS) unit is the footwall of the COPF/D pit. It comprises smooth foliation planes, which result in weak zones in the direction of the foliation. This unit, when classified using the graph produced by Laubscher (1990) it is a fair to good rock mass with medium-strong intact rock (Laubscher, 1990).

1.2 Problem Statement

Even though the recommendations from previous consulting reports were followed, structural slope failures on the south and east slopes have continued to occur, as shown in Figure 1-4. Figure 1-4 also shows the geological structures and the post-wedge failure scars on the footwall and south wall of the COPF/D pit, respectively. The consequence has been an exposure of both equipment and personnel to damage and injuries, respectively.

Figure 1-4: Geological structures on the COPF/D open pit footwall and south wall

1.3 Justification for Research

The geotechnical database of the COPF/D mine contains huge data sets of all rock formations, collected over many years. There is a relatively wide range between rock property values for each formation, some of which may not apply to the current slope wall positions. It is therefore difficult to determine representative values from the current database. Much of the data is from already mined-out positions from previous pit pushbacks and does not account for changes in the condition of the current face position. Conditions may also have deteriorated due to weathering, blasting and creep. This research will determine more representative rock mass data for numerical analyses, taking into account the current conditions of the rock mass and the current slope face positions. Such analyses are likely to be more relevant, translating into an optimised slope geometry with minimal slope failures. Execution of this research is expected to benefit the mine in terms of improved management of ground failure risk and optimised stripping ratio.

1.4 Research Objectives

The main objective of this research is to devise a slope stability management strategy that will enable the mining of the orebody safely and economically.

1.5 Research Methods

This study employed quantitative and qualitative research methods as described below:

a) determine new input rock mass strength parameters through new rock mass assessments using the Geological Strength Index (GSI), intact rock strength test data and Roclab software. The software is used to determine the strength parameters;
b) determine new input parameters for the discontinuities of the COPF/D pit by assessment of the discontinuities using the Q system;
c) investigate and describe the failure modes likely to occur by slope stability analyses using 2D numerical methods and kinematic analysis methods; and
d) optimise the slope geometry through/after stability and sensitivity analyses in both numerical and kinematic stability analyses.

1.6 Sources of Data

The data for this research includes the existing mine database (with new and updated information), laboratory test data and field assessments of slope data. The updated mine database includes diamond-drilled core data for empirical stability analysis and piezometer reading data for numerical stability analysis. Field assessment data included the use of the GSI charts to classify rock mass as well as slope face mapping data. The outdated and irrelevant data was deleted from the database.

1.7 Research Validation

Industry-recommended software and Standard empirical methods were used in the analysis, and results from the different methods were compared to validate the results. The source of information comprised approximately 20% from mine reports and 40% from laboratory tests and field mapping. Peer-reviewed material comprised 40%.

1.8 Structure of the Research Report

This research covers six chapters. Chapter 1 discusses the introduction and comprises the research background information, problem statement, research justification, and the research objectives. Other discussions were on the research methodologies, the information sources and the validation criteria of the research. Chapter 2 discusses the literature review, key concepts, theories and studies and key debates and controversies. Chapter 3 describes the approach of the research to the collection of data, design and the process of validation of data and analyses. Chapter 4 provides an analysis of the data collected for this research. Chapter 5 discusses the analysis and findings of the research. In Chapter 6, the conclusions and recommendations of the research are provided.

2 LITERATURE REVIEW

2.1 Introduction

Slope stability remains the most important aspect of open-pit mining ventures in the world (Rocscience, 2022). Therefore, slope stability management systems are a key component of open-pit mining. If set up effectively, occurrences of slope failures and the potential impacts of risks are minimised, especially where future failures are predicted. (Little, 2006). Other capabilities of effective slope management systems with accurate input data include predictions of modes of failures with indications of the size and location. This facilitates mitigation systems that ensure a safe mining environment is put in place by management (Kliche, 2018).

2.2 Key Concepts, Theories and Studies

The key concepts, theories and studies that this research used include:

- open pit slope geometry and its contribution to stability;
- types of slope failure;
- mapping techniques;
- causes of strength reduction in rock mass;
- stabilisation of slopes;
- rock mass classification;
- factor of safety, probability of failure and acceptability criterion;
- statistical analysis (measure of central tendency);
- stability evaluation of rock mass slopes using empirical methods;
- geotechnical software; and
- geotechnical instrumentation and monitoring of slope.

2.2.1 Open pit slope geometry

A Typical slope geometry for open pit slope design comprises the following components, as illustrated in Figure 2-1 (Wyllie & Mah, 2004):

- Bench face angle
- Bench height

- Bench stack
- Bench width
- Inter-ramp angle
- Overall slope angle
- Pit depth
- Pit crest
- Toe of slope

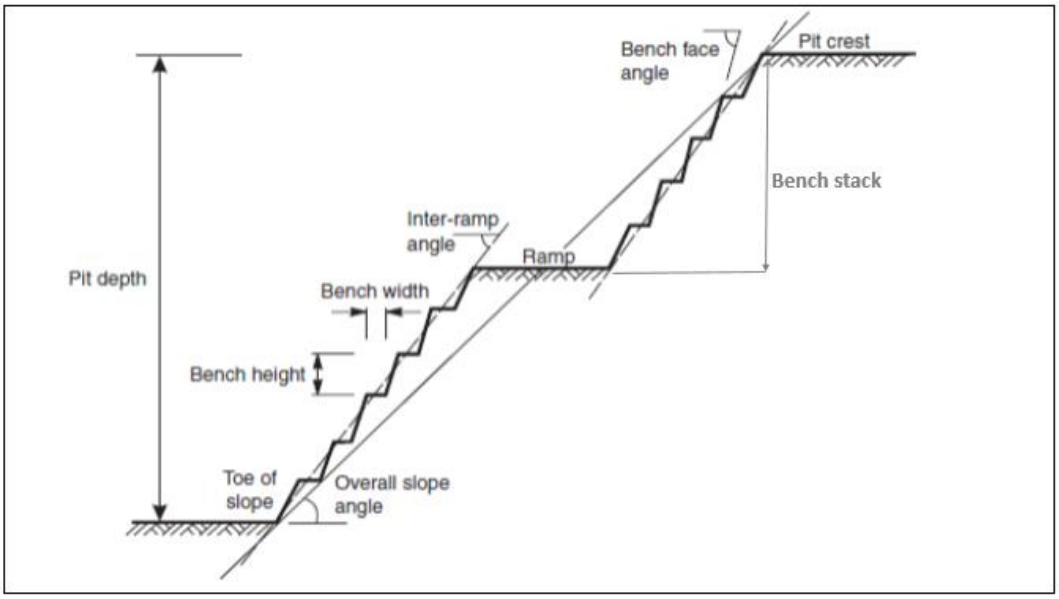

Figure 2-1: Typical open pit slope geometry (Wyllie & Mah, 2004)

2.2.2 Types of slope failure

In rock slope engineering, it is critical that stability analyses focused on the identification of failure modes that are likely to occur are conducted. The four common categories of failure modes include: plane failure, wedge failure, toppling or circular failure (Wyllie & Mah, 2004). The different types of failures are discussed below (Wyllie & Mah, 2004).

Plane Failure

A plane failure occurs when a planar block of rock mass slides on a plane surface when conditions are met (Wyllie & Mah, 2004). The following are the typical conditions for it to occur:

- The failure plane (Figure 2-2) must strike within approximately ±20° to the face of the slope;
- The failure plane should daylight in the face of the slope, that is, the dip of the plane must be shallower than that of the slope face, that is, $\psi p < \psi f$ (Figure 2-3);
- The friction angle of the failure plane must be shallower than the dip of the failure plane, that is, $\psi p >$;
- The upper end of the failure plane either makes an intersection with the slope above or gets terminated in a tension crack; and
- The lateral boundaries of the failure should be clearly defined by the release surfaces (Figure 2-2) on the sides of the sliding block. There should be negligible resistance to sliding on the release surfaces.

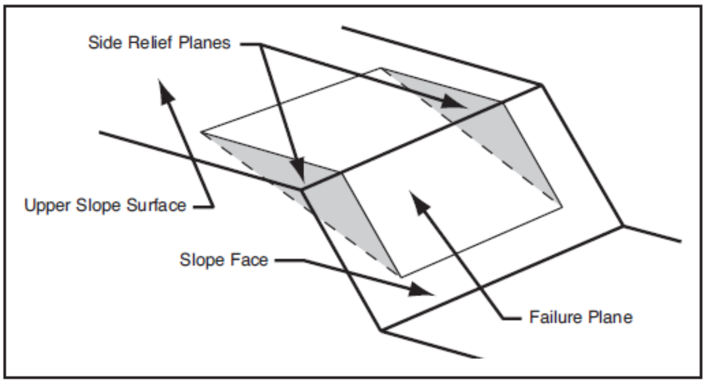

Figure 2-2: Plane failure showing release surfaces/relief planes at the ends of a plane *(Kliche, 2018)*

Where ψp is the friction angle of the failure plane and ψf is the slope face dip.

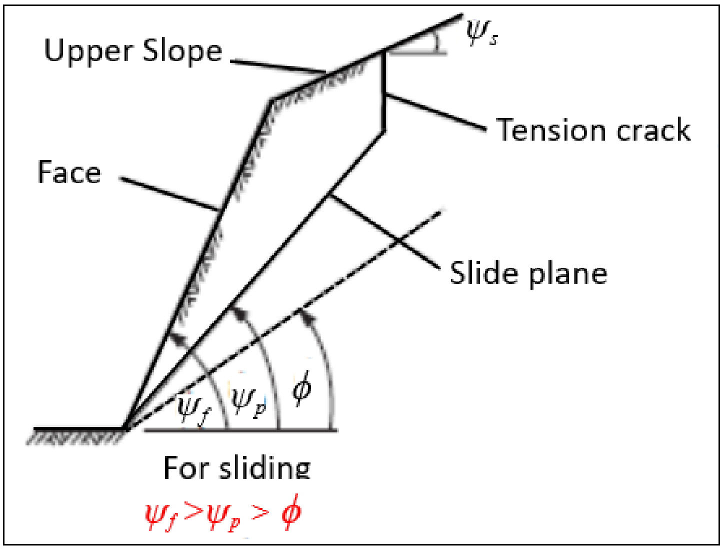

Figure 2-3: cross-section of planes forming a plane failure *(Wyllie & Mah, 2004)*

Wedge Failure

Wedge failure occurs when two discontinuity planes, which are obliquely oriented to the slope face, cause the sliding of a wedge along their line of intersection, as shown in Figure 2-4. However, sliding only occurs when the intersection of these two discontinuities daylight on the face of the slope. The occurrence of wedge failures is more common than plane failures, and therefore, their evaluation at mine sites is critical (Wyllie & Mah, 2004).

For wedge failure to occur, the following conditions must be satisfied:

- There should always be an intersection of two discontinuity planes whose line of intersection must daylight in the slope face; and
- The dip of the line of intersection must be shallower than the slope face dip, but greater than the average friction angle of both slide planes, that is, $\psi fi > \psi i > \varphi$ (Figure 2-5).

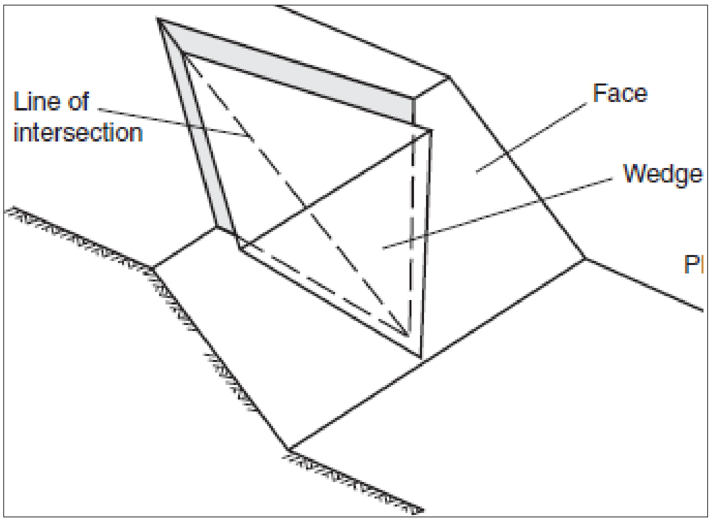

Figure 2-4: Isometric or 3D view of a wedge failure (Wyllie & Mah, 2004)

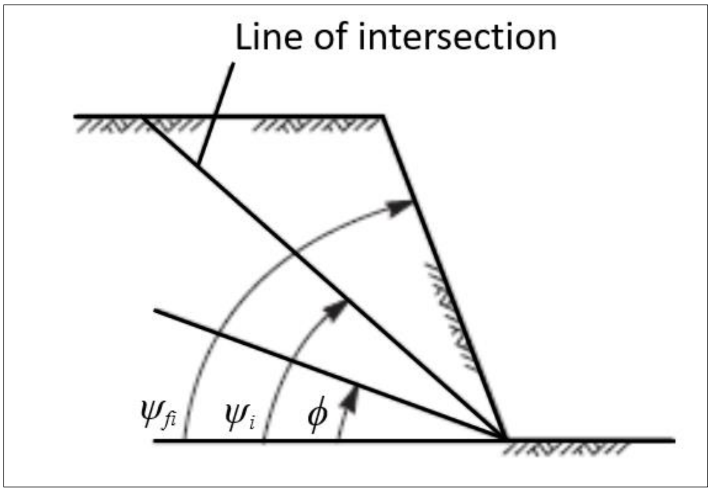

Figure 2-5: Cross-section of a wedge failure (Wyllie & Mah, 2004)

Toppling Failure

Toppling failure occurs when columns or blocks of rock rotate on a fixed base. For toppling failure to occur, the following conditions should be met (Wyllie & Mah, 2004);

- The dip direction of the structures dipping into the slope face should be within 10° of the dip direction of the slope face, forming slabs that are parallel to the slope face; and

- The dip angle of the planes must be steep for interlayer sliding to occur. Figure 2-6 shows toppling failure.

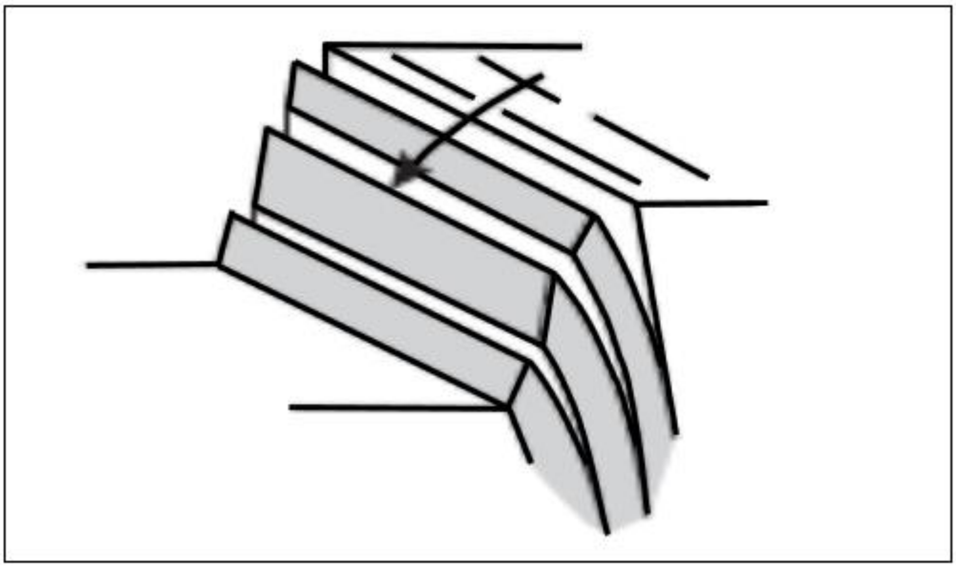

Figure 2-6: Toppling failure (Wyllie & Mah, 2004)

Types of toppling failures include:

- Block toppling;
- Flexural toppling; and
- Block-flexure toppling.

Block toppling: This type of failure occurs when steeply dipping Discontinuities into the face form individual columns whose height is defined by a second set of widely spaced orthogonal joints (Figure 2-7). This failure propagates up a slope as the shorter columns in the slope toe are pushed by the overturning longer columns, usually leaving a stepped base surface. Columnar basalt and bedded sandstone in which orthogonal jointing is well-developed are rocks where Block toppling is prevalent (Wyllie & Mah, 2004).

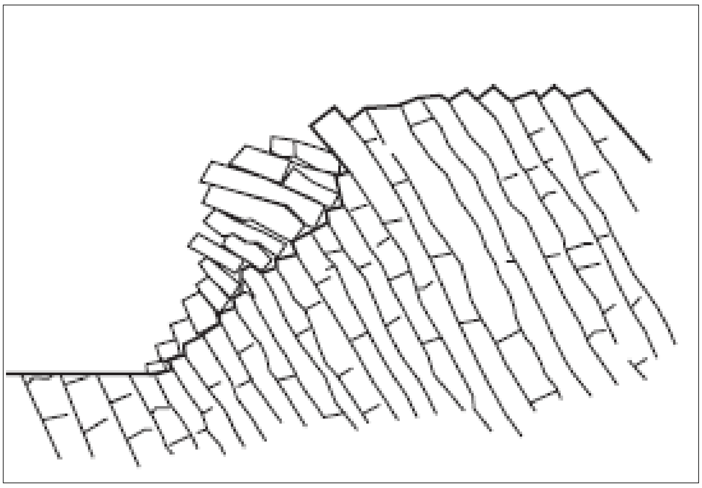

Figure 2-7: Block toppling *(Wyllie & Mah, 2004)*

Flexural toppling: This failure occurs when well-developed steeply dipping discontinuities form continuous columns which break in flexure and bend forward (Figure 2-8). This type of failure mechanism is common in thinly bedded sandstone and slate with orthogonal jointing, which is not well established. Some of the common triggering processes of the toppling process include sliding, excavation or erosion of the toe of the slope. These processes propagate into the rock mass, resulting in the formation of tension cracks (Wyllie & Mah, 2004).

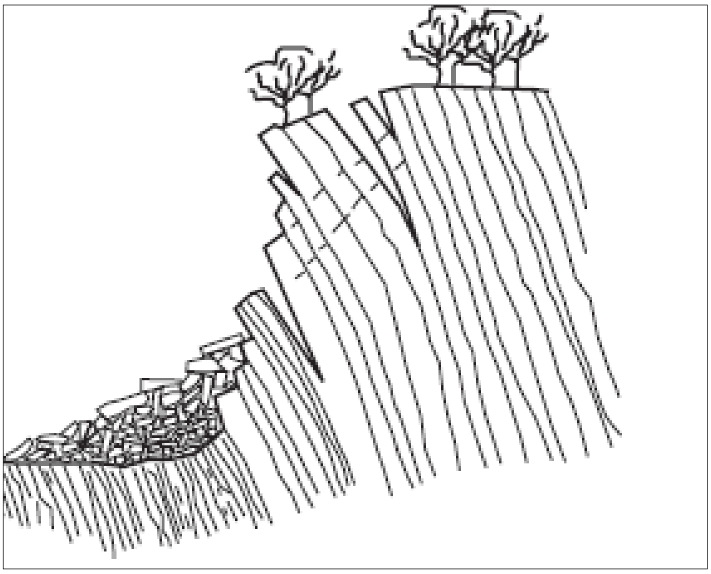

Figure 2-8: Flexural toppling *(Wyllie & Mah, 2004)*

Block-flexure toppling: Occurs when a relatively large number of cross joints divide pseudo-continuous flexure along long columns (Figure 2-9). The accumulated displacements on the cross-joints result in the toppling of the column. This type of failure results in fewer tension cracks compared to flexural toppling because of several small movements, which tend to close up the displaced spaces (Wyllie & Mah, 2004).

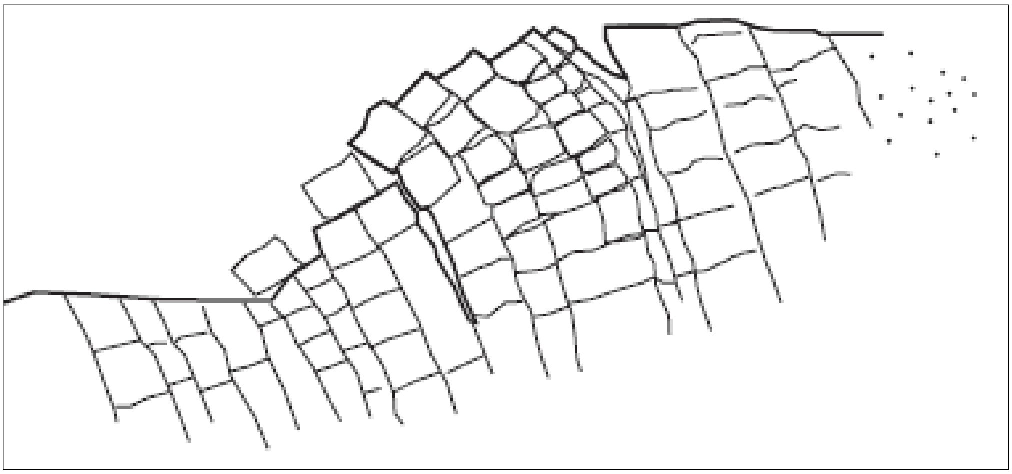

Figure 2-9:Block-flexure toppling *(Wyllie & Mah, 2004)*

Circular Failure

Circular failure occurs in materials that are low shear strength or highly jointed/weathered rock. The shape of the failure surface in such materials resembles a circular shape or an arc (Figure 2-10). The slip surface in this type of failure tends to find the line of minimum resistance through the slope. This is because the weathered or highly jointed rock has no structural pattern to result in significant resistance. For this failure to occur, the individual particles in the rock/soil material should be substantially smaller than the size of the slope. Therefore, it is recommended that slopes in these materials be designed with smaller heights and shallower batter angles to avoid circular failures (Wyllie & Mah, 2004).

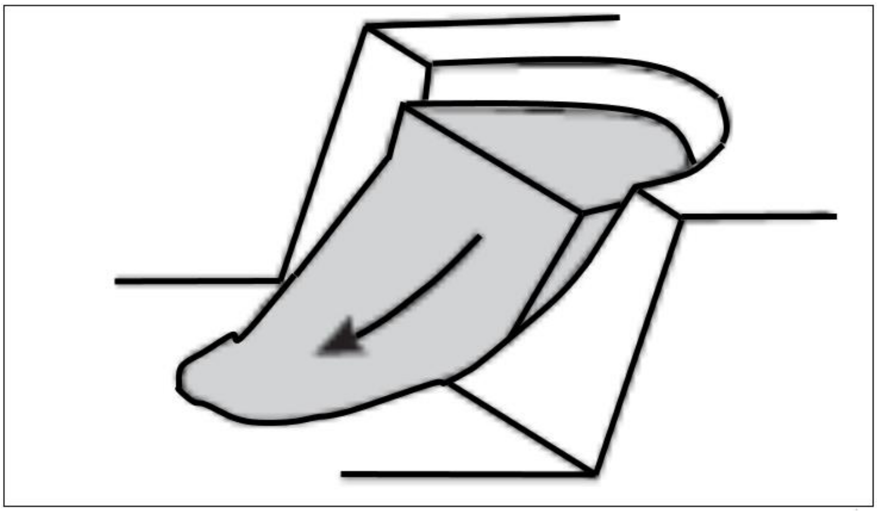

Figure 2-10: Circular failure (Wyllie & Mah, 2004)

2.2.3 Mapping techniques;

Structural Mapping is a complex undertaking that provides fundamental data on site conditions needed for slope design. This data is vital input for a range of analyses, including rock mass characterisation, rating and kinematic analyses (Wyllie & Mah, 2004). There are various methods of structural mapping, of which line mapping and window mapping methods are the most popular (Wyllie & Mah, 2004). However, the scanline method can result in a bias when small angles to the scanline are not accounted for. To correct this error, Terzaghi (1965) as cited in Tang et al. (2017) devised a four-step correction procedure which includes meshing the stereographic projection into grids, counting the poles within each grid. Further steps include calculating the frequencies according to the Terzaghi equation (Equation 2-1) and approximating the weighted frequencies to the nearest integer (Tang, et al., 2017).

$$N_{90} = \frac{N_\theta}{sin\theta} \qquad \textit{Equation 2-1}$$

Where θ is the angle of intersection between the discontinuity and the scanline, N_θ is the number of discontinuities intersected by the scanline at the angle θ ; and N_{90} is the number of discontinuities that would have been intersected at 90° and also the frequency of Discontinuities in a three-dimensional space.

A Rocscience software (DIPS) for kinematic analysis has an inbuilt Terzaghi weighting facility that can be applied to sampling bias from the data collection process (Rocscience, 2024).

2.2.4 Causes of strength reduction in the rock mass

Some of the prominent causes of reduction in the strength of rock mass include:

- weathering;
- groundwater; and
- blast effects.

Weathering

Weathering reduces the strength of rock and subsequently reduces the shear strength of discontinuities. Therefore, the reduced strength of intact rock results in the reduction of the shear strength of the rock mass. Weathering is caused by several conditions, which include soaking and drying, freezing and thawing, oxidation, hydration and carbonation (Wyllie & Mah, 2004).

Groundwater

Groundwater is defined as water below the water table. The cycle affecting Groundwater includes precipitation, evaporation, seepage and runoff. If not controlled, runoff water can cause erosion of the slope toes and alter the geometry. One of the most critical parameters in the stability assessments/analyses of slopes is the groundwater pressure. Groundwater pressure can reduce the effective shear strength and consequently cause instability of the slope. It can be measured using piezometers or determined by analysing the hydraulic properties such as permeability. The most satisfactory approach is measuring water pressure from representative locations with the piezometers and using this data in stability analyses (Kliche, 2018).

Blast Effect

Overbreak is one of the results of poor blast practices. It is usually caused by overcharging blast holes or poor drilling and blast designs. The overbreak, which can spread by 5 m- 10 m into the slope, can cause instability of the slope with time.

This occurs especially when water and ice fill the cracks, resulting in the dilatations and loosening of the blocks (Wyllie & Mah, 2004).

2.2.5 Stabilisation of slopes

Some amount of instability may be expected for Slopes. To stabilise the slopes, Kliche (2018) suggested some options that can be applied. These include grading, controlled blasting, mechanical stabilisation, structural stabilisation, vegetative stabilisation and water control:

Grading

Grading comprises modifying the slope geometry. The modifications may include introducing benches in the face of the slope and flattening the slope face angle.

Controlled Blasting

Controlled blasting is mainly for the prevention of the production blast from damaging the slope by overbreaking the rock mass. This is done to maintain or preserve a stable slope after blasts. Several techniques have been established to control overbreak.

Modified Production Blasting is a technique to reduce overbreak by reducing the explosive charge near the slope wall. To realise this, the explosive charges in the drilled row of holes which are nearest to the slope wall are reduced in the range of 30% to 60%. However, this technique still results in crack dilation or gas penetration to some extent.

Presplit blasting involves light charging and blasting closely spaced drilled holes hours or days before the production blast to prevent overbreaking of the slope wall. The prevention of overbreaking is achieved when closely spaced blasted holes create a fracture plane, which prevents the shock waves from the production blast from crossing.

Trim (cushion) blasting technique involves blasting a row of drilled blast holes hours or days or on delay after the production blast, mainly to remove blast overbreak to enhance slope stability. Removal of overbreak or loose material to enhance slope stability is one of the advantages of this method. However, it does not effectively/adequately protect the slope wall. Explosive charges similar to those used in the pre-split method are used in this method.

Line drilling is a technique where, during the blast, closely spaced holes drilled adjacent to the slope wall remain uncharged. This is to allow venting out of the gases through these uncharged holes, resulting in a crack extending from one hole to another. This prevents the propagation of shock waves into the slope, thereby protecting the wall from damage.

Mechanical stabilisation

The mechanical stabilisation method involves protecting the face of the slope. Erosion can be reduced if the slope is shielded with protective blankets and geotextiles. This method is also used to prevent rock falls where wire nets or mesh are used.

Structural stabilization

The structural stabilisation method involves the reinforcement of the rock mass structure at the slope surface using both primary and secondary support. Some of the commonly used methods include rock bolting, rock buttresses and shotcrete.

Vegetative stabilization

The vegetative stabilisation method is commonly used to stabilise areas experiencing minor instability, like ravelling and erosion. Some of the purposes of the vegetation include increasing cohesion as the roots spread and hindering water flow to limit erosion and enhance infiltration.

Water control

Slope stability is negatively impacted by water pressure, therefore, the stability can be improved by dewatering the slope. The two main sources of water pressure are groundwater and surface water. The negative impacts of surface water resulting from ponded and runoff water can be prevented by maintaining a topography that allows for effective flow and draining of water. This prevents the water from seeping into the tension cracks and causing dilation with consequential instability. Other measures of water control include lowering the water table to below the potential failure surfaces, thereby reducing the water pressure and improving stability. Some of the methods used to drain groundwater from slopes include dewatering boreholes, drainage galleries, adits and appropriately drilled drain holes. The water pore pressure can be determined from the borehole head by using suitable mathematical relationships. The critical pore pressure can then be determined from a sensitivity analysis in numerical software (as a pore pressure coefficient (Ru)). Pore water pressure and pore pressure coefficient are evaluated with Equation 2-2 and Equation 2-3, respectively:

$$U_w = \gamma_w h_w \qquad \textit{Equation 2-2}$$

$$R_u = U_w/\gamma_h \qquad \textit{Equation 2-3}$$

Where 'R_u' is the pore pressure coefficient, 'U_w' is the pore pressure, γ is the soil/rock unit weight and 'h' is the overburden height. 'h_w' is the height of water in a borehole and 'γ_w' is the unit weight of water.

2.2.6 Rock Mass Classification

Rock mass classification is one of the critical aspects of a slope stability management programme. In empirical methods, it is a key component in the development of geotechnical domains, estimating strength parameters and slope design. Using rock properties which control the behaviour of the rock mass, it can be used to assign numerical values for more meaningful uses, such as comparison of rock masses from different and distant locations (Brady & Brown, 2004). Several methods are discussed below.

Geomechanics Classification

The Geomechanics Classification or the Rock Mass Rating (RMR) system was developed by Bieniawski (1989). The classification is based on the following six parameters (Brady & Brown, 2004):

1. the uniaxial compressive strength (UCS) of the intact rock;
2. Rock Quality Designation (RQD), which is the percentage of pieces longer than 100 mm to the total length of the core;
3. spacing of discontinuity;
4. the condition of discontinuity surfaces;
5. groundwater conditions; and
6. orientation of discontinuities relative to the engineered structure.

The RMR classification is based on Table A-10 in Appendix A. The RMR classification value is obtained by adding the values of each of the six parameters.

Mining rock mass rating

Laubscher (1990) developed the Mining Rock Mass Rating (MRMR) system. This method uses parameters similar to those used in RMR. However, it combines the joint conditions and groundwater. The MRMR is based on four parameters, which include UCS, RQD, Joint spacing, condition and groundwater. The MRMR value is obtained by adding the values of each of the four parameters. The MRMR was developed to provide solutions for a range of situations in the mining industry. However, it is biased towards cavability. MRMR uses the tables and figures in Appendix A as a basis to classify the rock mass (Laubscher, 1990).

Based on conditions prevailing on site, the MRMR is adjusted based on weathering, joint orientation, blasting effects and mining-induced stresses to obtain the Adjusted MRMR (Laubscher, 1990). The Adjusted MRMR system classification is based on the tables and figures in Appendix A (Laubscher, 1990).

Q - system

The Q system was developed by Barton et al. (1974). This was after consideration of several case histories, which provided substantial levels of experience in the build-up of the system. The Q system was mainly developed for the design and support of tunnels. The classification by the Q system is done by calculating the rock mass quality index Q as shown in Equation 2-4. The classification is based on tables in Appendix B.

$$Q = (\frac{RQD}{J_n})\ x\ (\frac{J_r}{J_a})\ x\ (\frac{J_w}{SRF}) \qquad \textit{Equation 2-4}$$

Where: RQD is the Rock Quality Designation, J_r is the Joint roughness number, J_n is the Joint set number, J_a is the Joint alteration number, SRF is the Stress reduction factor, and J_w is the Water reduction number.

Q and other parameters such as the frictional component of discontinuities, RMR, deformation, support pressure and modulus of elasticity have been correlated.

The frictional component

The ratio (Jr/Ja) closely resembles the coefficient of friction for joints and discontinuities (Barton, 2002). Figure 2-11 Shows three illustrative shear strength-displacement graphs and back calculations of case records of relative magnitudes of $\tan^{-1}$(Jr/Ja). The friction angles evaluated using $\tan^{-1}$(Jr/Ja) (Tables B 1 and B 2 in Appendix B) provide near-accurate estimates (Barton, 2002). The determination of Jr can also be done by carrying out field measurements of an offset from a 0.5 m long ruler, as shown in Figure 2-12. The measurement obtained is then used on the graph in Figure 2-13 to read out the J_r (Watson, 2004). Figure 2-13 shows the relationship between the Jr and offset measurement of discontinuities on a logarithmic scale plot. The joint water reduction factor J_w (assigned using Table B- 3 in Appendix B) was added to include the effects of water. Evaluation of the frictional component (FC) can be done using Equation 2 - 5 (Barton, 2002):

$$FC = tan^{-1}\left(\left(\frac{Jr}{Ja}\right) x\, Jw\right) \qquad \textit{Equation 2-5}$$

Where J_r is the joint roughness number, J_a is the joint alteration number, and J_w is the joint water reduction factor.

After the Q system was updated in 2017, the shear resistance, τ, and the friction angle of geological structures could be approximated using the following equations 2-6 and 2-7, respectively (Bar & Barton, 2017):

$$\tau = \sigma_n tan^{-1}(\frac{Jr}{Ja}) \qquad \textit{Equation 2-6}$$

$$\phi = tan^{-1}(\frac{Jr}{Ja}) \qquad \textit{Equation 2-7}$$

where σ_n is the normal stress, ϕ is the friction angle of discontinuity, J_r is the joint roughness, and J_a is the joint alteration

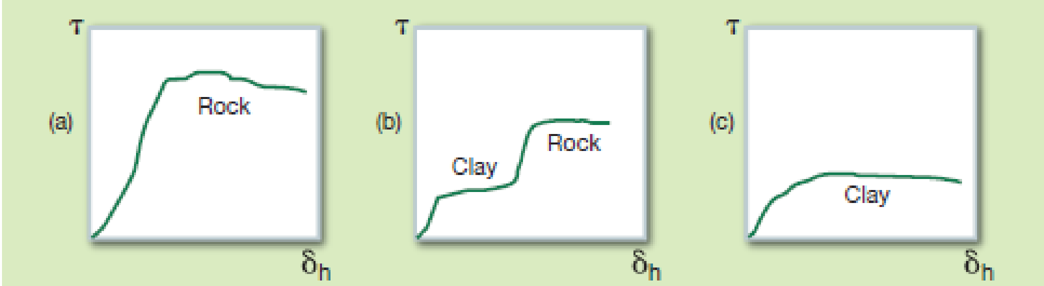

(a) Rock wall contact				(thin coatings)				
	Ja =	0.75	1.0	2	3	4		
	Jr			$\tan^{-1}$ (Jr/Ja)°				
A. Discontinuous joints	4	79°	76°	63°	53°	45°		
B. Rough, undulating	3	76°	72°	56°	45°	37°		
C. Smooth, undulating	2	69°	63°	45°	34°	27°		
D. Slickensided, undulating	1.5	63°	56°	37°	27°	21°		
E. Rough, planar	1.5	63°	56°	37°	27°	21°		
F. Smooth, planar	1.0	53°	45°	27°	18°	14°		
G. Slickensided, planar	0.5	34°	27°	14°	9.5°	7.1°		
(b) Rock wall contact when sheared				(thin fillings)				
	Ja =	4	6	8	12			
	Jr			$\tan^{-1}$ (Jr/Ja)°				
A. Discontinuous joints	4	45°	34°	27°	18°			
B. Rough, undulating	3	37°	27°	21°	14°			
C. Smooth, undulating	2	27°	18°	14°	9.5°			
D. Slickensided, undulating	1.5	21°	14°	11°	7.1°			
E. Rough, planar	1.5	21°	14°	11°	7.1°			
F. Smooth, planar	1.0	14°	9.5°	7.1°	4.7°			
G. Slickensided, planar	0.5	7°	4.7°	3.6°	2.4°			
(c) No rock wall contact when sheared				(thick fillings)				
	Ja =	5	6	8	12	13	16	20
	Jr			$\tan^{-1}$ (Jr/Ja)°				
Nominal roughness of discontinuity rock walls	1.0	11.3°	9.5°	7.1°	4.8°	4.4°	3.6°	2.9°

Figure 2-11: Inter-block frictional behaviour (a–c) (Barton, 2002).

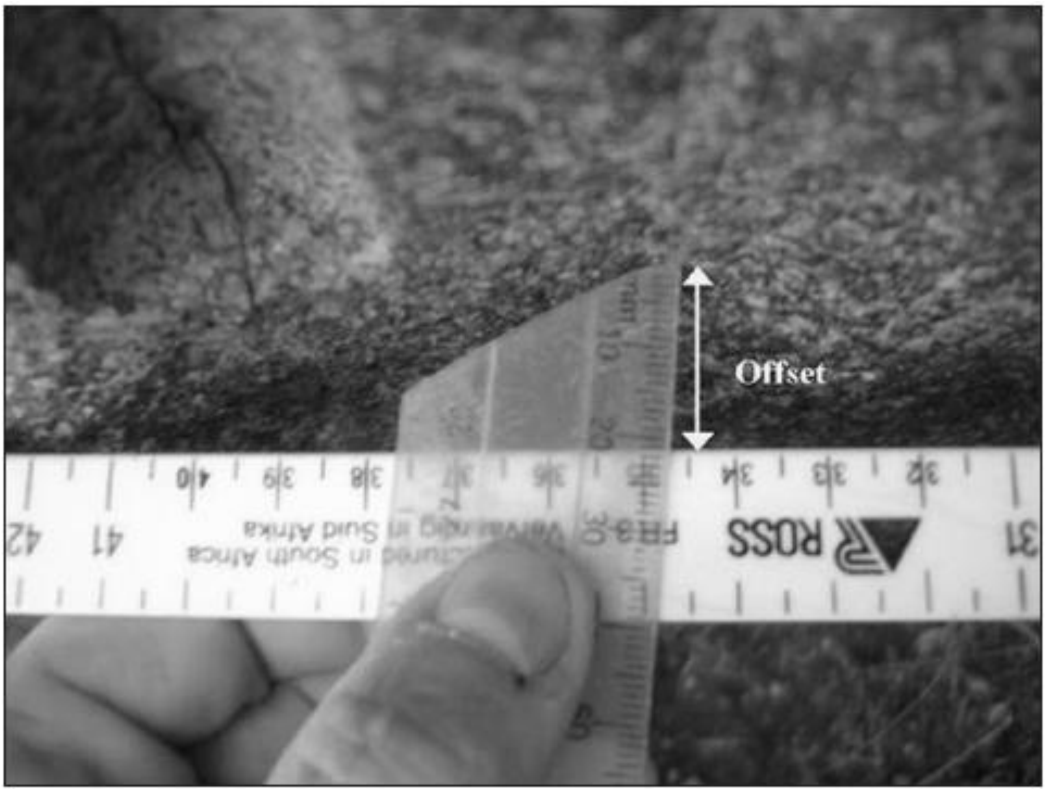

Figure 2-12: offset measurement for determining Jr (Watson, 2004)

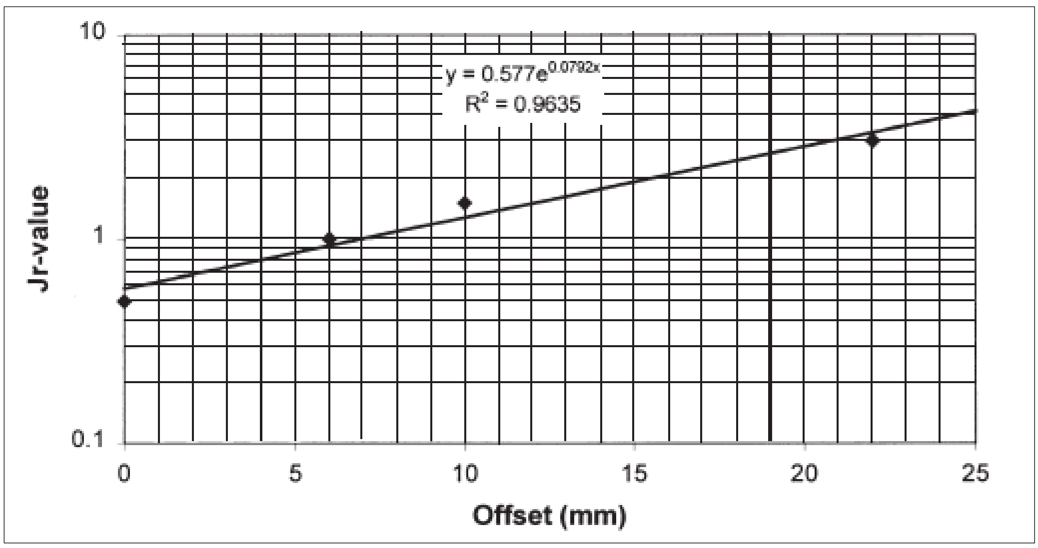

Figure 2-13: The relationship between Jr and offset (Watson, 2004)

Geological strength index

The Geological Strength Index (GSI) was developed by Hoek (1980). Wyllie and Mah (2004) argued that the GSI method can be used to estimate the strength of jointed rock masses on condition that their instability is not structurally controlled. The basis of the assessment is the interlocking of rock blocks and the surface conditions between these blocks for different geological conditions. Therefore, the GSI values were obtained to account for both the amount of fracturing and the surface condition of discontinuities (Wyllie & Mah, 2004). The GSI is currently the most widely used tool for rock mass quality classification. Marinos et al (2005) argue that the GSI can also be used to determine input data for stability analyses, which are based on the Hoek-Brown criterion.

Hoek and Brown established a correlation between GSI, Q and RMR, which can be used to estimate the GSI. These correlations are expressed in Equations 2-8 and 2-9 (Marinos, et al., 2005):

$$GSI = RMR'89 - 5 \; For \; GSI > 18 \; or \; RMR > 23 \qquad \text{Equation 2-8}$$

$$9lnQ' + 44 \; For \; GSI < 18 \qquad \text{Equation 2-9}$$

Where;

$$Q' = \frac{RQD}{Jn} \times \frac{Jr}{Ja} \qquad \text{Equation 2-10}$$

RMR’89 is the rating with groundwater rating at 15 and the joint adjustment rating at 0, and Q’ is the modified rock mass quality calculated using Equation 2-10. The GSI classification of different geotechnical conditions is based on Table A-11 in Appendix A.

2.2.7 Factor of safety, probability of failure and acceptability criterion

Factor of safety

The Factor of Safety (FoS) is the ratio of resisting forces acting on a slope to driving forces acting on the slope. This ratio is numerical with no units. It can be obtained from analysis methods such as the Limit Equilibrium Model (LEM) and the Shear Strength Reduction (SSR) (Macciotta, et al., 2020).

Probability of failure

The Probability of Failure (PoF) is a numerical parameter expressed in percentages which indicates the amount of uncertainty in slope stability analysis. Some of the sources of these uncertainties concerning the rock mass properties include spatial variability, material randomness, random sampling, errors during testing, inadequate information and systematic errors (Macciotta, et al., 2020).

Acceptability criterion

Open-pit slope engineering design optimisation should consider both the operation's profitability and the associated risks. During slope stability evaluations to determine an acceptable slope angle, a significant degree of uncertainty arises from various sources. Therefore, an optimal slope design must satisfy the Design Acceptance Criteria (DAC), accounting for the uncertainties and potential consequences of slope failure. Table 2-1 presents typical FoS and PoF acceptance criteria adopted as guidelines for the industry (Macciotta, et al., 2020).

Table 2-1: Typical acceptance criteria values of PoF and FoS for open-pit slopes at various scales by Wesseloo and Read (2009)

Slope scale	Consequence of failure	Minimum static FoS	Maximum PoF
Bench	Low-High	1.1	25%-50%
Inter-ramp	Low medium High	1.15-1.2 1.2 1.2-1.3	25% 20% 10%
Overall	Low Medium High	1.2-1.3 1.3 1.3-1.5	15%-20% 5%-10% <=5%

2.2.8 Statistical analysis (measure of central tendency)

Data collection processes usually gather unorganised data in a set. For this data to be usable as input data into various slope stability programmes, it should be processed into organised sets of data, each with a singular representative value (Wyllie & Mah, 2004). A measure of central tendency, identified as the central position of a data set, is used to singularly represent that data set. represents a data set by identifying a central position within that data set. The commonly used and valid measures of central tendency include the mean, median and mode (Laerd Statistics, 2018).

Mean

The mean is determined by adding all the values in the data set and dividing the sum by the number of entities in the data set, as shown in Equation 2-11. One of its advantages is that it minimises the error in the estimation of the representative value as all the entries in the data set are included in its calculations. However, its vulnerability to the influence of outliers is the main disadvantage. Therefore, the mean is not suitable for analysing skewed data (Laerd Statistics, 2018).

$$\textit{Mean} = \frac{x_1 + x_2 + \cdots + x_n}{n} \qquad \textit{Equation 2-11}$$

Median

The median is obtained by arranging the entities of a data set in order of magnitude and working out the central value. The central value is the median. Its main advantage is that it is less affected by outliers and skewed data. Therefore, the median is suitable for analysing skewed data (Laerd Statistics, 2018).

Mode

The Mode is obtained by determining the most popular of the entities in the data set. However, sometimes the mode results in problems of having more than one most popular entity in the data set. In other situations, the mode may also be far away from the other values or scores in the data set, thereby not being representative (Laerd Statistics, 2018).

Guide on when to use the mean, median and mode

Table 2-2 provides a guide on how to select the most suitable measure of central tendency for different types of variables.

Table 2-2: summary guide of the suitability of the measure of central tendency (Laerd Statistics, 2018)

Type of Variable	Best measure of central tendency
Nominal	Mode
Ordinal	Median
Interval/Ratio (not skewed)	Mean
Interval/Ratio (skewed)	Median

2.2.9 Stability evaluation of rock mass slopes using empirical methods

This involves the use of rock mass classification for preliminary evaluation of the stability of slopes. The Haines and Terbrugge method (1991), which was empirically derived, is one of the methods that is used. It is based on the correlation of the Adjusted MRMR, the slope angles, the bench stack slope height and the overall slope height (Haines, et al., 2006) as illustrated in the empirical chart in figure 2- 14. The empirical chart (Figure 2-14) is appropriate for the selection of inter-ramp or bench stack slope angles (Haines, et al., 2006). However, in situations where the stability of the slope is influenced by structures/discontinuities, the use of this method is not appropriate (Stacey, 2023).

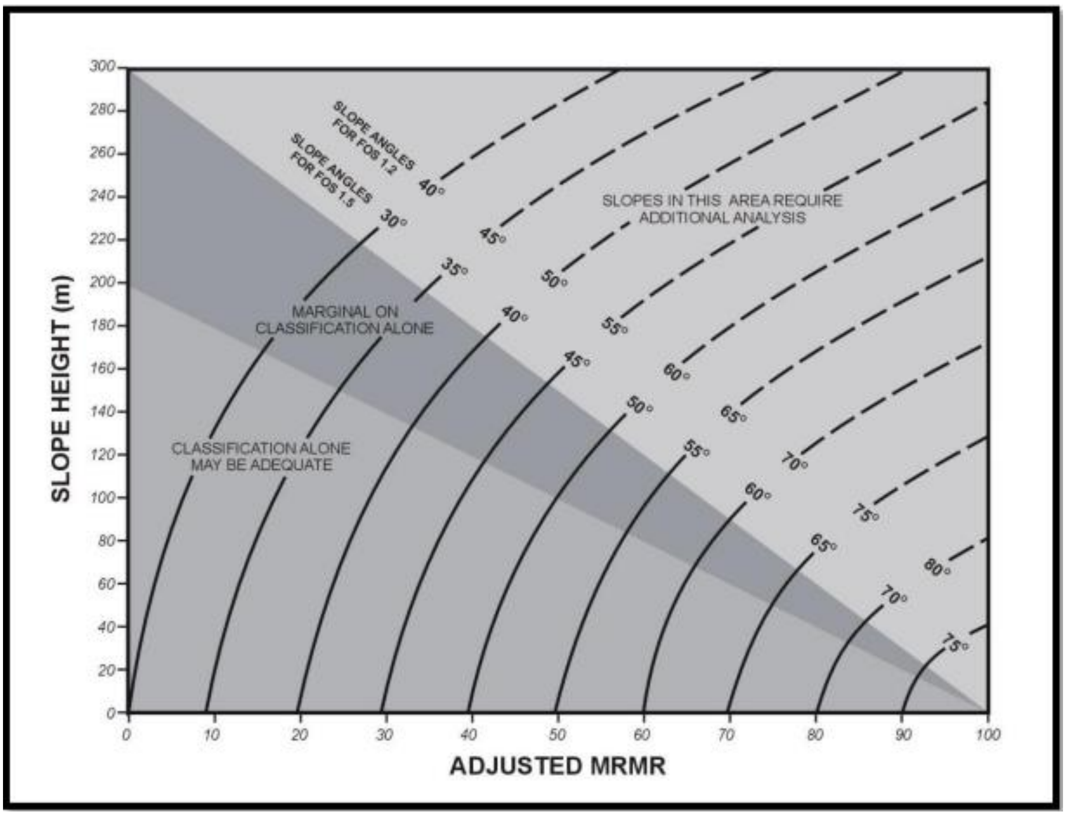

Figure 2-14: Empirical slope design chart (Haines, et al., 2006)

2.2.10 Geotechnical software

Stability analyses of slopes can be performed by several numerical programs including 2D and 3D Limit equilibrium (LEM), 2D and 3D Finite element (FEM), and kinematic analysis software (Rocscience, 2022). Rocscience software is one of the commonly used slope stability analysis software, which includes Slide2, RS2, RocData and Dips software.

Slide2 software

Slide2 is a 2D limit equilibrium slope stability program used to evaluate FoS and PoF in soil or rock slopes. It can evaluate both circular and non-circular failure surfaces (Rocscience, 2023). Other analyses which can be done using this software include finite element groundwater seepage analysis for both steady-state and transient conditions (Rocscience, 2023).

RS2 software

RS2 is a 2D finite element analysis program used to analyse geotechnical structures of both soil and rock in the Civil and mining industry. This software can be applied in a wide range of analyses such as surface excavation, underground excavations, foundations, slope stability, embankments, groundwater seepage dynamic analysis, tunnel and support design (Rocscience, 2023).

RSData

RSData is a program used to estimate rock and soil strength data, strength envelopes and other physical parameters. This program is based on generalised Hoek-Brown, Mohr-Coulomb, Power Curve and Barton-Bandis strength models. The results of the RSData program (material strength properties) are used as input for other numerical analysis programs (Rocscience, 2023).

Dips software

Dips is a program used to analyse structural orientation data. Other applications of this software include the determination of structural failure modes, joint spacing, joint sets and joint set statistics (Rocscience, 2023).

2.2.11 Geotechnical Instrumentation and Monitoring of Slopes

Mining activities or natural events create disturbances in the rock mass, which results in the redistribution of stresses. These redistributed stresses result in changes in deformations and strains, which are detectable and measurable with different types of slope monitoring tools. Monitoring includes observation of rock or soil structures visually or with a ground deformation monitoring tool. The monitoring can be done within the rock mass or on its surface. It is the visual or instrument-aided surveillance of engineering structures, which can either be done from within the rock mass or the boundary of the excavation. A slope monitoring programme's objectives include the following (Kliche, 2018):

a) To forewarn of potential instability. This enables the modification of excavation plans to reduce any impacts the instability may pose on the operation; and
b) Provision of rock/soil input data for the analysis of failure modes, allowing for proactive creation of corrective measures, including redesign of slopes that ensure stability and safety.

Kliche (2018) states that the two categories of slope monitoring techniques include observation and instrumentation.

Observational techniques- Commonly used observational techniques in the measurement of slope deformation include Global Positioning System, Slope Stability Radar (SSR), electronic and optical surveying and Slope Stability Monitoring (SSM). Other techniques include observations and photogrammetry. The design and Choice of the SSM systems are almost completely dependent on the geotechnical conditions of the slope (Cawood & Stacey, 2006). A guide called "Managing Slope Hazards, Making the Right Choice" can be useful for the selection of a suitable SSM system (Colin, 2022). Figure 2-15 provides a rough guide to managing slope hazards through the plot of a relationship between the mechanism of failure and suitable monitoring equipment.

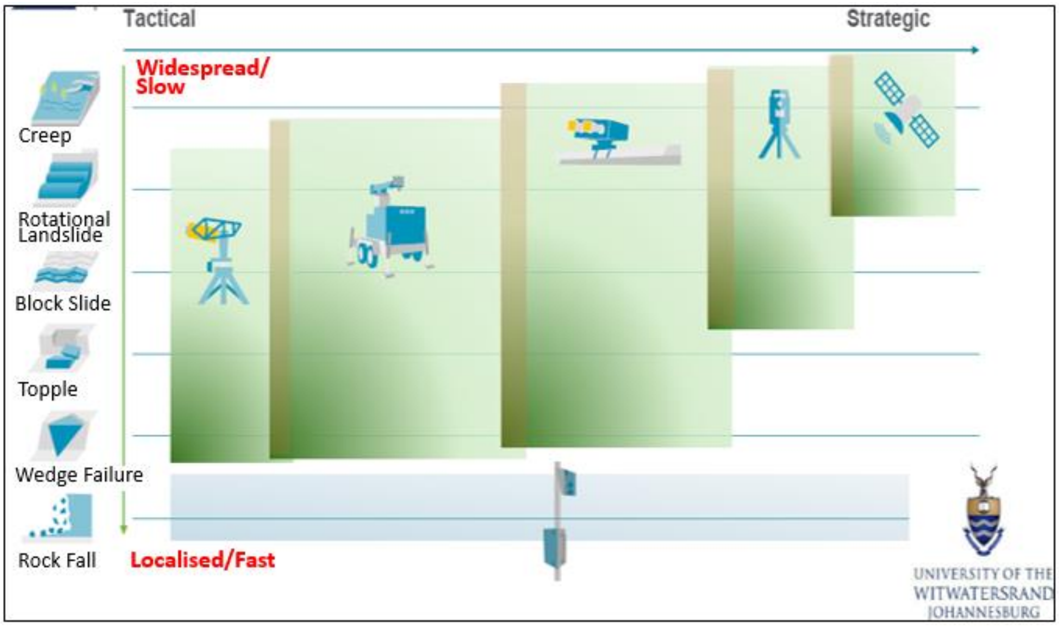

Figure 2-15: A guide to "Managing Slope Hazards, making the right choice", (Colin, 2022)

The SSR is the state-of-the-art slope stability monitoring technology being used in open-pit mines (Figure 2-16). This equipment provides real-time slope deformation measurement data through a live network continuously. Other important applications of the SSR include safe monitoring during production; background geotechnical monitoring to identify developing geotechnical hazards; post-failure recovery to clean up the slope and rescue equipment buried by failure; monitoring of subsidence, and monitoring of waste dumps. Other monitoring systems can be used to focus on small areas shown to be unstable by the SSR.

Figure 2-16: Slope stability radar image at COPF/D

Instrumentation technique involves the use of several mechanical and electronic instruments such as inclinometers, strain/stress gauges, and extensometers to measure rock mass deformation. These measurements are done on the surfaces of the rock mass or within the rock mass, where installation is done along fault planes and within the rock mass, respectively. Slope monitoring measures the displacement of the slope. The various categories of slope displacements include those which are stress-dependent, like creep movements, and those which are a reaction of rock mass unloading, like elastic movement. Cracking, dislocation and collapse are taken to mean failure. However, depending on the criticality of the situation, such as the rate of deformation, mode of failure, material type and where the instability is about the active mining operation, the displacements may not be worrisome (Kliche, 2018). Figure 2-17 shows the typical displacement-time curves for open pit slopes.

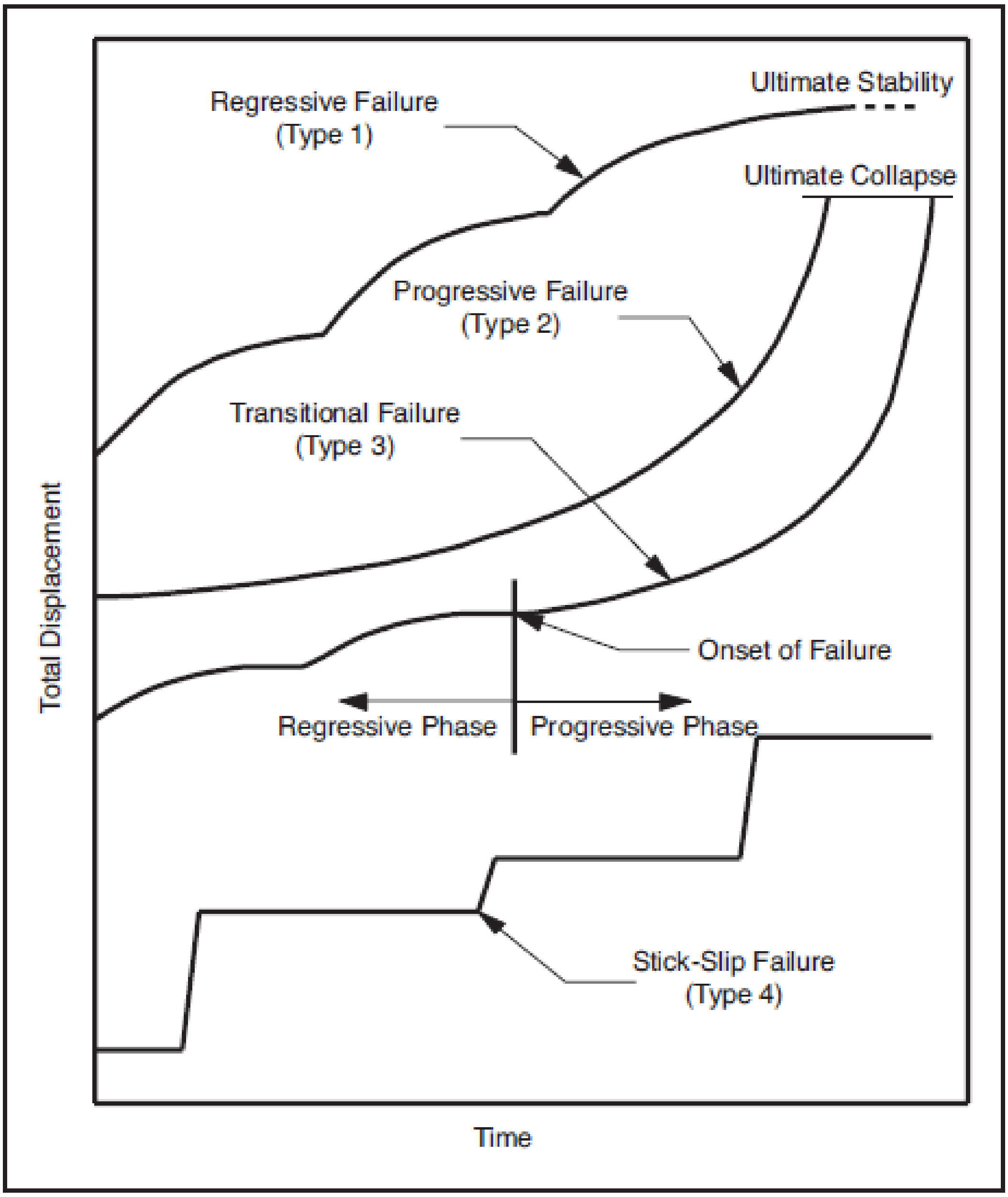

Figure 2-17: Typical displacement-time curves for open pit slope failures (Kliche, 2018)

One of the key objectives of setting up an open pit slope monitoring system is to detect the initial stages of slope instability. Other functions include a definition of the extent of the instability and provision of historical slope deformation data for the prediction of failure using methods like inverse velocity.

2.3 Key Debates and Controversies

Dana, et al. (2018) have argued that comparisons of 2D and 3D numerical modelling methods have been done by several researchers. McQuillan, et al. (2021) and Lam & Fredlund (1993) have discouraged the use of 2D in favour of 3D methods due to the limitations of the 2D methods. However, Cheng (2022) has encouraged the use of 2D methods because they are robust and user-friendly. McQuillan, et al. (2021) states that the failure to include end effects and various directional strengths in stability analyses is one of the main limitations of the 2D methods. The models will therefore produce lower/conservative values of FOS. Cala & Flisiak (2001), Arellano & Stark (2000) and Eid, et al (2006) found that for situations where the slope width (W) is greater than the slope height (H), 2D and 3D model analyses showed minimal differences. Figure 2-18 illustrates the slope width (W) and height (H) of a slope. The difference is about 20% for a W/H ratio of five, but increases rapidly below a ratio of four. Cheng (2022) argues that despite being modern and advanced, 3D models also produce results which are not satisfactory. He also highlighted the robustness of 2D models in somewhat complicated geological conditions. He further argued that for typical challenges, 2D and 3D results show minimal variances. Even the researchers who argued that 2D results were not satisfactory found minimal variances between 2D and 3D results. Further research is required to establish the conditions under which 2D and 3D slope stability software may be used in open pit analyses. This will make for easier and more timely decision-making regarding the choice between 2D and 3D software for various open pits.

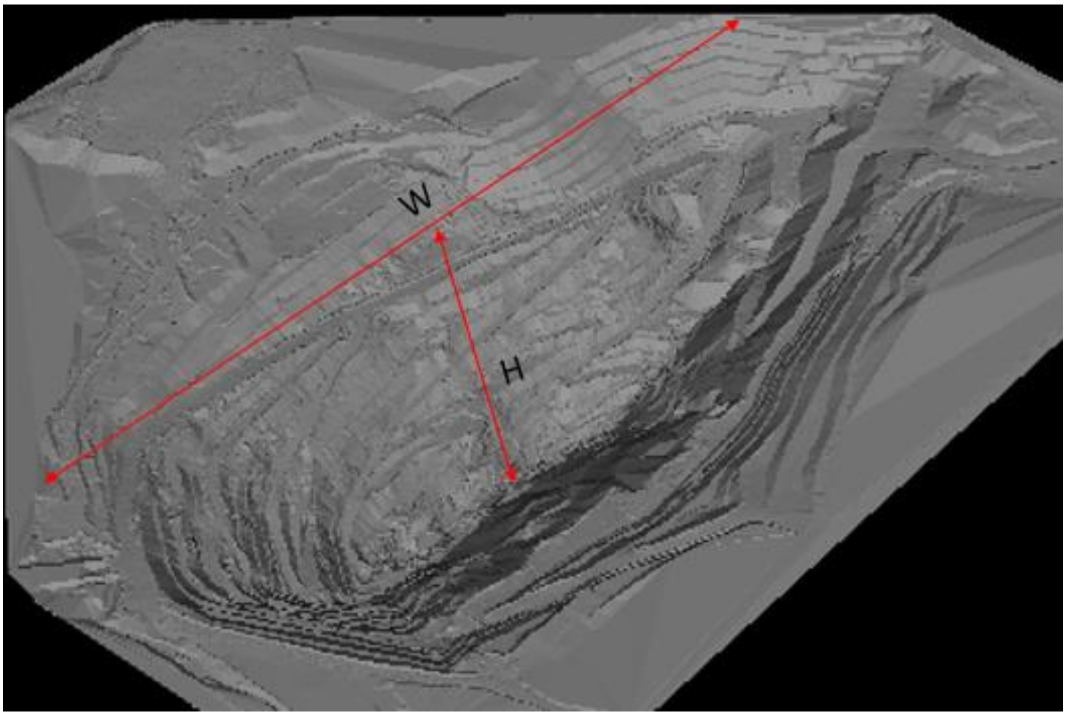

Figure 2-18: Slope width (W) and Slope Height (H) illustration for determining the W/H ratio

2.4 Chapter Summary

This chapter discussed various literature relevant to this research. The discussions covered techniques used in the management of slope stability. This included techniques used in data collection for use in numerical analyses and classification of rock mass, such as mapping, core logging and field rock mass assessments. Other techniques discussed were the stability analysis methods, validation of collected data and analysis results. Lastly, slope monitoring techniques and criteria for accepting risk levels in open pits were also discussed. 2D and 3D software were reviewed

3 RESEARCH APPROACH

3.1 Introduction

The chapter describes approaches that were employed to achieve the specific objectives of this research. The approaches are summarised in flow charts.

3.2 Research Design

The research involved quantitative assessments of the rock mass. The study included geotechnical logging and geomechanically testing of rock specimens. Relevant information was added from an existing mine database. The data collection was therefore a combination of primary and secondary sources.

3.3 Data Collection

The process of data collection is shown in the flow chart provided in Figure 3-1.

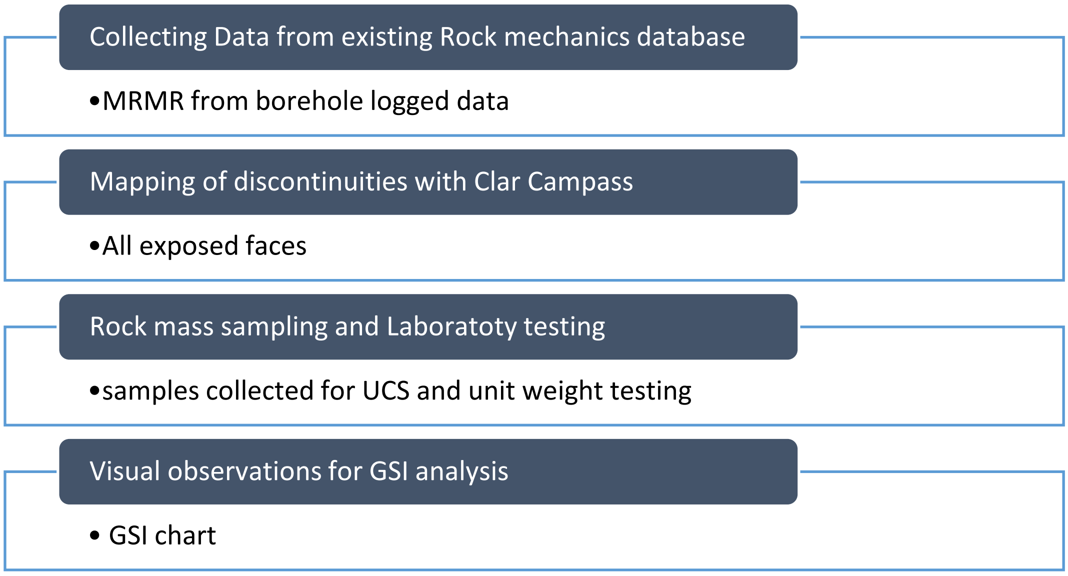

Figure 3-1: Data collection process chart for COPF/D

3.4 Data Validation Process

To validate the collected data, field sampling and laboratory tests were conducted using guidelines from the British Standards Institution (BSI) standards for sampling and testing rock (British Standards Institution, 2017). Field rock mass assessments were done using the GSI chart (Marinos, et al., 2005). Further validation was done by comparing the stability analysis results from three different analysis methods (empirical, deterministic and numerical).

3.5 Data Analysis Approach

The flow chart in Figure 3-2 shows the data analysis approach that was used in this research.

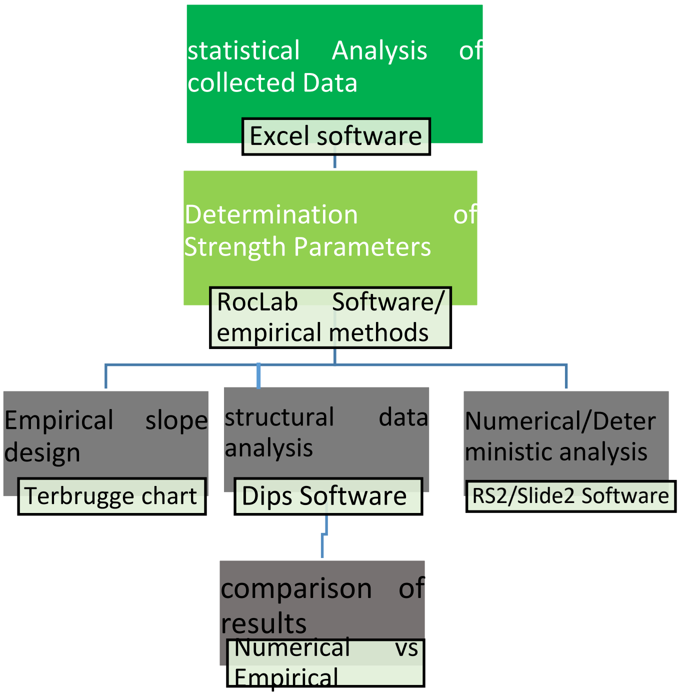

Figure 3-2: Data analysis approach process for the COPF/D pit

3.6 Chapter Summary

This chapter discussed details of the approach used in the collection of data, how the analysis was done, and techniques used to validate the results.

4 DATA FOR THE STUDY

4.1 Introduction

Data collection is one of the key aspects of any research. This research included data collection from the mine Database, field assessments, measurements and laboratory tests.

4.2 Collected Data

To carry out this research in line with the objectives, the following data were collected:

- Logged Borehole Geotechnical data;
- Division of the pit into three geotechnical domains;
- Piezometer readings data;
- UCS data;
- COPF/D GSI classification data;
- Strength parameter data(Cohesion and Friction angles);
- COPF/D rock properties (Unit weight and Modulus of elasticity);
- Mapping data (Discontinuities, surface orientations, and conditions data);
- Discontinuity friction angles; and
- Fall of Ground (FOG) data.

4.2.1 Logged borehole geotechnical data

Geotechnical data determined using drilled borehole data at current slope locations were collected from the mine database. A descriptive statistical analysis was done to organise the data as shown in Table 4-1. This data was used to determine geotechnical domains and calculate the Adjusted MRMR. The raw data for the calculations is provided in Tables A-7, A-8 and A-9 in Appendix A.

Table 4-1: Results of MRMR data from drilled boreholes for COPF/D

S/N	**Rock Formation**	**MRMR**		
		Median	**Mean**	**Standard deviation**
1	URD	31	33	12
2	SWG	41	40	13
3	CDOL	33	32	13
4	DOLSCH	36	39	13
5	UBS	33	33	9
6	TFQ	46	46	10
7	BSSU	35	37	10
8	PQ	40	40	9
9	BSSL	32	32	12
10	LBS	26	29	15
11	ARK	57	53	20
12	BAS	58	51	22

For effective analysis, the pit was divided into three geotechnical domains corresponding to the prevailing rock mass conditions. The domains were identified based on the MRMR and the failure criteria which have previously occurred. Planar failures are most likely in Domain 2, wedge failures in Domain 1 and topple and creep failures in Domain 3. Figure 4-1 shows the three domains at the COPF/D open pit.

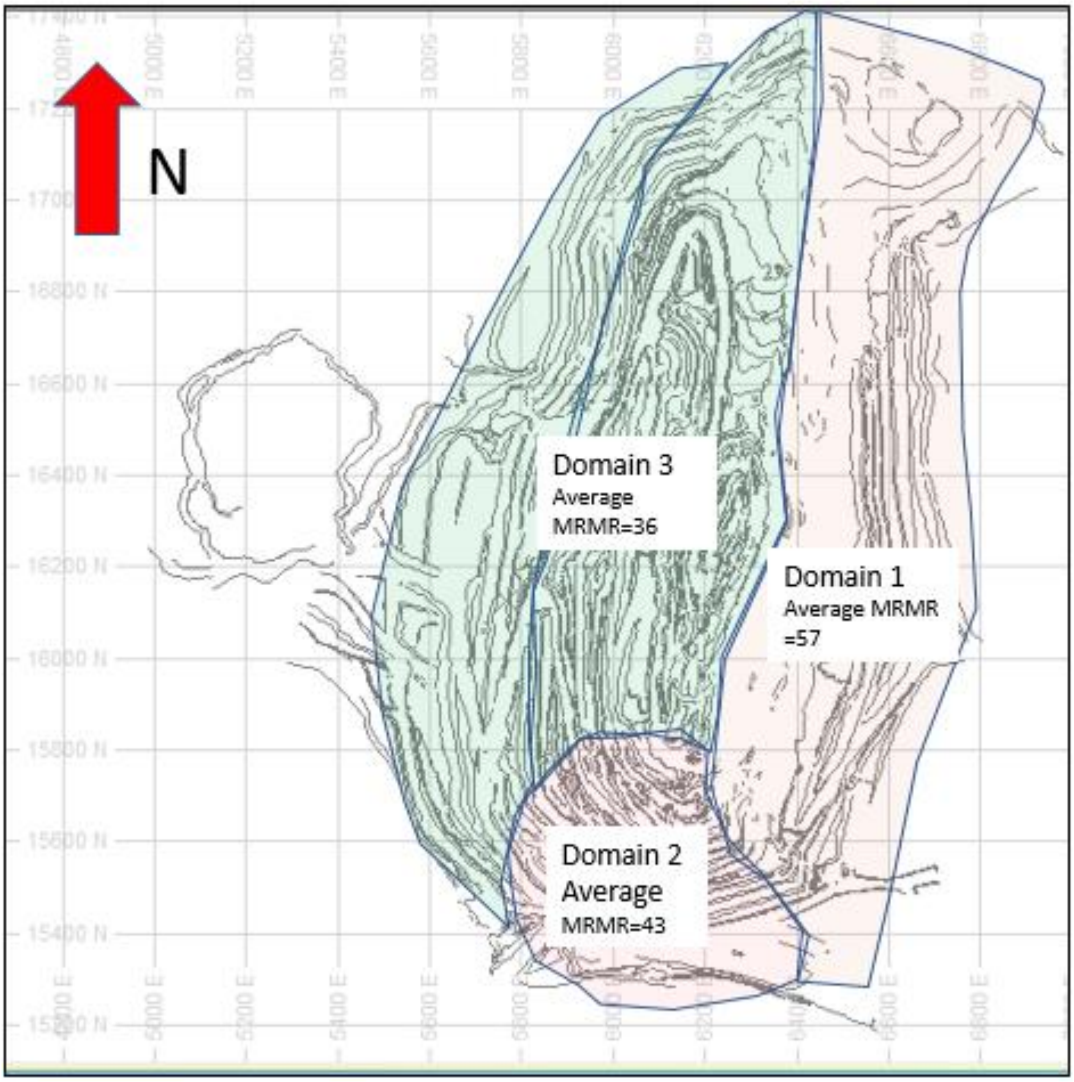

Figure 4-1: COPF/D Geotechnical domains

The adjusted MRMR was calculated based on field assessments, and the summary results are shown in Table 4-2. The depth below the surface is expressed as a metre Bench (mB) and indicated in Table 4-2. The surface at the COPF/D pit is given by 1333 m, which is the distance above sea level. The depth below the surface is the difference between the surface and the reduced level in the pit. Table A-7, Table A-8 and Table A-9 (Appendix A) show detailed calculations of adjusted MRMR for the footwall (Domain 1) and South wall (Domain 2) and hangingwall (Domain 3), respectively.

Table 4-2: Results of the Adjusted MRMR for COPF/D pit

Domain	Elevation (Depth below the surface) (m)	Thickness/Height (m)	Rock Formation	Adjusted MRMR	Stack Average Adjusted MRMR
1	0 mB -66 mB	66	weathered ARK	21.4	21.4
	66 mB-285 mB	233	ARK	53.0	53.0
2	0 mB-126 mB	126	Weathered BAS	23.1	24.8
			weathered ARK	57.4	
	126 mB-241 mB	115	BAS	24.8	34.8
			ARK	56.4	
			LBS	26.6	
			BSSL	32.8	
			PQ	44.7	
			BSSU	35.9	
			TFQ	33.0	
			UBS	33.8	
			DOLSCH	36.9	
3	0 mB-126 mB	126	Weathered URD	11.7	12.6
	126 mB-254 mB	128	URD	13.5	
			SWG	22.4	18.1
			CDOL	18.1	
			DOLSCH	19.7	
			UBS	18.1	
			TFQ	17.6	
			BSSU	17.9	
			PQ	21.9	
			BSSL	16.4	
			LBS	14.2	
			ARK	26.5	

4.2.2 COPF/D Pit Geometry Representative Sections

Three pit geometry representative sections of the current pit were simulated using the Datamine software for input into the numerical analysis software. Section A-A is likely realistic, and Section B-B will have a FoS built in due to the confining effects of the southern boundary of the pit. Section C-C is likely to have a large safety factor built in due to the confining effects of the eastern and western boundaries. section A-A and B-B have a W/H ratio of 6.4, while C-C has a W/H ratio of 4.3. Figure 4-2 shows the positions of the representative sections and piezometers.

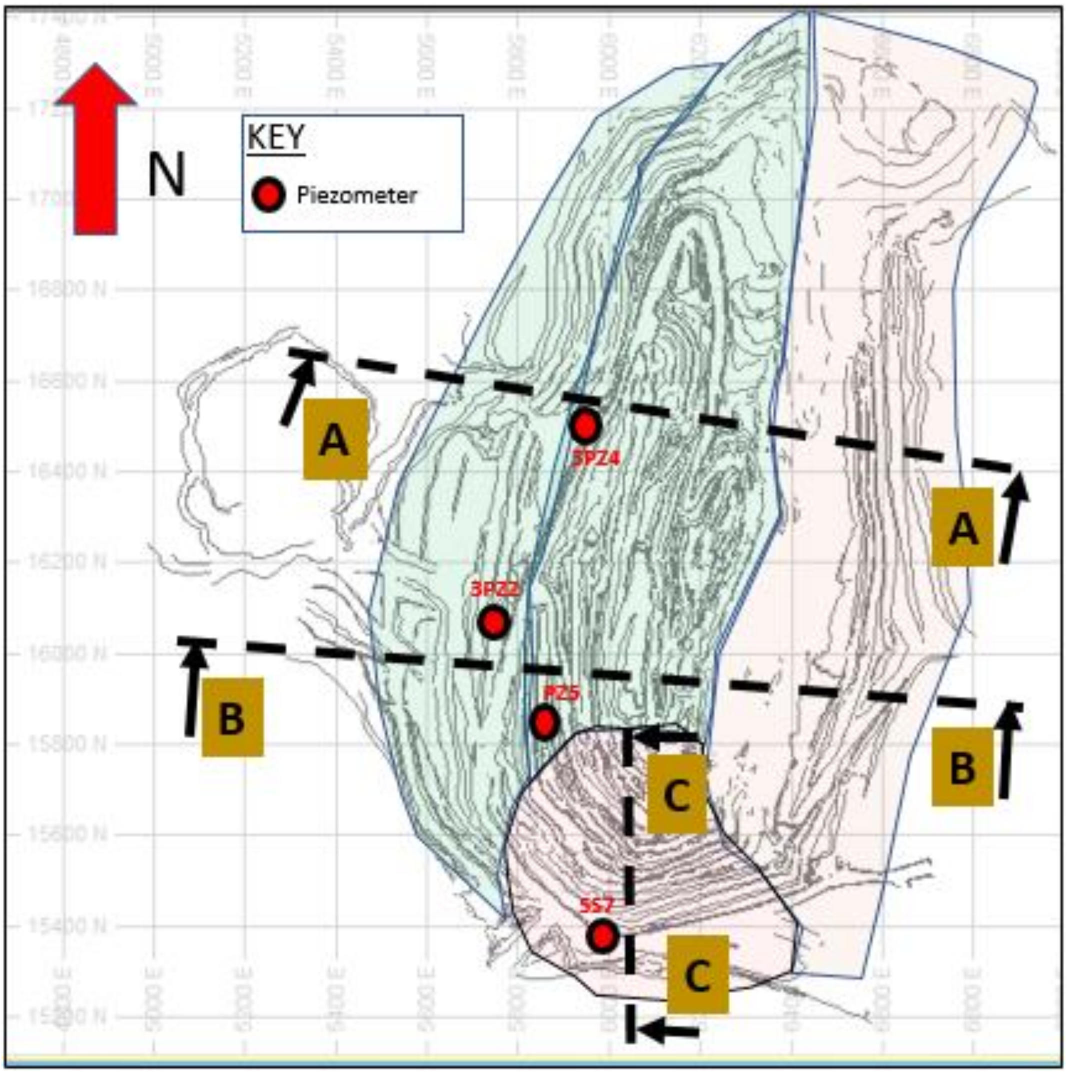

Figure 4-2: Piezometer locations and representative sections A-A, B-B and C-C positions

4.2.3 Piezometer Readings Data

Hydrogeological data include water levels collected from four piezometers located in the hangingwall and south wall of the pit, as shown in Table I-1 (Appendix I). The Piezometer reading data was used to determine the Ru for Domain 2 and Domain 3. The Ru was calculated using Equations 2-2 and 2-3 and was also used in the numerical stability analyses. Table 4-3 shows the domain maximum Ru values for the COPF/D pit.

Table 4-3: Ru for COPF/D pit domains determined from four piezometers

S/N	Domain	Maximum Ru
1	3	0.23
2	2	0.29

The current design geometry of COPF/D includes the bench face angle, the bench height, the bench width and the overall slope angle as shown in Table 4-4.

Table 4-4: COPF/D slope geometry

Region	Slope Geometry			
	Bench	**Bench face Angle (°)**	**Bench height (m)**	**Berm width (m)**
Hangingwall	0-75 mB	40	15	8
	75-300 mB	60	15	5
South wall	0 mB – 75 mB	60	15	5
	Below 75 mB	60	15	5
Footwall	0 mB – 30 mB	30	15	5
	Below 30 mB	40-45	-	-
Overall slope angle (°)	29			

4.2.4 UCS data

UCS data for all rock formations was determined from sampling and testing with a point load test machine. The data was subjected to a descriptive statistical analysis, and Table 4-5 shows the results. More detailed results are provided in Table D-1 (Appendix D).

Table 4-5: UCS data for all rock formations at COPF/D

Domain	Rock Type	Median UCS (MPa)	Standard deviation
1	ARK	260	44.37
2	BAS	345	5
	ARK	225	27.1
3	URD	200	42.6
	SWG	180	17.3
	CDOL	100	5.8
	DOLSCH	180	11.5
	UBS	130	16.3
	TFQ	180	7.1
	BSSU	35	1.5
	PQ	150	3.1
	BSSL	20	2.5
	LBS	170	11.5

4.2.5 COPF/D GSI classification data

COPF/D GSI classification data was used to determine the rock mass strength parameters using the RSData software from Rocscience (Rocscience, 2024). The input data included laboratory test data (UCS and E_i) and visual observations of the GSI as shown in Appendix C. The results were subjected to a descriptive statistical analysis in Excel software. Table 4-6 shows the strength parameter result of the analysis used as input data for numerical analysis. Detailed results are shown in Table C-1, Table C-2 and Table C-3 (Appendix C).

Table 4-6: Strength parameter results from the RSData software

Domain	Rock type	Cohesion (KPa)				Friction angle (°)			
		Median	Standard deviation	min	max	Median	Standard deviation	min	max
1	ARK	23.0	4.4	22.5	30.7	45.1	2.9	44.6	50.2
2	ARK	19.8	3.5	9.9	18.9	47.3	4.1	39.6	48.6
	BAS	39.7	21.2	0.1	46.3	50.1	17.0	17.0	52.3
3	URD	18.6	10.1	0.1	18.6	39.6	12.3	12.5	39.6
	SWG	21.0	2.3	16.4	21.0	37.6	0.9	35.8	37.6
	CDOL	5.5	0.1	5.4	5.5	32.5	0.2	32.2	32.5
	DOLSCH	20.5	1.7	17.6	20.5	43.7	1.0	42.0	43.7
	UBS	11.9	0.9	10.4	11.9	35.8	0.7	34.6	35.8
	TFQ	13.7	0.3	13.1	13.7	40.6	0.5	39.7	40.6
	BSSU	0.9	0.10	0.8	1.0	17.3	1.9	15.9	19.7
	PQ	17.5	1.4	15.0	17.5	47.6	1.2	45.5	47.6
	BSSL	0.8	0.10	0.7	0.8	26.5	1.3	24.3	26.5
	LBS	15.5	1.1	13.6	15.5	35.8	0.7	34.6	35.8
	ARK	19.0	1.7	16.4	19.7	47.6	1.3	46.4	49.0
	BAS	27.6	2.0	24.5	28.3	49.1	2.2	46.3	50.7

4.2.6 Strength parameter data

Strength parameter data was also obtained from the mine Database. Table 4-7 shows the median values of the previous and new strength parameters. Comparing the two data sets shows that the cohesion is higher while the friction angle is lower in the previous parameters. These results suggest that the previous parameters produced a conservative overall effect because the friction angle, which is directly proportional to the safety factor, was lower. This may be attributed to the fact that the pit was treated as one domain and therefore, data analysis could not be optimised.

Table 4-7: Previous and new strength parameters for COPF/D

ROCK Type	Previous median parameters		New median Parameters	
	Cohesion C(KPa)	**Friction Angle (°)**	**Cohesion C(KPa)**	**Friction Angle (°)**
URD	20.00	15.00	18.6	39.6
SWG	48.00	18.00	21.0	37.6
CDOL	30.00	18.00	5.5	32.5
DOLSCH	43.00	20.00	20.5	43.7
UBS	65.00	19.00	11.9	35.8
TFQ	78.00	28.50	13.7	40.6
BSSU	71.00	27.00	0.9	17.3
PQ	48.50	22.00	17.5	47.6
BSSL	78.00	22.00	0.8	26.5
LBS	76.00	23.50	15.5	35.8
ARK	50.00	20.00	19.0	47.6
BAS	42.00	17.00	27.6	49.1

4.2.7 COPF/D rock properties

COPF/D rock properties were obtained from the mine database and are shown in Table 4-8. This data was used in the numerical analyses and pore water pressure coefficient calculations.

Table 4-8: COPFD rock mass properties

Rock Formation	**In-situ unit weight (kN/m^3)**	**Modulus of Elasticity (MPa)**
URD	26.8	3.3
SWG	26.8	6.0
CDOL	26.8	3.8
DOLSCH	26.8	4.5
UBS	26.8	3.8
TFQ	26.8	7.9
BSSU	26.8	4.2
PQ	26.8	5.6
BSSL	26.8	3.5
LBS	26.8	2.5
ARK	28.0	14.0
BAS	28.0	16.0

4.2.8 Mapping data

Mapping data was obtained from field mapping of exposed discontinuities at various locations at the COPF/D pit. Tables 4-9 and 4-10 show mapping data at COPF/D. Detailed and other mapping data are shown in Table G-1, Table G-2 and Table G-3 (Appendix G). This data was used in the structural analysis of joint set data.

Table 4-9: Domain 1 mapping data

Domain	Discontinuity type	Dip (°)	Dip Direction (°)
1	Face	44	276
	Bedding plane (BD)	39	256
	BD	44	263
	BD	50	259
	BD	52	259
	BD	47	273
	BD	39	267
	BD	44	287
	BD	46	273
	BD	50	268
	BD	35	258
	BD	50	273
	BD	42	277
	BD	42	258
	BD	42	297
	BD	56	253
	Face	37	270
	Joint (JN)	75	98
	JN	70	94
	JN	75	98
	JN	70	96
	JN	75	3
	JN	75	10
	JN	75	4
	JN	90	4
	JN	75	16
	BD	40	295
	BD	40	254
	BD	45	265
	BD	30	260
	BD	40	251

Table 4-10: Domain 2 mapping data

Domain	Discontinuity type	Dip (°)	Dip Direction (°)
2	Face	65	347
	BD	40	319
	BD	44	311
	BD	70	315
	BD	71	328
	BD	45	312
	JN	84	214
	JN	62	204
	JN	77	81
	BD	45	314
	JN	82	244
	BD	45	303

4.2.9 Discontinuities friction angles

Discontinuity friction angles (Φ) were determined from the mapping data and offset measurement using Equation 2-7. The data was subjected to a descriptive statistical analysis, and the results are shown in Table 4-11. Detailed information is shown in Table H-1, Table H-2 and Table H-3 (Appendix H). This data was evaluated using the kinematic analysis in Dips. Comparing the two data sets, the difference is significant because the previous data was not measured from discontinuity surfaces but from intact rock mass. This may lead to different interpretations of results and potential instability resulting from incorrect input data in analysis software.

Table 4-11: Φ for discontinuities determined from offset measurement

Domain	Rock Type	New Φ (°)			Previous Φ (°)
		Mean	median	Standard deviation	Median
1	ARK	29.95	28.82	8.18	20.0
	BAS	31.18	33.04	7.19	17.0
2	ARK	35.6	30.93	16.37	20.0
	BAS	27.85	27.85	9.18	17.0
3	URD	20.78	15.38	13.44	15.0
	TFQ	31.97	24.24	12.64	28.5
	ARK	38.79	42.01	19.36	20.0
	PQ	28.85	28.85	22.87	22.0
	BSSU	61.65	61.65	27.78	27.0

4.2.10 Fall of Ground Data

The FOGs were mainly recorded on the southern slope of COPF/D. The mechanism of failure was wedge failure. Table 4-12 shows the FOG register for COPF/D (Geotechnical Database, 2008).

Table 4-12: Failure register of FOG at COPF/D pit (Geotechnical Database, 2008)

FOG Date	Area of FOG in the Pit	Mechanism of FOG	Quantity of Unstable area/ FOG (tons)	Remarks
2011	South wall	Wedge failure	80,000	Before recommendations from previous reports
2012	South wall	Wedge failure	75,000	After Recommendations to alter the slope angles to 60° on the south wall after previous failures and to increase the number of dewatering boreholes in the Hanging wall slope
2017	West wall	Creep (Circular failure)	420,000	
2018	South wall	Wedge failure	52,000	
2021	East wall	Planar failure	65,000	
2023	South wall	Wedge failure	85,000	

4.3 Chapter Summary

Various sets of data were collected for this study. This included geotechnical data used to classify the rock mass and to determine domains, pit geometry profile sections, design geometry and hydrogeological data for stability analyses. Other data collected included UCS, slope GSI classification for input into software for determination of strength parameters, rock mass data used in stability analyses and pore water pressure. The structures' mapping and offset measurements data for structural analysis and determination of the empirical friction angle were also collected.

5 ANALYSIS AND FINDINGS

5.1 Introduction

The evaluation of COPF/D consisted of three analysis methods, namely: empirical analysis, numerical analysis using software and structural analysis. The empirical analysis provided indicative slope geometry while the numerical and structural analyses validated the results. Figure 5-1 graphically shows the analysis process.

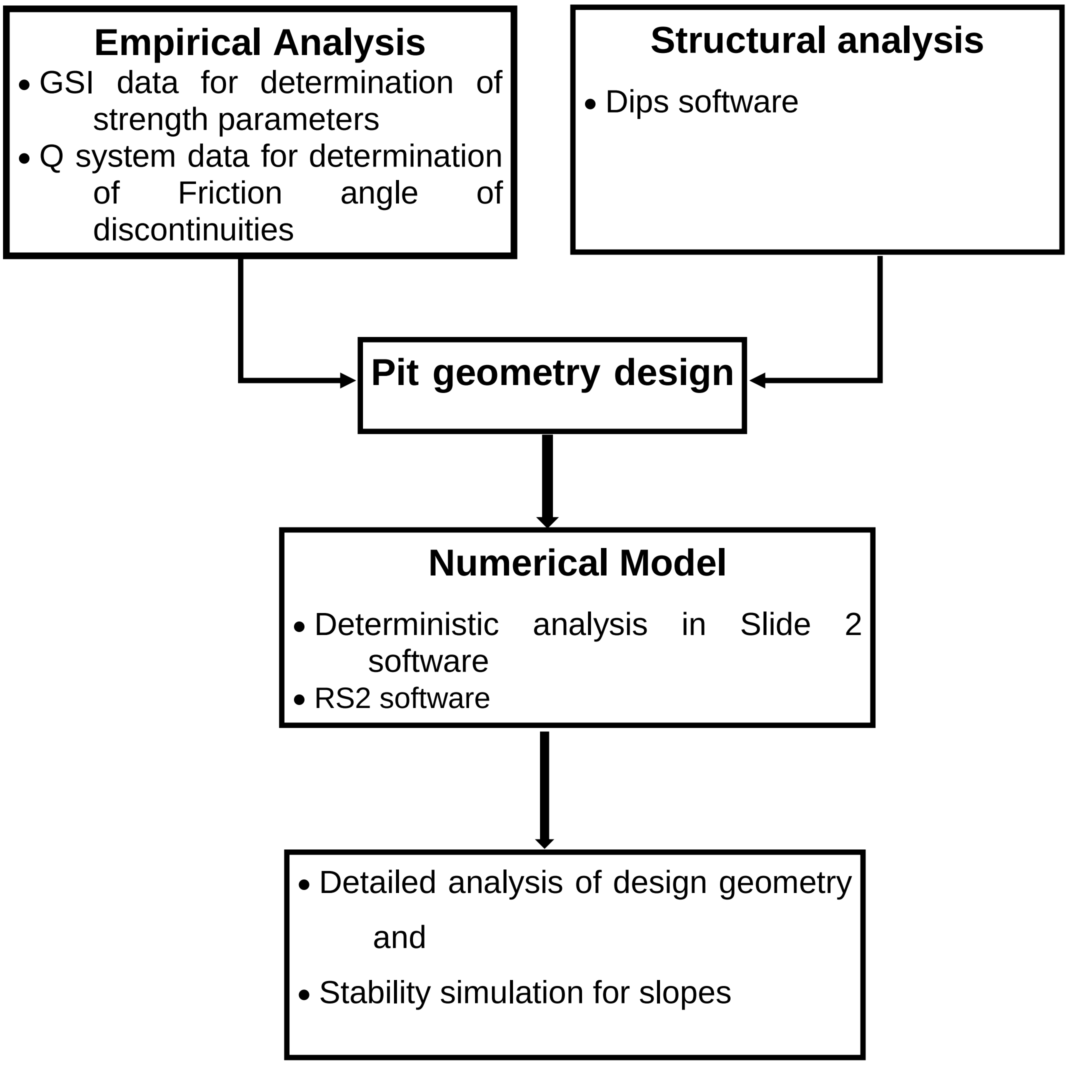

Figure 5-1:COPF/D slope stability analysis graphical representation

The results acceptance threshold by Wesseloo and Read (2009) was adopted and aligned with the mine site acceptability threshold indicated in Table 5-1 for all types of slope failures. The adopted consequence of failure is ‘’Low’’ due to the presence of a robust monitoring system put in place with which the mine can predict the instability and evacuate both equipment and personnel before the failure occurs.

Table 5-1: COPF/D acceptability criterion (Wesseloo & Read, 2009)

Slope scale	Consequence of failure	Minimum static FoS	Maximum PoF
Bench	Low-High	1.1	25%-50%
Inter-ramp	Low medium High	1.15-1.2 1.2 1.2-1.3	25% 20% 10%
Overall	Low Medium High	1.2-1.3 1.3 1.3-1.5	15%-20% 5%-10% <=5%

5.2 Empirical stability analysis of COPF/D slopes

The empirical stability analysis was carried out using empirically derived adjusted MRMR and the Terbrugge chart shown in Figure 2-14. The indicative stack angles and the overall slope angles were determined at a FoS of 1.2. Table 5-2 shows the results of the empirical stability analysis of COPF/D for various domains.

Table 5-2: Results of empirical stability analysis using adjusted MRMR and Terbrugge chart. The FoS of all results is 1.2.

Domain	Depth below surface (metre bench(mB))	Height (m)	Stack Average Adjusted MRMR	Overall Average Adjusted MRMR	Stack Angle(°)
1	0 mB- 75 mB	75	25.4	36.7	48
	75 mB-300 mB	225	36.9		43
2	0 mB- 75 mB	75	27.1	40.6	50
	75 mB-300 mB	225	54.1		48
3	0 mB- 75 mB	75	12.6	18.0	42
	75 mB-300 mB	225	18.1		43

5.3 Structural Analysis

Structural analysis was done using Dips software, which uses stereographic projections in the analysis. Figure 5-2 shows a sample result of stereographic projection analysis for Domain 1 of the COPF/D pit. The probability of the expected failure mechanism is shown as a percentage, as illustrated in the results summary table in the top right of Figure 5-2. Planar failure is analysed using pole plots of the orientations of discontinuities on the stereogram. The highlighted quarter moon in red (Zone 1) in Figure 5-2 is the zone where there is a probability for planar failure to occur. This zone is marked by the friction angle (friction cone) of the discontinuity and the daylight envelope plotted from the face orientation data of the slope. The daylight envelope is the boundary for all poles of discontinuities that daylight on the slope faces. All poles of Discontinuities that plot inside this boundary daylight on the slope face and are likely to slide. The friction cone plotted from the centre of the stereogram (polar friction cone) provides the boundary of the friction angle of the discontinuity. Poles which plot outside this boundary have planes steeper than the friction angle of the discontinuity plane and are likely to slide. Further, the plane on which sliding occurs should be approximately parallel (plus or minus 20° boundary or lateral limit) to the slope face (Wyllie & Mah, 2004). The lateral limits plotted (10° on either side (to make 20°) of the centre of the stereographic pole plot of the slope face) provide limits, and poles that plot inside these limits are likely to slide. The instability is probable when the poles of discontinuities plot in the zone of failure probability (Zone 1). Zone 1 is the zone beyond the friction cone boundary, within the daylight envelope boundary and the 20° lateral limits. An example is shown in Figure 5-2, where the Joint set J1 plot is in the zone of failure probability (Zone 1), which is beyond the friction cone, within the daylight envelope and the 20° lateral limits. This example shows that there is a 25.8% probability for sliding to occur.

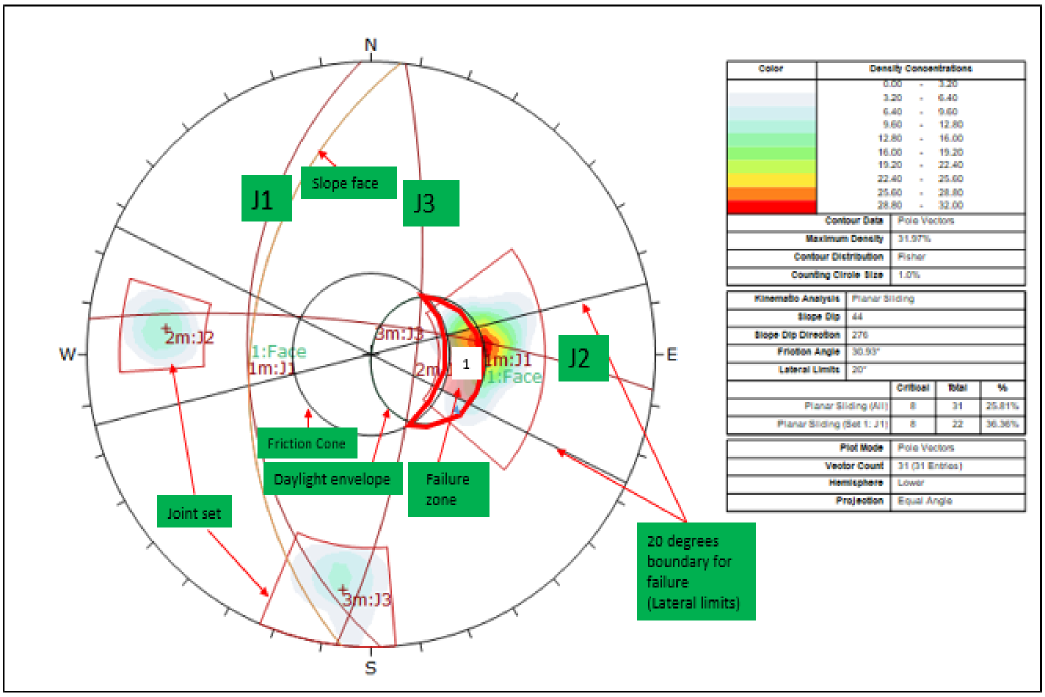

Figure 5-2: Dips software result of a kinematic analysis for planar failure in Domain 1

Wedge failure is analysed using great circle plots of the orientation of discontinuities on the stereogram. In Figure 5-3, the highlighted quarter moon in red (Zone 1) is the zone where there is a probability for wedge failure to occur. This zone is marked by the average friction angle of the discontinuity and the great circle of the slope face plotted on a great circle stereographic plot. The great circles are plotted from discontinuities with similar orientations, which form various joint sets. The friction cone measured/plotted from the outer boundary of the stereogram (planar friction cone) provides the boundary of the friction angle of the discontinuity. Great circles of discontinuities which intersect outside this boundary have intersection planes steeper than the friction angle of the discontinuity planes and are likely to slide. Further, the great circle of the slope face provide the daylighting boundary for intersecting discontinuity planes. Discontinuities which intersect beyond this boundary (in Zone 1) daylight in the slope face and are likely to slide. The instability is probable when the intersection of great circles of discontinuities plots in the zone of failure probability (Zone 1). Zone 1 is the zone beyond the friction cone boundary and the zone beyond the slope face boundary. Zone 2 shows the zone with a low probability of sliding. This zone is beyond the slope face boundary (therefore daylighting) but within the friction cone boundary. Therefore, sliding is unlikely for intersections in this zone. An example is shown in Figure 5-3, where three joint sets are plotted as three great circles. Joint sets J1 and J3 intersected in the zone of failure probability (Zone 1). This is beyond the friction cone boundary and the slope face boundary, indicating daylighting on the slope face. This example showed that there is a probability of 33.3% for sliding wedges to occur.

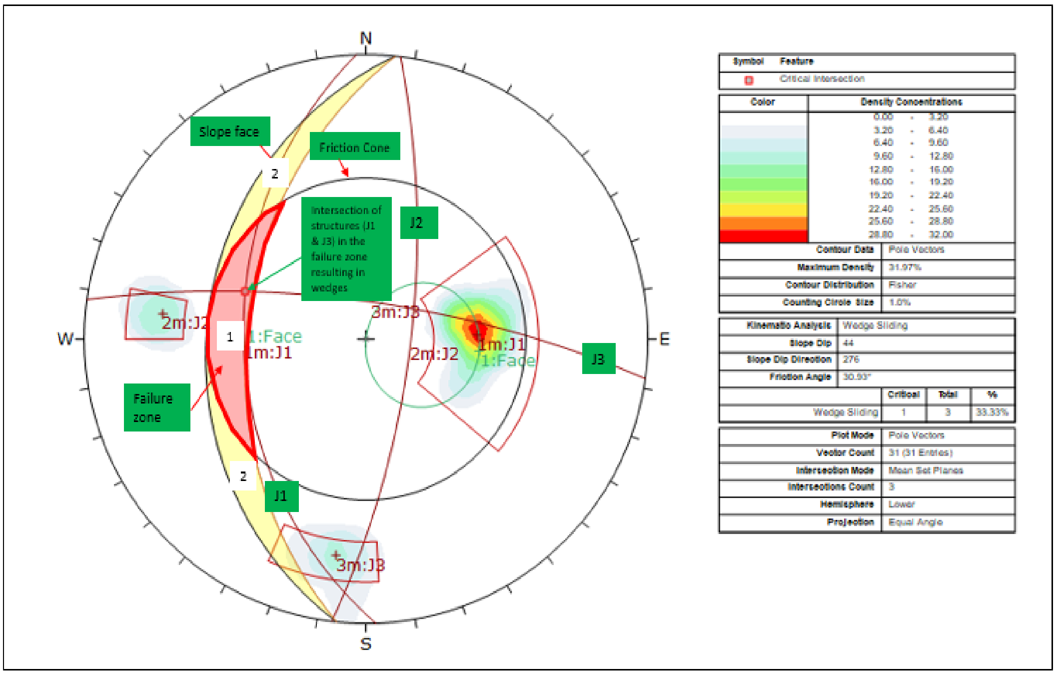

Figure 5-3: Dips software kinematic analysis for wedge failure in Domain 1

Toppling failure is analysed using both great circle plots and pole plots (for base planes) of discontinuities on the stereogram. In Figure 5-9, the highlighted triangular-shaped zone in red (Zone 1) is the zone where there is a probability for toppling to occur. This zone is marked by both the average planar and polar friction cones (friction angle) of discontinuities and 20° lateral limits. The friction cone provides the boundary of the friction angle of the discontinuity. Poles which plot out of this boundary (Zone 2 and Zone 3) for base planes have planes steeper than the friction angle of the discontinuity plane and are likely to slide. Planes or great circles which intersect beyond the planar friction cone boundary (Zone 1) are steeper than the friction angle of the discontinuity planes and are likely to slide. The base plane on which sliding occurs should be approximately parallel (plus or minus 20°) to the slope face. The lateral limits plotted provide limits, and only poles and intersections which plot inside these limits are likely to slide. The instability

(Direct Toppling) is probable when planes of discontinuities intersect in Zone 1 in conjunction with the base plane poles of discontinuities in Zone 2. Oblique toppling is probably when planes of Discontinuities intersect in Zone 1 in conjunction with the base plane poles of discontinuities in Zone 3. An example is shown in Figure 5-9, where no great circles of Joint sets intersect in the zone of failure probability (Zone 1), and no base plane poles are plotted in Zone 2 and Zone 3. This example showed that both direct toppling and oblique toppling were unlikely, with chances of 3.3% and 4.8%, respectively.

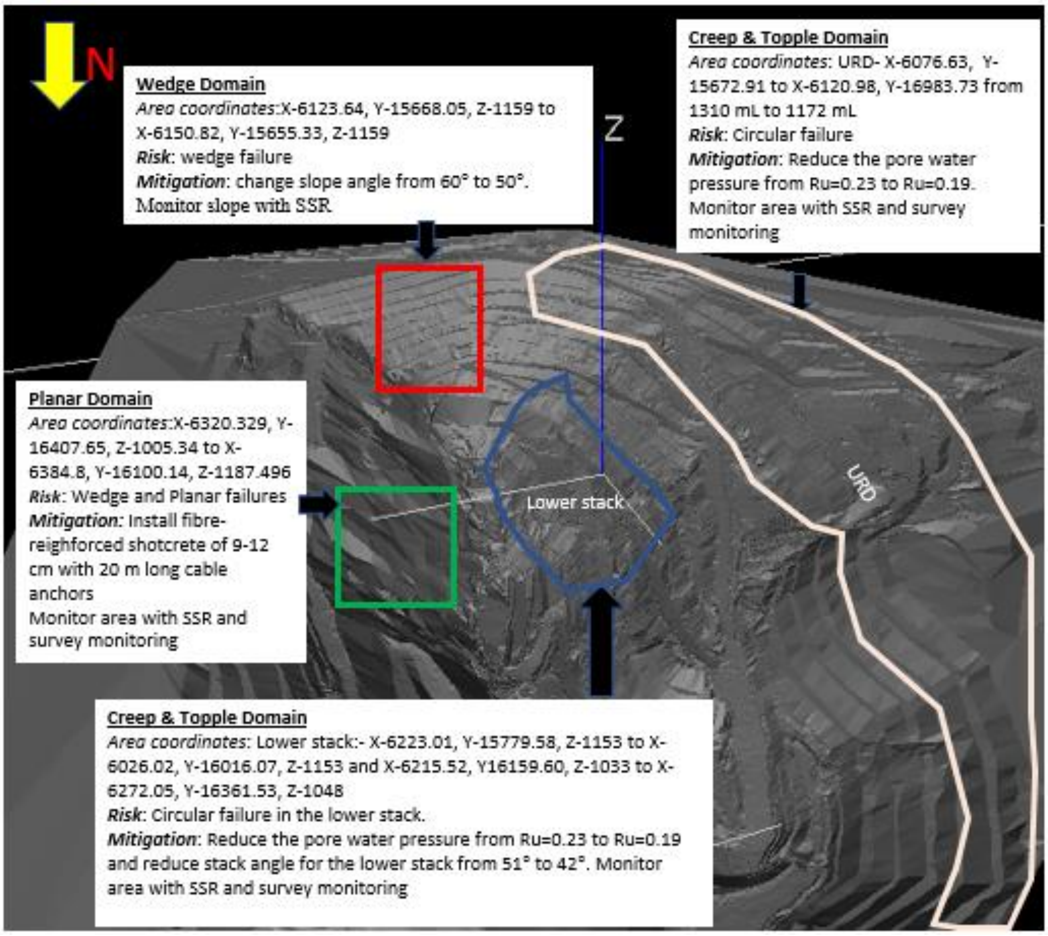

Figure 5-4: Potentially unstable areas at COPF/D pit

5.3.1 Domain 1

Domain 1 has an unterraced slope of 233 m high. The formation occurs with beddings of approximately 0.3 m thickness, which dip parallel to the dip of the slope. The structural analysis in the planar domain was carried out using Dips software. The results showed planar and wedge failures as two likely modes of failure. Wedge failure had the highest probability of occurrence with a probability of 33.3%, which was above the mine-acceptable threshold of 25%. The planar failure had a probability of occurrence of 25.8%, which was marginally above the mine-acceptable threshold of 25%. This is illustrated in Figure 5-2 and Figure 5-3, respectively. The slope angle in this domain increases the probability of failure. The result of other modes of failure showed that the occurrence was unlikely. The location of the potential planar instability is given by the coordinates and covers an area of 71,650 m^2 (Figure 5-4). A simulation to determine the slope angle that will minimise the chance of occurrence of wedge failure was done. The simulation involved altering the slope face orientation (Dip and Dip direction) to establish a safe orientation that will not result in failures. As shown in Figure 5-5 and Figure 5-6, the chance of planar and wedge failures would be reduced to within a mine-acceptable threshold of 16.1% and 18.6%, respectively, at a slope angle of 41°. Mining the slope to a simulated optimal slope angle of 41° may be uneconomical considering the potentially huge amount of waste (8,069,850 tons) that may be required to be mined (Table B-7 in Appendix B).

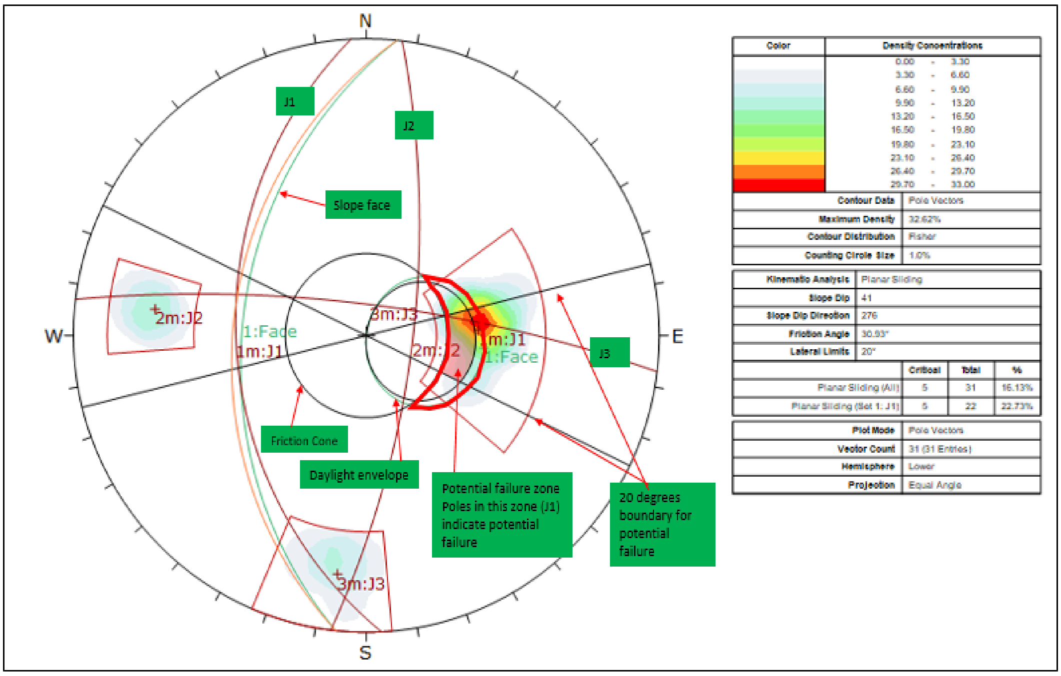

Figure 5-5: Dips software result of a simulated kinematic analysis for planar failure in Domain 1

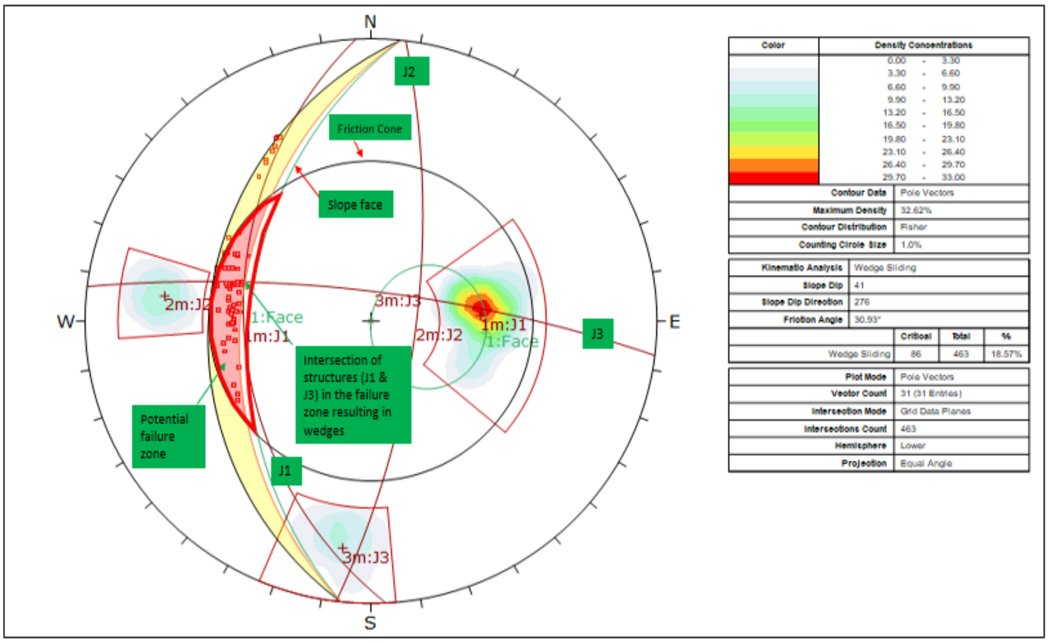

Figure 5-6: Dips software result of a simulated kinematic analysis for wedge failure in Domain 1

Support requirements for this potentially unstable zone were determined using the Q system (Barton, 2002) as shown in Table B-7 of Appendix B. This area was classified as a fair rock mass (Barton, 2002). To be made stable, fibre-reinforced shotcrete of 9-12 cm with 20 m long cable anchors should be installed. The total cost of this rock support was determined to be 6,096,615 United States Dollars (USD) (Table B-7 in Appendix B). The cost of mining this potentially unstable area to the recommended slope was determined to be 58,748,508 USD, as shown in Table B-7 of Appendix B. Considering both the cost of installing support and mining to the recommended slope angle, it is more economical for the unstable zone to be supported than to be mined. However, to ensure safety and efficiency during installation, a consulting company specialising in the installation of such long support should be engaged. This would ensure the safety of personnel and equipment operating below this portion of the slope.

5.3.2 Domain 2

The structural analysis in Domain 2 was carried out using Dips software. The results showed wedge failure as the likely mode of failure. Wedge failure had the highest probability of occurrence, with a probability of 34.9%, which is higher than the acceptable threshold of 25%. The result of other modes of failure showed that the occurrence was unlikely. This is illustrated in Figure 5-7. The location of the potential wedge instability is given by the coordinates and covers an area of 4,892 m^2 (Figure 5-4).

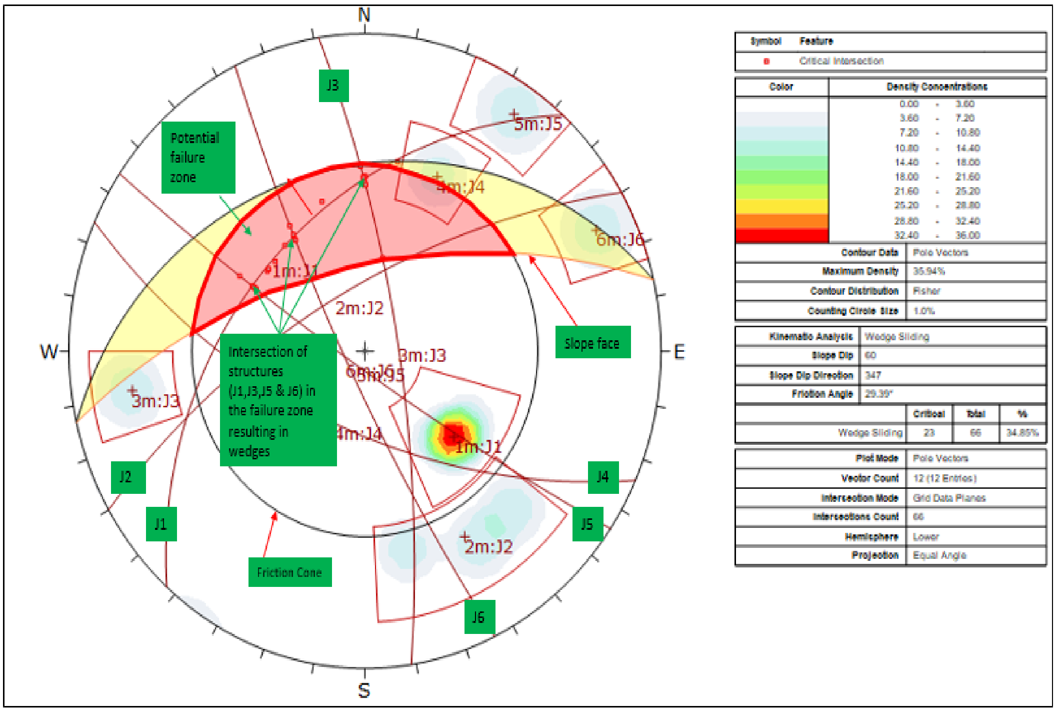

Figure 5-7: Dips software result of a kinematic analysis for wedge failure in Domain 2

A simulation to determine the slope angle that will minimise the probability of occurrence of wedge failure was done. As shown in Figure 5-8, the risk of wedge failures would be reduced to an acceptable threshold of 22.7% at a slope angle of 50°.

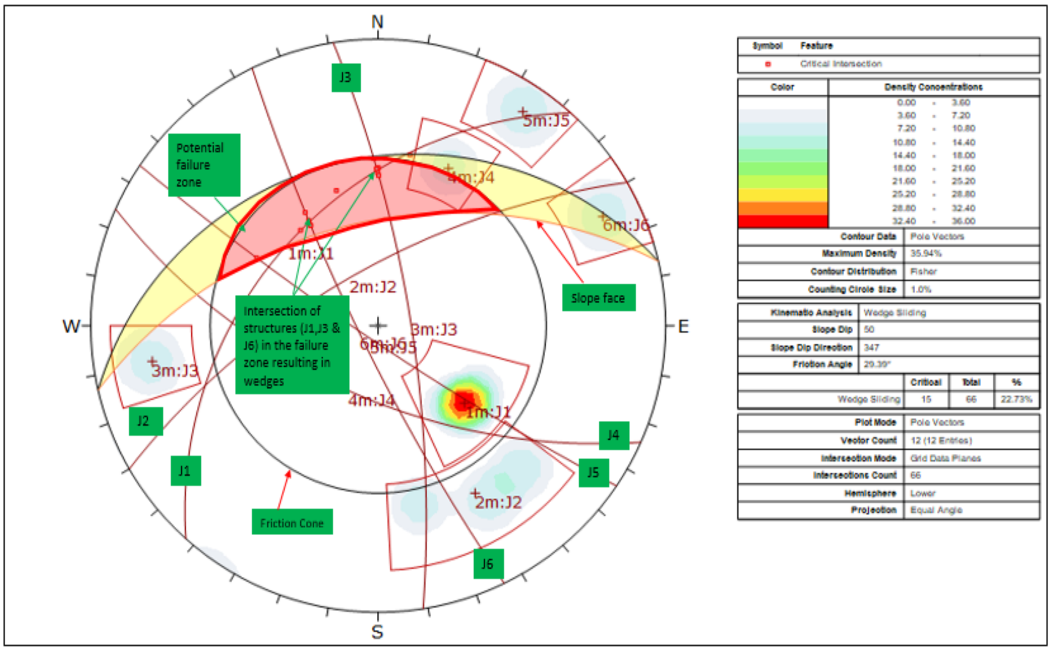

Figure 5-8: Dips software simulated result of a kinematic analysis for wedge failure in Domain 2

5.3.3 Domain 3

The structural analysis in Domain 3 was again carried out using Dips software. Domain 3 has several joint sets as shown by a greater number of great circles on the stereogram in Figure 5-9. The results showed Oblique toppling and wedge failures as the two likely modes of failure. Direct toppling in the TFQ rock formation had a probability of failure of occurrence of 3.3%. Wedge failure in URD rock formation had a probability of occurrence of 10.5%. Both failures were within the mine-acceptable threshold of 25%. Increasing the slope angle beyond 69° in this domain increases the probability of structural failures. The occurrence of other failure modes was not of major concern. This is illustrated in Figure 5-9 and Figure 5-10.

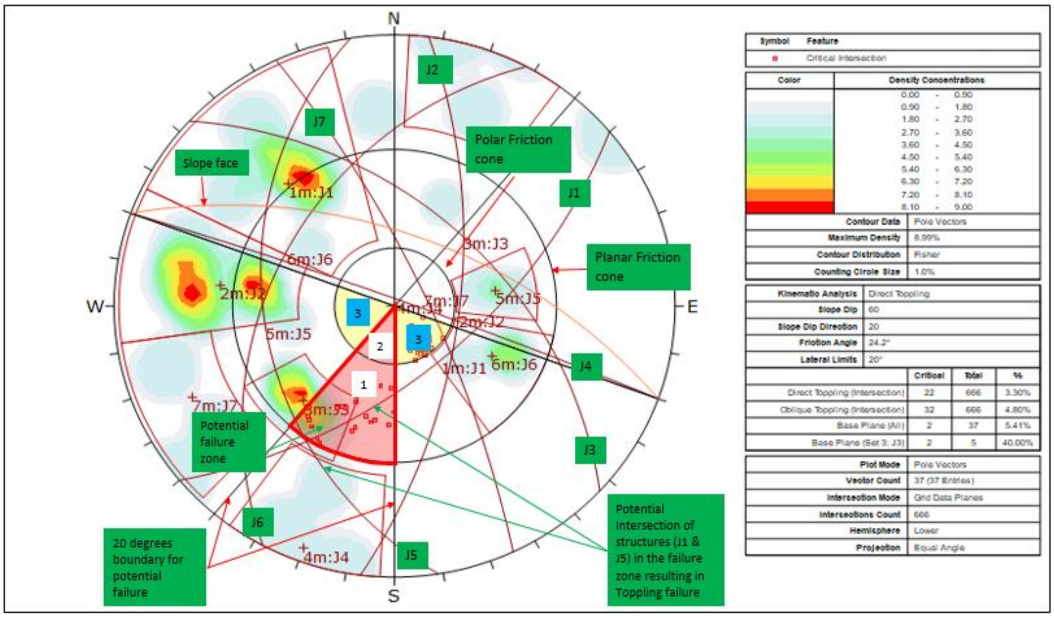

Figure 5-9: Dips software result of a kinematic analysis for flexural toppling failure in Domain 3

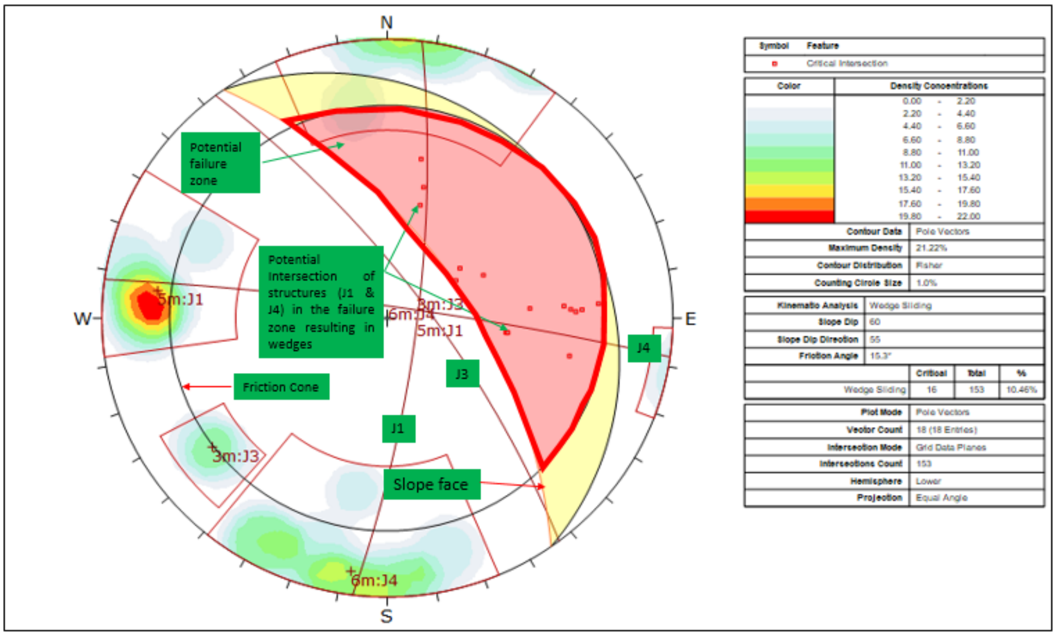

Figure 5-10: Dips software result of a kinematic analysis for wedge failure in Domain 3

5.4 Groundwater Analysis

Groundwater levels were monitored using piezometers installed in the pit at 1213 m (120 mB) and 1243 m (90 mB) on the Hangingwall, and on the surface at 1333 m (0 mB) on the south wall, as shown in Figure 4-2. The boreholes labelled PZ5, 3PZ2 and SS7 were drilled on the southern side of the pit at depths below the surface of 120 mB, 90 mB and 0 mB, respectively. 3PZ4 was installed on the northern side of the pit at 120 mB. The water levels were plotted on the graph to determine the trend of the water surface during the rain period when water recharge is expected to be at its highest. The piezometer readings revealed that the groundwater levels were steadily rising, as shown in Figure 5-10. The groundwater level increased by an average of 0.2 m over six months, resulting in the pore water pressure coefficient (Equation2-3) ranging from 0.21 to 0.29 (Appendix Table I). The rising water levels may negatively impact the slope by reducing the shear strength of the discontinuities within the rock mass. The rising water levels were partially attributed to frequent power cuts at the mine, which often disrupted the pumping operations.

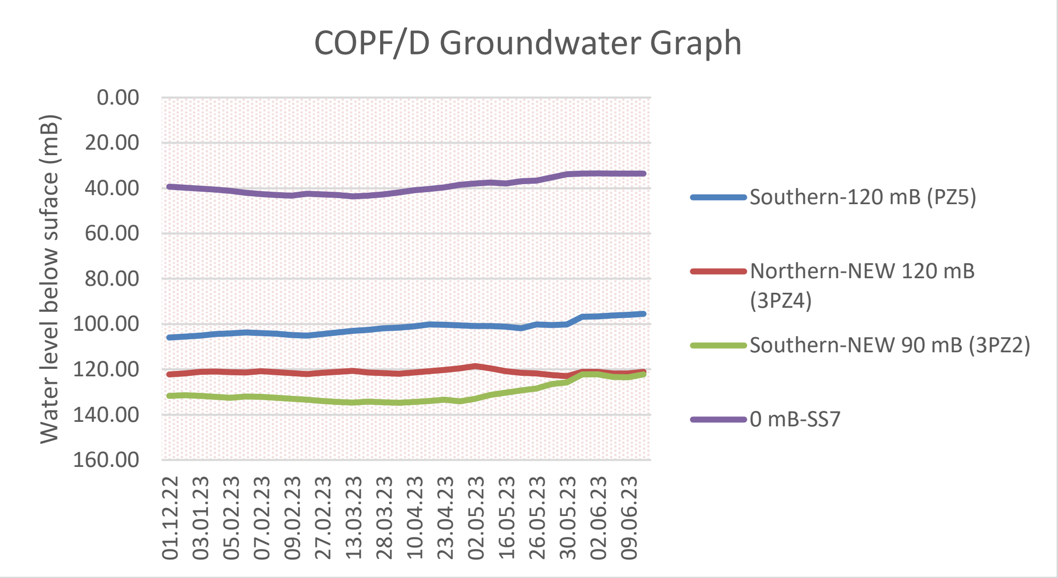

Figure 5-11: Groundwater level monitoring from piezometers on the hangingwall and south wall at the COPF/D pit.

5.5 Numerical Stability Analysis

The stability analysis was carried out using the 2D deterministic approach and the 2D numerical modelling approach. Slide2 Rocscience software was used for the deterministic analysis approach, and RS2 was used for the numerical analysis approach. The stability analysis was based on the Mohr-Coulomb failure criterion. The numerical analysis was focused on assessing the circular type failures in each domain, while other types of failure were assessed using empirical and structural analysis methods. The input data for all the numerical analyses included the strength parameters (Cohesion and Φ) in Appendix C and Table 4-6, and the unit weight of rock formations shown in Appendix F. Other input data included the Pore water pressure data in Appendix I. The stability analyses for all the domains were carried out, and the results are shown below.

5.5.1 Domain 1

Table 5-3 shows a summary of the results of the deterministic analysis from Slide 2 for Domain 1. The domain was stable with both the FoS and PoF compliant to the set acceptance threshold.

Table 5-3: Results of a deterministic stability analysis from the Slide2 software for COPF/D Domain 1 on the eastern wall slope.

Section	Bench Stack	FoS	PoF (%)	Acceptability		Remarks
				FoS	PoF(%)	
B-B	upper	2.32	0	Acceptable	Acceptable	The slope is stable
	Lower	1.34	0.1	Acceptable	Acceptable	The slope is stable
	Overall	1.34	0.1	Acceptable	Acceptable	The slope is stable

Figure 5-12 shows the result of RS2 numerical software. The FoS from the RS2 numerical analysis was 1.25, which was compliant with the set acceptance threshold of 1.2. The results of the FoS from RS2 were consistent with the results of the Slide2 software, which showed that the slope would be stable.

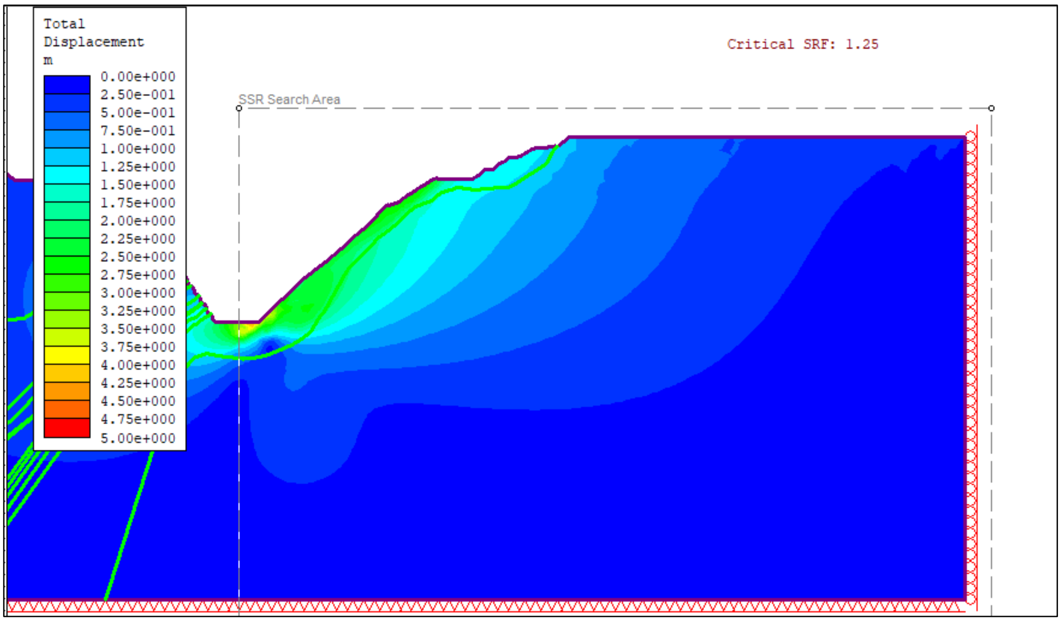

Figure 5-12: Stability analysis results for Domain 1.

5.5.2 Domain 2

Table 5-4 shows the summary of the results of the deterministic analysis from Slide2 for Domain 2. The domain was stable, with both the FoS and PoF compliant with the set acceptance threshold.

Table 5-4: Results of a deterministic stability analysis from the Slide2 software for COPF/D Domain 2 on the southern wall slope.

Section	Bench Stack	FoS	PoF (%)	Acceptability		Remarks
				FoS	PoF(%)	
C-C	upper	1.5	0	Acceptable	Acceptable	The slope is stable
	Lower	1.15	13.2	Acceptable	Acceptable	The slope is stable
	Overall	1.33	1.4	Acceptable	Acceptable	The slope is stable

Figure 5-13 shows the result of the RS2 numerical software. The FoS from the RS2 numerical analysis was 1.23, which was marginally compliant with the set acceptance threshold of 1.15. The FoS from RS2 was consistent with the results of the Slide2 software, indicating the slope was stable.

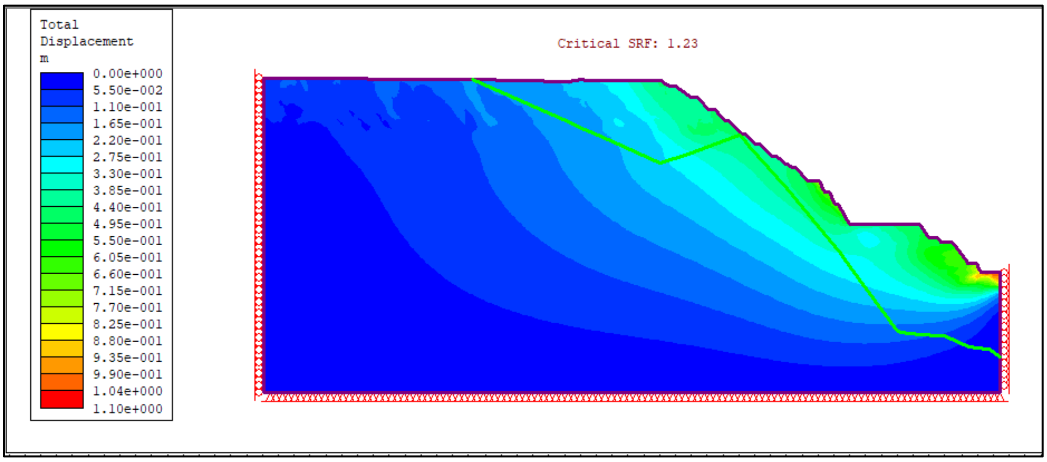

Figure 5-13: Section C-C stability analysis results for Domain 2

5.5.3 Domain 3

Two representative sections A-A and B-B, obtained at positions shown in Figure 4-2, were used for stability analyses. Table 5-5 shows the section A-A summary of the results of the deterministic analysis from the Slide2 Rocscience software for Domain 3. The domain was generally unstable. Figure 5-14 shows an example of the analysis using slide software. The deterministic result was a FoS of 0.94 with a PoF of 39%. The FoS was below 1, showing that the slope was unstable, while the PoF was above the COPF/D mine acceptable threshold of 25%.

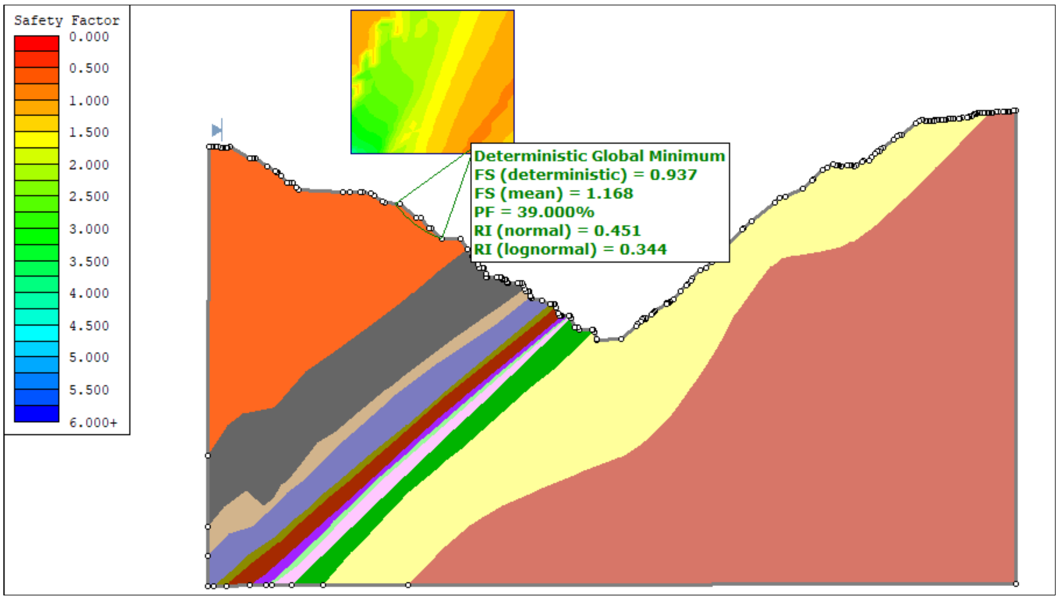

Figure 5-14: Section A-A Stability analysis result from Slide2 software for COPF/D Domain 3 on the western wall slope

Table 5-5: Section A-A results of a deterministic stability analysis from Slide2 software for COPF/D Domain 3 on the western wall slope.

Section	Bench Stack	FoS	PoF (%)	Acceptability		Remarks
				FoS	PoF(%)	
A-A	upper	0.94	39	Not Acceptable	Not Acceptable	The 44 m stack in URD at 70 m from the surface is unstable. The instability is due to high pore water pressure
	Lower	0.69	100	Not Acceptable	Not Acceptable	One 15m bench in CDOL 170 m from the surface affected. The failure may affect the access ramp above
	Overall	0.96	32	Not Acceptable	Not Acceptable	Unstable slope

Table 5-6 shows the section B-B summary of results of the deterministic analysis from the Slide2 Rocscience software for Domain 3. The domain was unstable in the lower stack of the slope.

Table 5-6: Section B-B Results of a deterministic stability analysis from Slide2 software for COPF/D Domain 3 on the western wall slope.

Section	Bench Stack	FoS	PoF (%)	Acceptability		Remarks
				FoS	PoF(%)	
B-B	upper	1.22	4.7	Acceptable	Acceptable	The slope is stable
	Lower	0.14	100	Not Acceptable	Not Acceptable	One 15m bench in CDOL 160 m from the surface is affected. The failure may affect the access ramp above
	Overall	1.22	9	Acceptable	Acceptable	The slope is stable

Figure 5-15 shows section A-A displacement results from the RS2 numerical software. Prevailing pore water pressure at at COPF/D was determined and used in the analysis. The results showed that the position of the failure slip surface and the FoS were consistent with the results of Slide2 software. The FoS from the RS2 numerical analysis was 1.00 which was below the acceptance threshold of 1.15 with a potential total displacement range of 0.7 m – 1.2 m. The area of concern was a 19 m high slope in CDOL 170 m from the surface. A failure in this area may affect the access ramp directly above.

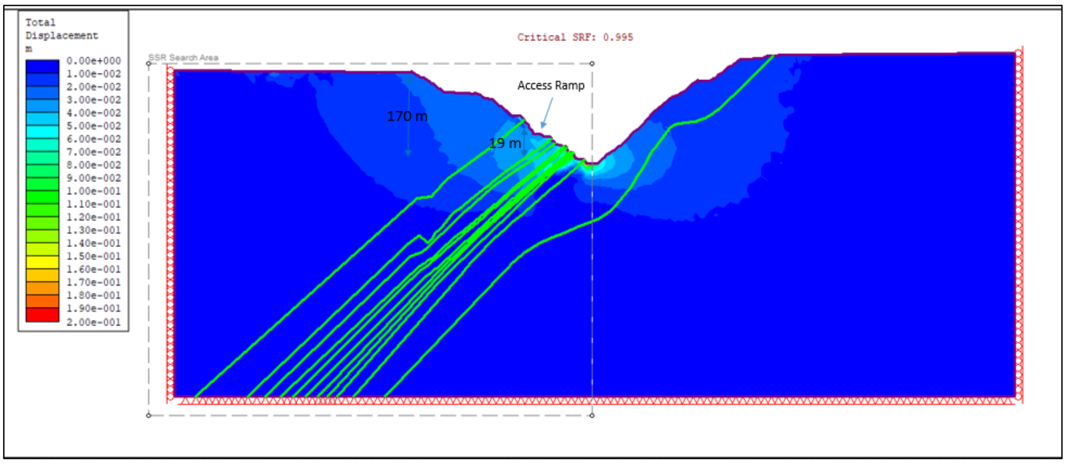

Figure 5-15: Section A-A stability analysis results for Domain 3.

Figure 5-16 shows the result of the RS2 numerical analysis along section B-B. The results showed that the position of the failure slip surface and the FoS were consistent with the results of the Slide2 software, which were both in the lower stack. The FoS from the RS2 numerical analysis was 0.35, which was below the acceptance threshold of 1.15, having a potential total displacement range of 1.5 m – 2.4 m. The area of concern was a 39 m high slope in CDOL at 197 m from the surface.

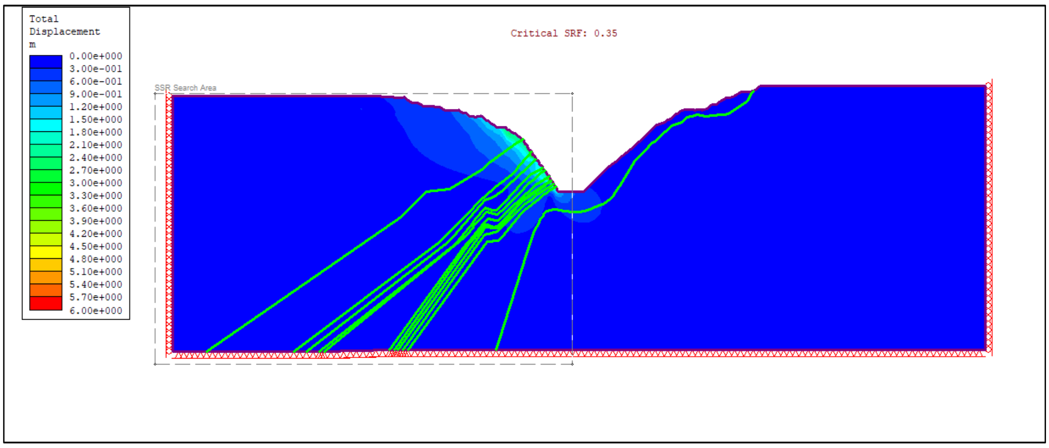

Figure 5-16: Section B-B stability analysis results for Domain 3.

For Domain 3, the areas of concern were in the lower stack and the upper stack (URD formation). The instability was caused by increased pore water pressure in the upper stack and a steep stack angle in the lower stack. The lower stack was located by coordinates as shown in Figure 5-4. The instability was a circular failure potentially covering an area of 20,685 m^2. The upper stack was located by coordinates as shown in Figure 5-4. The instability was caused by circular failure, potentially covering an area of 1,556,769 m^2. To mitigate this unstable domain, sensitivity analyses were done on groundwater and slope angle. Table 5-7 shows the results which should be implemented to attain a stable slope. The groundwater analysis showed that the level should be drawn down to an equivalent average pore pressure coefficient (Ru) of 0.19. At this point, the URD and CDOL rock formations showed that they were stable.

Table 5-7: Results of the simulated Domain 3 slope stability analysis

Section	Bench Stack	FoS	PoF (%)	Acceptability		Remarks
				FoS	PoF(%)	
A-A	upper	1.16	5.4	Acceptable	Acceptable	Maintain the stack angle but reduce the Ru from 0.23 to 0.19
	Lower	1.15	0.0	Acceptable	Acceptable	Mine the slope to stack angle of 36°
	Overall	1.2	9.6	Acceptable	Acceptable	The slope was stable at an overall slope angle of 28° - 31°
B-B	upper	1.15	8.8	Acceptable	Acceptable	The slope was stable at a stack angle of 38°
	Lower	1.15	0.0	Acceptable	Acceptable	The slope was stable at a stack angle of 42°
	Overall	1.2	11.4	Acceptable	Acceptable	The overall slope was stable at a stack angle of 31°

5.5.4 Summary of unstable zones and comparison of results

The areas with potential instability identified through structural and stability analyses were outlined in the COPF/D plan shown in Figure 5-4. The analysis shows that the results are consistent with the actual Falls of Ground (FOG) that have been observed in the COPF/D pit, particularly on the southern slope wall (Figure 1-4). The failures that have been occurring in the current design have been predicted accurately in the analysis. Table 5-8 shows the comparison of results from different analysis methods. The analyses show that the 2D deterministic method and the numerical modelling method were generally consistent with each other, but conservative compared to the empirical method. This is because the 2D analysis methods do not include the end effects and various directional strengths in the computation (McQuillan, et al., 2021). However, for COPF/D, the error relating to conservatism is minimal due to the pit's favourable dimensions (2.1 km wide and 330 m deep), translating into a W/H of 6.4. The average error between the empirical and numerical modelling results of the COPF/D pit is 16%. According to Cala & Flisiak (2001), Arellano & Stark (2000) and Eid, et al (2006), the error in results is about 20% for a W/H ratio of five but increases rapidly from the ratio of four and below. Ultimately, with the unavoidable 20% error, there will still be some conservatism in the results, as exhibited in the comparison between the numerical and empirical analysis results of COPF/D.

Table 5-8: comparison of results from Empirical Analysis,Slide2 and RS2 software

Domain	Bench Stack Height	Design Stack angle (°)	Empirical analysis		Slide2 Analysis	RS2 Analysis	Remarks
			Stack angle(°)	FoS	FoS	FoS	
1	Upper(69 m)	23	51	1.2	1.34	1.25	The numerical and empirical methods show similar results, indicating the slopes are generally stable
	Lower (233 m)	42	43	1.2	2.32		
2	Upper(126 m)	34	47.5	1.2	1.52	1.23	The numerical and empirical methods show positive results, indicating the slopes are generally stable
	Lower (115 m)	30	53	1.2	1.15		
3	Upper(126 m)	23	42	1.2	0.94	0.9	The numerical methods show negative results, but are conservative compared to the empirical method
	Lower (128 m)	36	52.5	1.2	0.69		

5.6 Slope Monitoring

To effectively detect and manage potential failure risks, each domain should be monitored with an appropriate slope monitoring system, depending on the FOG risks identified from the stability analysis. To this effect, an appropriate monitoring system for each domain was selected using the guide “Managing Slope Hazards, Making the Right Choice" proposed by Collin (2022) in Figure 2-15. Table 5-9 shows the results of the selected appropriate monitoring system for each domain.

Table 5-9: SSM equipment selection results using a guide in Figure 2-15

Domain	Failure Mechanism	Monitoring Requirements	Suitable Monitoring Strategy
1	Wedge and planar failure	Real-time scanning, high resolution, Tactical positioning, Focus monitoring	Slope stability radar, Survey monitoring
2	Wedge failure	Real-time scanning, high resolution, Tactical positioning, Focus monitoring	Slope stability radar
3	Circular failure/creep	Wide area coverage, Capability to resolve very slow movement	Slope stability radar, Survey monitoring for long-term monitoring

5.7 Comparison between FOGs and current pit slope design

The most frequent FOGs were Structural failures, mainly occurring on the south slope of the COP F/D pit on the current design. Other failures were planar failure and creep on the eastern and western walls, respectively. The register of previous failures is shown in Table 4-12 in Chapter 4 above. The back analyses outlined the following:

1. The mapping of the structures/discontinuities was not done effectively and consequently resulted in vital structures not being captured and included in the kinematic analysis, which resulted in wedge failures. The recommendation was that the slope on the southern slope face be mined to 60° and re-oriented to a dip direction of 020° to prevent wedge failures.
2. The groundwater level increased steadily over time, showing that the dewatering boreholes were ineffective and resulted in an increase in the pore water pressure in the slope. This resulted in creep/circular failures. The recommendation was that the water table on the western slope should be lowered further by drilling more dewatering boreholes. This was to reduce the pore water pressure in the slope and prevent creep/circular

failures. The back analysis, however, did not specify any thresholds of pore water pressure.

5.8 Comparison between current and recommended pit slope design

Table 5-11 shows the comparison between the current and recommended pit slope design for COPF/D pit.

Table 5-10: Current versus recommended pit slope design

Domain	Parameter/ Support	Current Design	Recommended Design
1	Overall Slope angle (°)	44	44
	Support	Not supported	Cable anchor Support recommended
2	Bench face angle (°)	60	50
3	Lower Stack angle (°)	51	42
	Pore water Pressure (Ru)	0.23	0.19

5.9 Mitigation Strategies to Cater for a Low FOS

The Analysis results showed that the low FoS were in the Topple & Creep domain. To mitigate the low FoS, the strategies included reducing the groundwater pore pressure coefficient from 0.23 to 0.19 and slackening the lower stack angle of the slope from 51° to 42°.

5.10 Chapter Summary

This chapter discussed the results of the empirical, kinematic and numerical analyses of the slopes at COPF/D. The mine site acceptability criteria for FoS (1.15-1.2) and PoF (20% -25%) were used for all stability assessments. The analysis involved dividing the pit into three geotechnical domains (1, 2 and 3) for the analysis to be effective.

The empirical analysis used the adjusted MRMR and the Terbrugge chart to analyse the preliminary appropriate stack angles for the slopes. This analysis showed that the design geometry was stable (FoS of 1.2) and conservative.

The kinematic analysis was done using Dips software for all the domains. Domain 1 had a 33.3% and 25.8% chance of occurrence of wedge and planar failures, respectively. The mitigation was to support the affected slope by installing fibre-reinforced shotcrete of 9-12 cm with 20 m long cable anchors. Domain 2 had a 34.9% chance of occurrence of wedge failures. The mitigation was to reduce the bench face angle of the slope from 60° to 50° over an area of 4,892 m^2. Domain 3 had a 10.5% and 3.3% chance of occurrence of wedge and direct toppling failures, respectively.

The groundwater analysis was done and showed that the groundwater level generally increased by 0.2 m over the year. The pore pressure coefficient (Ru) was calculated from the piezometer readings and used in the stability analyses. The Ru ranged from 0.21 to 0.29.

The numerical stability analyses were done using Slide2 and RS2 Rocscience software. The results from both software showed that Domain 1 and Domain 2 were stable, while Domain 3 was generally unstable. The instability was caused by increasing pore water pressure in the URD formation and unfavourable geometry in the lower stack.

The simulation results showed that in Domain 2, the design slope angle should be reduced from 60° to 50° to prevent structural failures. Domain 3 was stabilised by reducing the pore water pressure and reducing the stack angle of the lower stack from 51° to 42°. The simulation also showed that there is potential for the slope in Domain 1 to be optimised from 29° to 31°. This analysis generally showed that if the recommendations provided were applied, the wedge and circular failures currently occurring at the COPF/D pit would not have occurred.

6 CONCLUSIONS AND RECOMMENDATIONS

6.1 Introduction

The main objective of this research was to devise a slope stability management strategy that will enable the mining of the orebody safely and economically by identifying specific locations and sizes of unstable areas. The sub-objectives were to determine new input rock mass strength parameters, determine new input parameters for the discontinuities of the COPF/D pit, investigate and describe the failure modes likely to occur and optimise the slope geometry.

6.2 Summary of Chapters

This report has presented six chapters, which cover the following:

- Chapter 1 discussed the research background and context, the problem statement, the research justification, the objectives and the sources of data for the research. The chapter also discussed the research validation and the structure of the research report.
- Chapter 2 was a review of the literature relevant to this research. The main discussions covered slope stability management, which included areas of data collection, classification of rock masses, empirical and numerical analyses of slopes, water control, slope monitoring and the acceptance criteria for various risk levels.
- Chapter 3 discussed the research design, the data collection process, the data validation process and the data analysis approach.
- Chapter 4 provided the input data collected for this research.
- Chapter 5 presented the analysis and results of the research.
- Chapter 6 provided the conclusions of the project. The chapter also highlighted the research contributions, limitations and recommendations for future research work.

6.3 Research Observations

6.3.1 Initial and complementary studies

Initial and complementary studies included desk studies to assess the data required for the research and data already available from the mine database. The database had borehole data and strength parameter data from previous logging and testing, respectively.

6.3.2 Key findings and observations

COPF/D pit was divided into three distinctive domains (Domain 1, Domain 2 and Domain 3) based on the observed failure mechanisms and rock mass strength. The main problem at COPF/D was the lack of an effective slope management plan to address the safety and economic uncertainties. This matter was resolved through the development of set objectives.

Main objective

Structural and numerical analyses were conducted, and the results were used to identify specific locations and potential sizes of areas with a high risk of failure. In Domain 1, the potentially high-risk area had a high possibility of structural failure and was located by coordinates covering an area of 71,650 m^2 (Figure 5-4). In Domain 2, the potentially high-risk area had a high possibility of structural failure and was located by coordinates covering an area of 4,892 m^2 (Figure 5-4). The areas of concern in Domain 3 were in the lower and upper stacks (URD formation). The instability was a circular failure caused by increased pore water pressure in the upper stack and a steep stack angle in the lower stack. The lower stack covers an area of 20,685 m^2 (Figure 5-4). The upper stack covers an area of 1,556,769 m^2 (Figure 5-4). The instability was caused by circular failure.

Sub-objective one

The rock mass input parameters were determined from the laboratory tests and down-rated to represent the rock mass using the GSI method. The input parameters derived were used in the slope stability numerical analyses in RS2 and slide software (Rocscience, 2024). The derived rockmass strength parameters are shown in Table 4-6.

Sub-objective two

The new input parameters for the discontinuities were determined and are shown in Table 4-11. The new strength parameters were used in the kinematic analysis to determine structural failure mechanisms at COPF/D slopes.

Sub-objective three

Kinematic and numerical analysis was conducted using Dips software, RS2 and Slide software, respectively. From the structural analysis, the results showed that Domain 1 had a 33.3% and 25.8% chance of wedge and planar failures, respectively. Both results were above the acceptable PoF threshold of 25%. To effectively manage the potential failure risk, the SSR and survey monitoring systems should be used to monitor the slope. Domain 2 had a 34.9% chance of occurrence of wedge failures, which was above the acceptable PoF threshold of 25%. To mitigate this potential instability, the slope angles should be reduced from 60° to 50°, and an SSR should be used to monitor the slope for effective failure risk management. Domain 3 had a 10.5% and 3.3% chance of occurrence of the wedge and direct toppling failures, respectively. Both results were within the acceptable PoF threshold of 25%.

From the numerical analysis, Domain 3 showed that the slope would fail by a circular failure mechanism in the upper and lower stacks of the slope. The instability was caused by increasing pore water pressure in the upper stack and a steep stack angle (51°) in the lower stack. To mitigate this potential instability, the pore water pressure in the upper stack slope should be reduced from Ru of 0.23 to 0.19, and the lower stack slope angle should be reduced from 51° to 42°. Survey monitoring and SSR monitoring should be installed as part of the slope stability management programme to proactively manage potential instability.

The overall structural and stability analysis showed that Domain 1 and Domain 2 were susceptible to wedge and planar failures, while Domain 3 was susceptible to circular failures.

Sub-objective four

The rock mass assessment for slope optimisation involved determining the GSI and using it to derive strength parameters for input into stability analyses. Based on these parameters, the overall slope angle for Domain 3 was optimised from 29° to 31°. The optimisation in Domain 2 resulted in reducing the slope angle from 60° to 50° to prevent wedge failures.

The other key findings and observations made from the analyses conducted were:

- The strength parameters used in the previous kinematic analyses were not for discontinuity faces/surfaces but for the intact rock. Therefore, this may have resulted in wrong results and recommendations.
- The numerical methods showed similar results but were conservative compared to the empirical method.
- It is more economical to install support on Domain 1 than to mine the slope to the recommended slope angle of 41°.

6.3.3 Recommendations

- To effectively manage the pore water pressure and operate within the recommended threshold of RU of 1.9, a standby/alternative power system like a diesel genset should be introduced. This is to ensure that pumping is sustained throughout the current erratic power supply at COPF/D.
- In Domain 2, where the slope angle is critical, it should be ensured that good blast practices are employed to avoid back breaks and excessive ground vibrations. The back breaks may compromise the recommended slope angle of 50°, while excessive ground vibrations may open up the joints and hasten structural failures.
- In Domain 1, where the slope poses a significant risk, it should be supported with cable anchors. The support should be supplemented with fibre-reinforced shotcrete to further confine loosening rock slabs between installed support elements.

6.4 Research Contributions

The main outcome of this research was to provide a slope management solution for the stability of COPF/D for at least three years. An effective slope management plan identifies areas of the pit with potential risk of instability and then provides mitigation measures. This research identified areas at COPF/D with potential risk of wedge failure on the southern slope, planar and wedge failures on the footwall slope and circular failures on the hangingwall slope. The research also highlighted the increasing pore water pressure at COPF/D south wall and hangingwall slopes, which was potentially causing instability. In light of the identified instabilities, this research proposed mitigation measures which included: pumping out water to reduce the pore water pressure on the south wall and hangingwall slopes; optimised the slope geometry of the south wall and hangingwall slopes and recommending the right/appropriate slope monitoring equipment for an effective slope monitoring regime that will effectively pick developing slope instability for effective risk management.

6.5 Research Limitations

During data collection relating to rock mass assessments for rock mass classification, access to some benches was a challenge. This was due to the lack of availability of technologies on site, such as a drone. This situation made it difficult to carry out close-range assessments for accurate results. However, long-range binoculars were used to observe the faces during assessments, thereby improving the quality of the data and consequently the findings of the research.

6.6 Recommendations for Future Research Work

One of the areas highlighted in this research where a different approach would be beneficial is in data collection, particularly in field assessments for rock mass classification. New technologies, such as drones and data acquisition scanners, that would improve quality assessments, should be employed if near-accurate analysis results are to be obtained. However, even with these tools, the results of the assessment may be misleading where the rock mass surface is weathered only to a shallow depth and Unweathered beyond that depth. Therefore, assessments using drilled cores are recommended.

REFERENCE LIST

Arellano, D. & Stark, T., 2000. *Importance of Three-Dimentional Slope Stability Analyses in Practice.* 101 ed. Colorado: Geotech Special Publication.

Bar, N. & Barton, N., 2017. The Q-Slope method for Rock Slope Engineering. *Rock Mechanics and Rock Engineering,* Volume 50, pp. 3307-3322.

Barton, N., 2002. Some new Q-value correlations to assist in site characterisation and tunnel design. *International Journal of Rock Mechanics & Mining Science,* Volume 39, pp. 185-216.

Barton, N., Lien, R. & Lunde, J., 1974. Engineering Classification of Rock Masses for the Design of Tunnel Support. *Rock Mechanics Felsmechanik Mecanique des Roches,* Volume 6, pp. 186-236.

Brady, B. H. G. & Brown, E. T., 2004. *Rock Mechanics for Underground.* 2nd ed. Dordrecht: Springer Science + Business Media, Inc..

British Standards Institution, 2017. *Geotechnical investigation and testing - Identification, description and classification of rock.* BS EN ISO 14689 ed. Geneva: BSI.

Cala, M. & Flisiak, J., 2001. *Slope stability analysis with FLAC and limit equilibrium methods.* Lyon, FLAC and Numerical Modelling in geomechanics, pp. 111-114.

Cawood, F. T. & Stacey, T. R., 2006. Survey and Geotechnical Slope Monitoring Considerations. *South African Institute of Mining and Metallurgy,* Volume 106, pp. 495-502.

Cheng, Y. M., 2022. Critical Review of Two-dimensional Slope Stability Analysis by Discontinuity Layout Optimization, Limit Equilibrium and. *Global Journal of Researches in Engineering,* 22(4), pp. 1-17.

Colin, T., 2022. *Slope Stability Monitoring Course.* Johannesburg: s.n.

Dana, Z. H., Kakaie, K. R., Rafiee, R. & Bafghi, Y. R., 2018. Effects of geometrical and geomechanical properties on slope stability of open-pit mines using 2D and 3D finite difference methods. *Journal of Mining and Environment,* 9(4), pp. 941-958.

Eid, T. H., Elleboudy, G. A., Elmarsafawi, G. H. & Salama, G. A., 2006. Stability analysis and charts for slopes susceptible to translational failure. *Canadian Geotechnical Journal,* 43(12), pp. 1374-1388.

Geotechnical Database, 2008. *\\10.1.2.3\RockMech,* Chingola: Geotechnical Department.

Haines, A. & Terbrugge, P. J., 1991. *Preliminary estimation of rock slope stability using rock mass classification systems.* Aachen, Proc 7th International Congress on Rock Mechanics, pp. 887-892.

Haines, A., Voulgaris, P., Walker, D. & Bruyn, I. D., 2006. *GEOTECHNICAL DESIGN CONSIDERATIONS FOR THE PROPOSED OYU TOLGOI OPEN PITS, SOUTHERN MONGOLIA.* Johannesburg, Proceedings of the International Symposium on Stability of Rock Slopes in Open Pit Mining and Civil Engineering. The Southern African Institute of Mining and Metallurgy.

Kliche, C. A., 2018. *Rock Slope Stability.* 2nd ed. Colorado: Society for Mining, Metallurgy, and Exploration (SME).

Laerd Statistics, 2018. *Measures of Central Tendency: Laerd Statistics.* [Online] Available at: https://statistics.laerd.com/statistical-guides/measures-central-tendency-mean-mode-median.php
[Accessed 25 April 2023].

Lam, L. & Fredlund, G. D., 1993. A general limit equilibrium model for three-dimensional slope stability analysis. *Canadian Geotechnical Journal,* 30(6), pp. 905-919.

Laubscher, D. H., 1990. A geomechanics classification system for the rating of rock mass in mine design. *Journal of the South African Institute of Mining and Metallurgy,* 90(10), pp. 257-272.

Little, M., 2006. *Slope Monitoring Strategy at PPRust Open Pit Operation.* Cape Town, International Symposium on Stability of Rock Slopes in Open Pit Mining and Civil Engineering.

Macciotta, R., Creighton, A. & Martin, D., 2020. Design acceptance criteria for operating open-pit slopes: An update. *CIM Journal,* 11(4), pp. 248-265.

Marinos, V., Marinos, P. & Hoek, E., 2005. The Geological Index: Applications and Limitations. *Bulleting of the Engineering Geology and the Environment,* 64(1), pp. 55-65.

McQuillan, A., Bar, N. & Yacoub, T., 2021. *On the Comparison of 2D and 3D stability analyses of an anisotropic slope.* RIC2021 ed. Toronto: Rocscience International.

Nchanga Open Pit Geotechnical, 2012. *COP F/D South Wall Stability Analysis,* Chingola: Geotechnical section.

Onestopmap, 2023. *Onestopmap.com.* [Online]
Available at: http://www.onestopmap.com/zambia/zambia-60
[Accessed 15 May 2023].

Rafiei, R. H. & Cai, M., 2022. Forty-Year Review of the Hoek-Brown Failure Criterion for Jointed Rock Masses. *Rock Mechanics and Rock Engineering,* Volume 55, pp. 1-23.

Rocscience, 2022. *Geotechnical Software for Open Pit Mining: Rocscience.* [Online]
Available at: https://www.rocscience.com/learning/geotechnical-software-for-open-pit-mining
[Accessed 25 April 2023].

Rocscience, 2023. *Rocscience.* [Online]
Available at: https://www.rocscience.com/help/rs2/overview
[Accessed 16 October 2023].

Rocscience, 2024. *Geotechnical Software for Open Pit Mining: Rocscience.* [Online]
Available at: https://www.rocscience.com/help/dips/stereonet-plots/terzaghi-weighting
[Accessed 24 June 2024].

Stacey, T. R., 2023. *Rock Mass Classification in Rock Engineering.* Johannesburg: University of the Witwatersrand School of Mining Engineering.

Tang, h.,Huang, L., Bobet, A., Ez, E. M., Wang, L., Wu, Y. & Hu, X. 2017. Identification and Mitigation of Error in the Terzaghi Bias Correction for Inhomogeneous Material Discontinuities. *Strength of Materials,* Volume 48, pp. 825 - 833.

Watson, B. P., 2004. A rock mass rating system for evaluating stope stability on the Bushveld Platinum mines. *The Journal of The South African Institute of Mining and Metallurgy,* pp. 229-238.

Wesseloo , J. & Read, J., 2009. Acceptance Criteria. In: P. Stacey & J. Read, eds. *Guidelines for Open Pit Slope Design.* Collingwood: CSIRO Publishing, pp. 83-139.

Wyllie, D. C. & Mah, C. W., 2004. *Rock Slope Enginnering.* 4th ed. London: CRC Press.

APPENDIX A. RMR, GSI, MRMR AND ADJUSTED MRMR CLASSIFICATION TABLES, GRAPHS AND MRMR CALCULATIONS

Parameter	Range of Values										
RQD	100-97		96-84	83-71	70-56	55-44	43-31	30-17	16-4	3-0	
Rating (= *RQD* x 15/100)	15		14	12	10	8	6	4	2	0	
UCS (MPa)	185	184-165	164-145	144-125	124-105	104-85	84-65	64-45	44-25	24-5	4-0
Rating	20	18	16	14	12	10	8	6	4	2	0
Joint Spacing	Refer to Figure on "Joint spacing rating"										
Rating	25										
Joint condition including groundwater	Refer to Figure on "Adjustments for Joint Condition and Groundwater"										
Rating	40										

Figure A- 1: MRMR classification table showing rating (Laubscher, 1990)

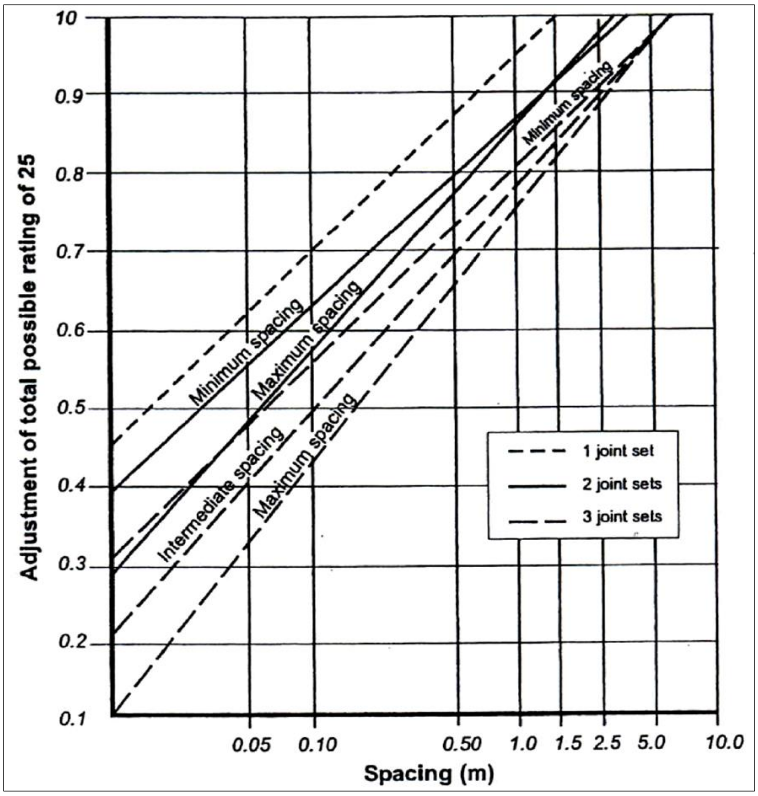

Figure A- 2 : MRMR joint spacing rating (Stacey, 2023)

Table A- 1: MRMR Groundwater and Joint Condition adjustments (Laubscher, 1990)

Parameter	Description		Dry Condition	Wet Conditions		
				Moist	Moderate pressure 25-125 1/mm	Severe Pressure >125 1/min
A Joint Expression (large scale irregularities)	Wavy	Multi-Directional	100	100	100	95
		Uni-Directional	95 90	95 90	90 85	80 75
	Curved		89 80	85 75	80 70	70 60
	Straight		79 70	74 65	60	40
B Joint Expression (small scale irregularities or roughness	Very rough		100	100	95	90
	Striated or rough		99 85	99 85	80	70
	Smooth		84 60	80 55	60	50
	Polished		59 50	50 40	30	20
C Joint Wall Alteration Zone	Stronger than wall rock		100	100	100	100
	No alteration		100	100	100	100
	Weaker than wall rock		75	70	65	60
D Joint Filling	No fill – surface staining only		100	100	100	100
	Non softening and sheared material (clay or talc free	Coarse Sheared	95	90	70	50
		Medium Sheared	90	85	65	45
		Fine Sheared	85	80	60	40
	Soft sheared material (eg talc)	Coarse Sheared	70	65	40	20
		Medium Sheared	65	60	35	15
		Fine Sheared	60	55	30	10
	Gouge thickness < amplitude of irregularity		40	30	10	
	Gouge thickness < amplitude of irregularity		20	10	Flowing material 5	

Table A- 2: Adjustment for Weathering (Laubscher, 1990)

Rate of weathering and adjustments (%)					
Description of weathering extent	**6 months**	**1 year**	**2 years**	**3 years**	**4 + years**
Fresh	100	100	100	100	100
Slightly	88	90	92	94	96
Moderately	82	84	86	88	90
Highly	70	72	74	76	78
Completely	54	56	58	60	62
Residual soil	30	32	34	36	38

Table A- 3: MRMR joint orientation adjustment (Laubscher, 1990)

Number of joints defining the block	Adjustment (%) Number of faces inclined away from the vertical				
	70	75	80	85	90
3	3	-	2	-	-
4	4	3	-	2	-
5	5	4	3	2	1
6	6	5	4	3	2 or 1

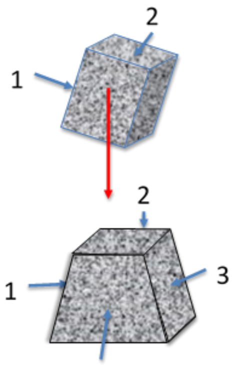

Table A- 4: MRMR adjustment for effects of blasting (Laubscher, 1990)

EXCAVATION TECHNIQUE	Adjustment (%)
Boring	100
Smooth wall blasting	97
Good conventional blasting	94
Poor blasting	80

Table A- 5: Adjustments for mining-induced stresses (Laubscher, 1990)

Stress Adjustments based on judgement
Good confinement enhances stability – maximum positive adjustment is 120%
Poor confinement, associated with numerous closely spaced joint sets does not promote stability – maximum negative adjustment is 60%

Table *A- 6: MRMR rock mass classification data from logged bore holes at COPF/D*

Collar Coordinates	Hole ID	From	To	Rock Type	UCS	RQD	Joint Spacing	Joint Condition and Ground water	Laubscher
X =6486.679	DGT04	0	3.88	ARK	0.2	1.1	11.3	2.5	15
Y = 16067.032	DGT04	3.88	5.83	ARK	0.2	3.6	10.5	0.7	15
Z =1304.025	DGT04	5.83	8.83	ARK	0.2	0.0	13.8	1.0	15
	DGT04	8.83	11.83	ARK	0.2	0.0	14.6	0.2	15
	DGT04	11.83	14.83	ARK	1.2	2.7	7.2	12.9	24
	DGT04	14.83	17.83	ARK	1.9	8.5	12.1	13.5	36
	DGT04	17.83	20.83	ARK	1.9	6.9	14.9	16.4	40
	DGT04	20.83	23.83	ARK	1.9	7.4	11.5	9.3	30
	DGT04	23.83	26.83	ARK	3.3	7.7	8.5	12.5	32
	DGT04	26.83	29.83	ARK	3.3	11.7	7.6	3.4	26
	DGT04	29.83	32.83	ARK	4.1	7.1	12.0	22.8	46
	DGT04	32.83	35.83	ARK	4.1	6.9	10.9	27.1	49
	DGT04	35.83	38.83	ARK	3.3	8.5	10.0	20.2	42
	DGT04	38.83	41.83	ARK	3.3	16.3	12.3	16.0	48
	DGT04	41.83	42	ARK	4.1	26.7	11.1	7.1	49
	DGT04	42	44.55	ARK	7.0	8.2	8.7	8.0	32
	DGT04	44.55	47.55	ARK	8.1	13.5	10.4	8.0	40
	DGT04	47.55	50.55	ARK	8.1	10.6	16.9	32.4	68
	DGT04	50.55	53.55	ARK	8.1	15.3	13.3	21.4	58
	DGT04	53.55	56.55	ARK	8.1	18.3	14.2	19.5	60
	DGT04	56.55	59.55	ARK	3.8	12.5	10.4	19.3	46
	DGT04	59.55	62.55	ARK	3.8	9.1	11.3	21.9	46
	DGT04	62.55	65.55	ARK	3.8	6.4	11.6	24.2	46
	DGT04	65.55	68.55	ARK	3.8	9.4	11.4	21.4	46
	DGT04	68.55	71.55	ARK	3.8	3.5	12.0	29.8	49
	DGT04	71.55	74.55	ARK	4.5	6.7	10.1	22.8	44
	DGT04	74.55	77.55	ARK	8.1	16.3	10.1	18.5	53
	DGT04	77.55	80.55	BAS	10.4	15.3	9.8	16.5	52
	DGT04	80.55	83.55	BAS	10.8	18.9	12.0	20.2	62
	DGT04	83.55	86.55	BAS	11.7	17.5	10.4	18.4	58
	DGT04	86.55	89.55	BAS	11.7	12.2	9.2	22.0	55
	DGT04	89.55	92.55	BAS	12.5	17.7	10.1	19.7	60
	DGT04	92.55	94	BAS	0.0	6.4	8.9	20.7	36
X =6078.658	DGT06	0	3.68	URD	0.3	3.1	10.4	1.2	15
Y = 16071.113	DGT06	3.68	5.83	URD	0.7	6.3	7.8	0.2	15
Z =1312.356	DGT06	5.83	8.83	URD	0.7	4.9	8.2	1.2	15
	DGT06	8.83	10.58	URD	0.4	3.1	9.8	25.7	39
	DGT06	10.58	11.83	SWG	0.4	0.0	11.1	20.4	32
	DGT06	11.83	14.83	SWG	0.4	1.1	8.7	15.7	26
	DGT06	14.83	17.83	SWG	0.4	10.7	10.3	10.5	32
	DGT06	17.83	20.83	SWG	0.4	5.1	9.1	8.4	23
	DGT06	20.83	23.83	SWG	0.4	5.3	10.5	15.8	32
	DGT06	23.83	26.83	SWG	0.0	0.0	14.2	0.8	15
	DGT06	26.83	29.83	SWG	0.0	0.0	14.9	0.1	15
	DGT06	29.83	32.4	SWG	0.0	0.0	14.2	0.8	15
	DGT06	32.4	32.83	CDOL	5.8	0.0	9.4	19.8	35
	DGT06	32.83	35.83	CDOL	2.9	0.0	9.2	15.9	28
	DGT06	35.83	38.83	CDOL	0.4	0.0	10.3	21.3	32
	DGT06	38.83	41.83	CDOL	0.0	0.0	0.1	14.9	15
	DGT06	41.83	44.83	CDOL	6.1	0.0	8.9	21.0	36
	DGT06	44.83	47.83	CDOL	0.9	1.7	7.9	13.5	24
	DGT06	47.83	50.83	CDOL	0.7	2.7	11.4	11.2	26
	DGT06	50.83	53.83	CDOL	0.4	1.4	7.4	8.7	18
	DGT06	53.83	56.83	CDOL	0.3	0.0	8.6	17.1	26
	DGT06	56.83	59.83	CDOL	0.3	1.2	8.7	9.8	20
	DGT06	59.83	62.83	CDOL	0.3	2.0	9.4	14.4	26
	DGT06	62.83	65.83	CDOL	0.3	0.0	8.4	11.3	20

Collar Coordinates	Hole ID	From	To	Rock Type	UCS	RQD	oint Spacir	Joint Condition and Ground water	Laubscher
	DGT06	65.83	68.83	DOLSCH	2.9	1.6	11.3	15.2	31
	DGT06	68.83	71.83	DOLSCH	2.9	4.9	12.0	19.2	39
	DGT06	71.83	74.83	DOLSCH	2.9	2.3	11.6	14.3	31
	DGT06	74.83	77.83	DOLSCH	2.4	0.8	11.1	26.7	41
	DGT06	77.83	80.83	DOLSCH	5.8	4.3	10.9	14.0	35
	DGT06	80.83	83.83	DOLSCH	3.3	1.9	8.0	15.7	29
	DGT06	83.83	86.83	DOLSCH	4.1	5.2	11.5	11.2	32
	DGT06	86.83	89.83	DOLSCH	2.4	3.4	13.5	19.7	39
	DGT06	89.83	92.83	DOLSCH	2.4	3.0	12.6	19.0	37
	DGT06	92.83	95.83	DOLSCH	2.4	0.0	10.6	19.0	32
	DGT06	95.83	97.18	DOLSCH	2.4	2.0	8.6	12.0	25
	DGT06	97.18	98.83	DOLSCH	2.4	1.2	8.3	13.0	25
	DGT06	98.83	101.83	DOLSCH	1.2	2.3	8.9	12.5	25
	DGT06	101.83	104.83	DOLSCH	2.4	2.1	10.7	19.8	35
	DGT06	104.83	107.83	DOLSCH	3.3	5.5	10.7	14.5	34
	DGT06	107.83	108	DOLSCH	2.9	0.0	10.3	20.8	34
	DGT06	108	110.05	DOLSCH	5.2	0.0	6.5	19.3	31
	DGT06	110.05	110.55	DOLSCH	5.2	10.3	11.8	19.7	47
	DGT06	110.55	112.7	DOLSCH	5.2	5.5	9.1	21.3	41
	DGT06	112.7	113.55	DOLSCH	5.2	3.9	10.9	12.0	32
	DGT06	113.55	116.55	DOLSCH	5.2	9.9	10.2	12.7	38
	DGT06	116.55	119.55	DOLSCH	5.2	4.1	7.7	15.0	32
	DGT06	119.55	122.55	DOLSCH	5.2	10.3	8.5	21.0	45
	DGT06	122.55	125.55	DOLSCH	5.8	6.3	11.2	28.8	52
	DGT06	125.55	128.55	DOLSCH	5.8	9.6	9.1	5.4	30
	DGT06	128.55	131.55	DOLSCH	6.4	1.8	8.1	19.7	36
	DGT06	131.55	134.55	DOLSCH	7.0	4.0	8.6	15.4	35
	DGT06	134.55	137.55	DOLSCH	7.0	1.0	8.3	12.8	29
	DGT06	137.55	140.55	DOLSCH	6.7	0.7	8.5	12.1	28
	DGT06	140.55	143.55	UBS	5.2	4.3	8.6	13.9	32
	DGT06	143.55	146.55	UBS	5.2	1.6	7.2	15.0	29
	DGT06	146.55	149.55	UBS	3.3	0.0	6.9	15.7	26
	DGT06	149.55	152.81	UBS	3.8	4.5	7.3	7.5	23
	DGT06	152.81	155.55	TFQ	4.5	14.5	10.0	4.0	33
	DGT06	155.55	158.55	TFQ	4.5	5.4	8.6	8.5	27
	DGT06	158.55	159.8	TFQ	3.8	0.0	6.9	13.3	24
	DGT06	159.8	161.55	TFQ	2.9	1.4	7.7	11.0	23
	DGT06	161.55	164.55	TFQ	6.4	12.7	10.0	7.9	37
	DGT06	164.55	167.55	TFQ	5.2	11.5	9.7	5.5	32
	DGT06	167.55	170.55	TFQ	5.2	17.0	12.2	3.5	38
	DGT06	170.55	173.55	TFQ	5.2	11.3	9.9	5.6	32
	DGT06	173.55	176.55	TFQ	5.2	13.9	9.5	6.3	35
	DGT06	176.55	179.55	TFQ	5.2	12.0	9.7	2.1	29
	DGT06	179.55	182.55	TFQ	5.2	8.8	9.6	8.4	32
	DGT06	182.55	183.3	TFQ	4.5	6.3	9.2	8.0	28
	DGT06	183.3	187.2	UBS	5.2	1.5	7.7	14.7	29
	DGT06	187.2	188.55	UBS	5.2	0.0	5.5	10.3	21
	DGT06	188.55	191.55	UBS	2.9	0.8	6.8	9.5	20
	DGT06	191.55	192.88	TFQ	4.5	1.9	9.0	27.6	43
	DGT06	192.88	194.55	TFQ	5.8	6.2	10.5	19.5	42
	DGT06	194.55	197.55	TFQ	8.1	9.3	8.8	14.8	41
	DGT06	197.55	199.55	TFQ	7.5	11.1	10.4	16.0	45
	DGT06	199.55	200.55	TFQ	8.6	4.5	9.2	21.7	44
	DGT06	200.55	203.55	TFQ	5.8	12.7	9.7	13.8	42
	DGT06	203.55	206.55	TFQ	5.8	16.8	10.7	11.7	45
	DGT06	206.55	209.55	TFQT	3.8	1.9	6.9	20.5	33
	DGT06	209.55	212.55	BSSU	0	0.0	6.7	17.1	24
	DGT06	212.55	215.55	BSSU	0	0.0	7.8	15.9	24
	DGT06	215.55	219.14	PQ	4	0.6	6.8	9.8	21
	DGT06	219.14	219.76	PQ	1	9.3	8.5	8.3	27
	DGT06	219.76	221.55	BSSL	1	0.0	1.7	11.1	14

Collar Coordinates	Hole ID	From	To	Rock Type	UCS	RQD	oint Spacin	Joint Condition and Ground water	Laubscher
	DGT06	221.55	224.55	BSSL	1	0.8	6.8	12.3	21
	DGT06	224.55	227.55	BSSL	1	1.4	8.2	16.2	27
	DGT06	227.55	230.55	BSSL	0	0.0	4.1	10.7	15
	DGT06	230.55	230.85	BSSL	0	0.0	3.7	12.0	16
	DGT06	230.85	233.55	TR	8	0.0	2.6	23.4	34
	DGT06	233.55	236.55	TR	9	15.0	9.9	17.0	51
	DGT06	236.55	239.55	TR	9	17.7	11.2	11.0	49
	DGT06	239.55	243.19	TR	9	14.0	10.5	5.4	39
	DGT06	243.19	245.55	ARK	14	19.2	14.3	28.1	76
	DGT06	245.55	248.55	ARK	14	20.3	13.5	28.8	77
	DGT06	248.55	251.55	ARK	15	19.4	15.2	27.6	77
	DGT06	251.55	254.55	ARK	15	18.3	11.5	12.4	57
	DGT06	254.55	257.55	ARK	15	17.1	14.1	24.1	70
	DGT06	257.55	260.55	ARK	16	20.6	14.3	14.9	66
	DGT06	260.55	263.55	ARK	16	19.4	15.2	24.2	75
	DGT06	263.55	266.55	ARK	15	17.7	12.9	20.9	67
	DGT06	266.55	268.85	ARK	15	20.4	12.9	13.2	62
	DGT06	268.85	269.55	ARK	15	10.9	10.8	37.8	75
	DGT06	269.55	272.55	ARK	6	12.1	8.3	16.8	43
	DGT06	272.55	275.55	ARK	12	9.0	8.9	14.6	45
	DGT06	275.55	278.55	ARK	14	18.1	13.5	20.0	66
	DGT06	278.55	281.55	ARK	15	18.5	11.3	9.4	54
	DGT06	281.55	284.55	ARK	15	17.9	13.6	21.8	68
	DGT06	284.55	287.55	ARK	15	15.8	12.3	26.8	70
	DGT06	287.55	290.55	ARK	15	18.7	13.0	20.9	68
	DGT06	290.55	293.55	ARK	15	13.7	12.2	26.0	67
	DGT06	293.55	296.55	ARK	15	17.4	10.9	21.2	65
	DGT06	296.55	299.55	ARK	15	17.9	10.4	24.3	68
X =5919.569	DGT13	0	0.55	URD	0.0	0.0	13.3	1.7	15.0
Y = 15878.543	DGT13	0.55	3.68	URD	0.0	0.0	12.9	2.1	15.0
Z = 1308.700	DGT13	3.68	5.58	URD	0.0	0.0	13.7	1.3	15.0
	DGT13	5.58	8.58	URD	0.9	9.3	4.1	0.8	15.0
	DGT13	8.58	11.58	URD	0.4	0.0	9.4	5.2	15.0
	DGT13	11.58	14.58	URD	0.9	12.6	8.8	1.3	23.6
	DGT13	14.58	17.58	URD	0.9	9.8	9.1	6.7	26.6
	DGT13	17.58	20.58	URD	5.2	1.7	8.4	19.2	34.5
	DGT13	20.58	23.58	URD	5.2	0.8	6.5	18.2	30.8
	DGT13	23.58	26.58	URD	5.2	4.4	6.1	12.1	27.8
	DGT13	26.58	29.58	URD	3.3	4.7	6.1	10.9	25.1
	DGT13	29.58	32.58	URD	3.8	2.3	7.0	11.4	24.4
	DGT13	32.58	35.58	URD	3.8	0.0	5.0	15.6	24.4
	DGT13	62.58	65.58	SWG	5.8	2.8	6.4	20.9	35.9
	DGT13	65.58	68.58	SWG	5.8	2.6	9.1	24.4	41.9
	DGT13	68.58	71.58	SWG	9.5	5.4	7.0	21.3	43.3
	DGT13	71.58	74.58	SWG	10.8	2.4	7.6	25.6	46.4
	DGT13	74.58	77.58	SWG	10.8	4.7	6.4	21.5	43.5
	DGT13	77.58	80.58	SWG	10.8	3.0	7.0	25.7	46.4
	DGT13	80.58	83.58	SWG	10.8	3.4	6.0	23.2	43.4
	DGT13	83.58	86.3	SWG	12.5	0.0	4.4	28.7	45.6
	DGT13	86.3	89.3	SWG	12.5	0.7	5.6	28.8	47.6
	DGT13	89.3	92.3	SWG	12.5	3.6	6.7	27.8	50.6
	DGT13	92.3	95.3	SWG	10.8	7.4	6.3	14.9	39.3
	DGT13	95.3	98.3	SWG	7.0	8.7	6.9	6.4	28.9
	DGT13	113.3	116.3	SWG	7.0	4.7	5.6	17.8	35.0
	DGT13	116.3	119.3	SWG	3.3	4.0	5.4	6.2	18.9
	DGT13	119.3	122.3	SWG	3.3	8.0	6.6	10.3	28.1
	DGT13	122.3	125.3	SWG	2.9	0.0	5.0	9.7	17.6
	DGT13	125.3	128.3	SWG	2.9	10.2	8.8	13.3	35.1
	DGT13	128.3	131.3	SWG	8.6	13.7	7.7	7.8	37.8

Collar Coordinates	Hole ID	From	To	Rock Type	UCS	RQD	Joint Spacing	Joint Condition and Ground water	Laubscher
	DGT13	131.3	134.3	SWG	9.0	12.8	8.0	3.7	33.6
	DGT13	134.3	137.3	SWG	10.8	14.3	7.5	12.2	44.8
	DGT13	137.3	140.3	SWG	11.7	11.9	7.2	21.2	51.9
	DGT13	140.3	143.3	SWG	5.8	14.3	8.6	16.9	45.7
	DGT13	143.3	146.3	SWG	12.5	12.8	8.0	10.9	44.3
	DGT13	146.3	149.3	SWG	12.5	10.9	5.8	15.2	44.3
	DGT13	149.3	152.3	SWG	12.5	16.9	9.7	10.4	49.5
	DGT13	152.3	155.3	SWG	11.7	14.2	10.9	11.4	48.2
	DGT13	155.3	158.3	SWG	8.1	14.2	7.5	10.8	40.5
	DGT13	158.3	161.3	SWG	12.5	13.1	8.5	22.9	57.0
	DGT13	161.3	164.3	SWG	5.8	11.1	6.8	3.1	26.8
	DGT13	164.3	167.3	SWG	5.8	16.9	9.9	2.1	34.8
	DGT13	167.3	170.3	SWG	5.8	8.5	6.7	5.8	26.8
	DGT13	170.3	173.3	SWG	5.8	12.4	7.5	1.1	26.8
	DGT13	173.3	176.3	SWG	5.8	12.1	6.9	2.0	26.8
	DGT13	176.3	179.3	SWG	5.8	14.8	9.9	8.0	38.6
	DGT13	179.3	182.3	SWG	5.8	13.8	7.5	4.7	31.8
	DGT13	182.3	185.3	CDOL	7.0	14.3	8.9	4.4	34.7
	DGT13	185.3	188.3	CDOL	7.0	13.1	9.7	4.8	34.7
	DGT13	188.3	191.3	CDOL	5.8	6.7	7.0	8.1	27.6
	DGT13	191.3	194.3	CDOL	5.8	13.6	8.8	8.1	36.3
	DGT13	194.3	197.3	CDOL	5.8	15.7	9.5	8.3	39.3
	DGT13	197.3	200.3	DOLSCH	8.1	8.8	6.9	23.4	47.1
	DGT13	200.3	203.3	DOLSCH	8.1	9.3	6.7	14.4	38.5
	DGT13	203.3	206.3	DOLSCH	8.1	5.6	6.5	18.4	38.5
	DGT13	206.3	209.3	DOLSCH	8.1	7.2	6.6	14.9	36.8
	DGT13	209.3	212.3	DOLSCH	8.1	10.9	7.4	12.2	38.5
	DGT13	212.3	215.3	UBS	8.1	11.6	8.1	22.3	50.1
	DGT13	215.3	218.3	UBS	8.1	7.6	7.0	15.9	38.5
	DGT13	218.3	221.3	UBS	8.1	8.0	6.9	13.8	36.8
	DGT13	221.3	224.3	TFQ	8.1	11.8	8.6	8.3	36.8
	DGT13	224.3	227.3	TFQ	8.1	12.2	7.7	1.6	29.5
	DGT13	227.3	230.3	TFQ	8.6	6.2	7.2	10.8	32.8
	DGT13	230.3	233.3	TFQ	2.4	0.8	7.8	19.8	30.8
	DGT13	233.3	236.3	TFQ	3.8	4.7	6.3	11.6	26.4
	DGT13	236.3	236.53	BSSU	5.8	3.4	7.0	23.1	39.3
	DGT13	236.53	237.6	PQ	8.1	9.3	7.8	8.6	33.8
	DGT13	237.6	239.3	BSSL	8.1	14.4	8.8	2.4	33.8
	DGT13	239.3	242.3	BSSL	8.1	17.7	11.3	11.6	48.6
	DGT13	242.3	245.3	BSSL	12.5	19.5	10.4	8.6	51.0
	DGT13	245.3	248.3	LBS	9.0	2.5	8.1	16.9	36.6
	DGT13	248.3	251.3	TR	4.1	2.5	5.6	9.6	21.9
	DGT13	251.3	254.3	ARK	7.0	4.3	6.8	10.6	28.7
	DGT13	254.3	257.3	ARK	9.0	5.6	7.1	9.8	31.6
	DGT13	257.3	260.3	ARK	12.5	15.3	12.8	23.1	63.6
	DGT13	260.3	263.3	ARK	12.5	14.6	10.5	15.9	53.4
	DGT13	263.3	266.3	ARK	12.5	15.9	10.7	18.0	57.0
	DGT13	266.3	269.3	ARK	12.5	16.6	11.3	13.7	54.0
	DGT13	269.3	272.3	ARK	11.7	9.3	7.9	23.7	52.5
	DGT13	272.3	275.3	ARK	9.0	20.6	10.4	14.6	54.6
	DGT13	275.3	278.3	ARK	11.7	17.5	10.3	9.4	48.9
	DGT13	278.3	281.3	ARK	11.7	11.0	5.5	13.9	42.2
	DGT13	281.3	284.3	ARK	10.8	17.9	9.0	5.4	43.1
	DGT13	284.3	287.3	ARK	9.0	15.5	8.5	0.5	33.6
	DGT13	287.3	290.3	ARK	7.0	11.1	6.0	0.3	24.4
	DGT13	290.3	293.3	ARK	12.5	18.5	11.2	14.7	57.0
	DGT13	293.3	296.3	ARK	14.4	18.5	11.0	11.6	55.5
	DGT13	296.3	299.3	ARK	14.4	19.4	11.6	7.9	53.3
	DGT13	299.3	302.3	ARK	14.4	18.8	20.0	18.3	71.5

Collar Coordinates	Hole ID	From	To	Rock Type	UCS	RQD	Joint Spacing	Joint Condition and Ground water	Laubscher
	DGT13	302.3	305.3	ARK	14.4	19.3	15.2	24.8	73.7
	DGT13	305.3	308.3	ARK	14.4	20.3	13.0	21.0	68.7
	DGT13	308.3	311.3	ARK	14.4	19.0	13.6	24.7	71.7
	DGT13	311.3	314.3	ARK	14.4	18.4	12.4	23.5	68.7
	DGT13	314.3	317.3	BAS	14.4	18.2	11.9	27.1	71.7
	DGT13	317.3	320.3	BAS	16.2	17.7	10.9	22.7	67.5
X =6147.610	DGT14	0	4.08	URD	0.4	0.0	14.1	0.5	15.0
Y= 15760.435	DGT14	4.08	5.83	URD	0.4	0.0	9.2	5.4	15.0
Z =1317.714	DGT14	5.83	8.83	URD	0.4	0.0	8.5	6.1	15.0
	DGT14	8.83	11.83	URD	0.4	0.0	10.1	4.5	15.0
	DGT14	11.83	14.83	URD	0.4	0.0	10.2	4.4	15.0
	DGT14	14.83	17.83	URD	0.3	9.3	11.2	10.8	31.6
	DGT14	17.83	20.83	URD	0.3	5.4	9.9	7.7	23.3
	DGT14	20.83	23.83	URD	0.6	8.1	9.3	5.4	23.4
	DGT14	23.83	26.83	URD	1.9	5.8	9.5	13.1	30.3
	DGT14	26.83	29.83	URD	2.4	6.0	9.7	7.5	25.6
	DGT14	29.83	32.83	URD	1.9	13.3	9.2	-0.1	24.3
	DGT14	32.83	35.83	URD	2.4	5.7	8.3	5.4	21.8
	DGT14	35.83	38.83	URD	5.2	1.7	7.9	16.7	31.5
	DGT14	38.83	41.83	URD	3.8	4.5	9.3	8.8	26.4
	DGT14	41.83	44.83	URD	5.8	10.4	10.0	12.3	38.6
	DGT14	44.83	47.83	URD	7.0	3.5	7.3	14.6	32.4
	DGT14	47.83	50.83	URD	5.2	4.3	7.8	14.3	31.5
	DGT14	50.83	53.83	URD	4.5	3.3	8.2	14.4	30.5
	DGT14	53.83	56.83	URD	1.2	5.4	8.0	12.2	26.8
	DGT14	56.83	59.83	SWG	0.7	1.1	7.4	9.3	18.5
	DGT14	59.83	62.83	SWG	1.5	2.3	9.2	14.0	27.0
	DGT14	62.83	65.83	SWG	0.9	0.0	5.2	11.8	17.8
	DGT14	65.83	68.83	SWG	0.9	6.7	9.2	9.0	25.8
	DGT14	68.83	71.83	SWG	0.9	0.0	5.0	9.7	15.6
	DGT14	71.83	74.83	SWG	1.2	2.5	8.0	12.1	23.8
	DGT14	74.83	77.83	SWG	1.9	1.1	7.9	10.5	21.3
	DGT14	77.83	80.83	SWG	1.2	3.8	9.1	9.7	23.8
	DGT14	80.83	83.83	SWG	1.2	3.6	8.4	7.6	20.8
	DGT14	83.83	86.55	SWG	0.9	1.3	5.9	10.5	18.6
	DGT14	86.55	89.54	SWG	1.9	10.3	8.9	6.3	27.3
	DGT14	89.54	92.55	SWG	1.9	11.4	9.1	2.0	24.3
	DGT14	92.55	95.55	SWG	2.4	12.2	10.7	2.5	27.8
	DGT14	95.55	98.55	SWG	4.1	9.1	8.7	2.0	23.9
	DGT14	98.55	101.55	SWG	5.2	11.9	8.7	-0.3	25.5
	DGT14	101.55	104.55	SWG	5.2	7.0	8.4	10.9	31.5
	DGT14	104.55	107.55	SWG	5.2	6.4	8.1	5.8	25.5
	DGT14	107.55	110.55	SWG	5.2	8.9	8.4	9.0	31.5
	DGT14	110.55	113.55	SWG	4.1	9.7	8.6	1.5	23.9
	DGT14	113.55	116.55	SWG	4.1	9.5	7.4	5.9	26.9
	DGT14	116.55	119.55	SWG	4.1	11.5	6.1	2.1	23.9
	DGT14	119.55	122.55	SWG	5.2	15.8	9.7	0.0	30.8
	DGT14	122.55	125.55	CDOL	5.2	1.2	6.4	12.7	25.5
	DGT14	125.55	128.55	DOLSCH	4.1	2.5	7.3	10.0	23.9
	DGT14	128.55	131.55	DOLSCH	3.8	6.1	9.9	18.5	38.3
	DGT14	131.55	134.55	DOLSCH	4.1	7.1	8.7	20.1	40.1
	DGT14	134.55	137.55	DOLSCH	5.8	2.3	7.2	17.3	32.7
	DGT14	137.55	140.55	DOLSCH	4.1	0.8	7.2	18.0	30.1
	DGT14	140.55	143.55	DOLSCH	2.9	3.8	9.0	18.9	34.5
	DGT14	143.55	146.55	UBS	3.8	10.0	9.7	6.0	29.4
	DGT14	146.55	149.55	TFQ	3.3	7.6	8.0	3.9	22.9
	DGT14	149.55	152.55	TFQ	4.5	13.5	9.3	6.2	33.6
	DGT14	152.55	155.55	TFQ	4.5	9.1	8.0	17.7	39.3
	DGT14	155.55	158.55	BSSU	3.8	0.8	7.9	20.2	32.6

Collar Coordinates	Hole ID	From	To	Rock Type	UCS	RQD	Joint Spacing	Joint Condition and Ground water	Laubscher
	DGT14	158.55	161.55	BSSU	3.8	0.9	5.8	17.1	27.6
	DGT14	161.55	164.55	PQ	2.9	1.0	7.5	22.1	33.5
	DGT14	164.55	167.55	BSSL	2.4	0.7	6.8	12.6	22.6
	DGT14	167.55	170.55	BSSL	1.9	4.7	8.1	10.4	25.1
	DGT14	170.55	173.55	BSSL	2.4	8.5	9.6	8.1	28.6
	DGT14	173.55	176.55	BSSL	2.9	6.7	9.6	18.0	37.2
	DGT14	176.55	179.55	TR	2.4	3.3	8.2	8.6	22.6
	DGT14	179.55	182.55	TR	11.7	2.3	11.9	34.1	60.0
	DGT14	182.55	185.55	TR	12.5	2.5	6.8	35.6	57.4
	DGT14	185.55	188.55	TR	12.5	13.7	11.0	29.2	66.4
	DGT14	188.55	191.55	ARK	12.1	15.3	9.1	18.6	55.1
	DGT14	191.55	194.55	ARK	11.3	8.9	7.5	19.3	47.0
	DGT14	194.55	197.55	ARK	14.4	20.4	16.5	28.0	79.4
	DGT14	197.55	200.55	ARK	14.8	20.2	20.0	27.5	82.4
	DGT14	200.55	203.55	ARK	14.8	20.6	16.6	20.4	72.3
	DGT14	203.55	206.55	ARK	15.1	18.5	11.6	16.2	61.4
	DGT14	206.55	209.55	ARK	14.4	15.5	13.6	29.9	73.3
	DGT14	209.55	212.55	ARK	16.2	17.7	13.5	34.5	81.9
	DGT14	212.55	215.55	ARK	16.2	19.9	13.6	16.9	66.5
	DGT14	215.55	218.55	ARK	16.2	17.2	14.3	33.3	80.9
	DGT14	218.55	221.55	ARK	16.2	20.6	15.2	21.9	73.9
	DGT14	221.55	224.55	ARK	12.5	17.9	11.3	9.3	51.0
	DGT14	224.55	227.55	ARK	12.5	17.5	11.2	18.0	59.1
	DGT14	227.55	230.55	ARK	10.0	7.2	8.8	17.2	43.2
	DGT14	230.55	233.55	ARK	12.5	15.9	9.5	9.4	47.3
	DGT14	233.55	236.55	BAS	14.0	11.9	9.2	13.4	48.5
	DGT14	236.55	239.55	BAS	14.4	18.1	10.1	19.1	61.7
	DGT14	239.55	242.55	BAS	16.2	20.1	13.0	24.3	73.5
	DGT14	242.55	245.55	BAS	16.2	19.9	13.0	21.5	70.5
	DGT14	245.55	248.55	BAS	15.5	14.8	9.5	15.8	55.7
	DGT14	248.55	251.55	BAS	14.4	19.6	12.0	13.3	59.3
X =6132.697	DGT20	0	3.78	LAT	1.2	0.0	9.1	4.7	15.0
Y = 16339.726	DGT20	3.78	5.83	LAT	1.2	0.0	8.2	5.6	15.0
Z =1308.175	DGT20	5.83	8.83	URD	0.4	0.0	8.9	5.7	15.0
	DGT20	8.83	11.83	URD	0.4	0.0	10.2	4.4	15.0
	DGT20	11.83	14.83	URD	0.4	0.0	11.0	3.6	15.0
	DGT20	14.83	17.83	SWG	0.4	0.0	12.5	2.1	15.0
	DGT20	17.83	20.83	SWG	0.4	0.0	10.4	4.2	15.0
	DGT20	20.83	23.83	SWG	0.4	0.0	9.8	4.8	15.0
	DGT20	23.83	26.83	SWG	0.4	0.0	11.1	3.5	15.0
	DGT20	26.83	29.83	SWG	0.4	0.0	9.7	4.9	15.0
	DGT20	29.83	32.83	SWG	0.7	0.0	12.1	2.2	15.0
	DGT20	32.83	35.83	SWG	0.7	0.0	10.7	3.6	15.0
	DGT20	35.83	38.83	URD	0.7	0.0	12.2	2.1	15.0
	DGT20	38.83	41.83	URD	5.2	9.5	10.4	25.5	50.6
	DGT20	41.83	44.83	URD	5.2	13.4	11.8	22.3	52.6
	DGT20	44.83	47.83	URD	3.8	3.4	6.5	20.9	34.5
	DGT20	47.83	50.83	URD	3.3	0.0	9.3	32.3	45.0
	DGT20	50.83	53.83	SWG	2.9	0.0	11.0	23.4	37.4
	DGT20	53.83	56.83	SWG	2.4	0.0	7.6	26.5	36.5

Table A- 7: Calculation of Adjusted MRMR values for the footwall (Domain 1) of COPF/D pit

Area	Domain	Rock Formation	MRMR	Weathering Adjustment		Joint Orientation adjustment		Adjustment for mining induced stresses		Blating effects adjustments		Adjusted MRMR
			Median	Description	Rating (%)	Description	Rating (%)	Description	Rating (%)	Description	Rating (%)	
Footwall	1	weathered ARK	57	Highly weathered	76	3 faces inclines away	85	poor confinment due to shallow depth	60	smooth wall blasting	97	21.4
		ARK	57	Slightly weathered	94	3 faces inclines away	85	good confinement due to pit depth	120	smooth wall blasting	97	53.0

Table A- 8: Calculation of Adjusted MRMR values for the South wall (Domain 2) of COPF/D pit

Area	Domain	Rock Formation	MRMR	Weathering Adjustment		Joint Orientation adjustment		Adjustment for mining induced stresses		Blating effects adjustments		Adjusted MRMR
			Median	Description	Rating (%)	Description	Rating (%)	Description	Rating (%)	Description	Rating (%)	
South Wall	2	Weathered BAS	58	Highly weathered	76	2 faces inclines away	90	poor confinment due to shallow depth	60	smooth wall blasting	97	23.1
		BAS	58	Fresh	100	3 faces inclines away	85	good confinement due to pit depth	60	smooth wall blasting	97	28.7
		weathered ARK	57	moderately weathered	88	3 faces inclines away	85	poor confinment due to shallow depth	60	smooth wall blasting	97	24.8
		ARK	57	Fresh	100	3 faces inclines away	85	poor confinment due to shallow depth	60	smooth wall blasting	97	28.2
		LBS	26	moderately weathered	88	2 faces inclines away	100	poor confinment due to shallow depth	60	smooth wall blasting	97	13.3
		BSSL	32	moderately weathered	88	2 faces inclines away	100	poor confinment due to shallow depth	60	smooth wall blasting	97	16.4
		PQ	40	Slightly weathered	96	2 faces inclines away	100	poor confinment due to shallow depth	60	smooth wall blasting	97	22.3
		BSSU	35	moderately weathered	88	2 faces inclines away	100	poor confinment due to shallow depth	60	smooth wall blasting	97	17.9
		TFQ	46	Slightly weathered	88	6 faces inclined away	70	poor confinment due to shallow depth	60	smooth wall blasting	97	16.5
		UBS	33	moderately weathered	88	2 faces inclines away	100	poor confinment due to shallow depth	60	smooth wall blasting	97	16.9
		DOLSCH	36	moderately weathered	88	2 faces inclines away	100	poor confinment due to shallow depth	60	smooth wall blasting	97	18.4

Table A- 9: Calculation of Adjusted MRMR values for the Hangingwall (Domain 3) of COPF/D pit

Area	Domain	Rock Formation	MRMR	Weathering Adjustment		Joint Orientation adjustment		Adjustment for mining induced stresses		Blating effects adjustments		Adjusted MRMR
			Median	Description	Rating (%)	Description	Rating (%)	Description	Rating (%)	Description	Rating (%)	
Hangingwall	3	Weathered URD	31	Highly weathered	76	3 faces inclines away	85	poor confinment due to shallow depth	60	smooth wall blasting	97	11.7
		URD	31	moderately weathered	88	3 faces inclines away	85	poor confinment due to shallow depth	60	smooth wall blasting	97	13.5
		SWG	41	Slightly weathered	94	2 faces inclines away	100	poor confinment due to shallow depth	60	smooth wall blasting	97	22.4
		CDOL	33	Slightly weathered	94	2 faces inclines away	100	poor confinment due to shallow depth	60	smooth wall blasting	97	18.1
		DOLSCH	36	Slightly weathered	94	2 faces inclines away	100	poor confinment due to shallow depth	60	smooth wall blasting	97	19.7
		UBS	33	Slightly weathered	94	2 faces inclines away	100	poor confinment due to shallow depth	60	smooth wall blasting	97	18.1
		TFQ	46	Slightly weathered	94	6 faces inclined away	70	poor confinment due to shallow depth	60	smooth wall blasting	97	17.6
		BSSU	35	moderately weathered	88	2 faces inclines away	100	poor confinment due to shallow depth	60	smooth wall blasting	97	17.9
		PQ	40	Slightly weathered	94	2 faces inclines away	100	poor confinment due to shallow depth	60	smooth wall blasting	97	21.9
		BSSL	32	moderately weathered	88	2 faces inclines away	100	poor confinment due to shallow depth	60	smooth wall blasting	97	16.4
		LBS	26	Slightly weathered	94	2 faces inclines away	100	poor confinment due to shallow depth	60	smooth wall blasting	97	14.2
		ARK	57	Slightly weathered	94	3 faces inclines away	85	poor confinment due to shallow depth	60	smooth wall blasting	97	26.5

Table A- 10: Rock mass rating system classification table (after Bieniawski, 1989)

A. CLASSIFICATION PARAMETERS AND THEIR RATINGS

	Parameter		Range of values				
1	Strength of intact rock material	Point-load strength index	>10 MPa	4 - 10 MPa	2 - 4 MPa	1 - 2 MPa	For this low range - uniaxial compressive test is preferred
		Uniaxial comp. strength	>250 MPa	100 - 250 MPa	50 - 100 MPa	25 - 50 MPa	5 - 25 MPa; 1 - 5 MPa; < 1 MPa
	Rating		15	12	7	4	2; 1; 0
2	Drill core Quality *RQD*		90% - 100%	75% - 90%	50% - 75%	25% - 50%	< 25%
	Rating		20	17	13	8	3
3	Spacing of discontinuities		> 2 m	0.6 - 2 . m	200 - 600 mm	60 - 200 mm	< 60 mm
	Rating		20	15	10	8	5
4	Condition of discontinuities (See E)		Very rough surfaces Not continuous No separation Unweathered wall rock	Slightly rough surfaces Separation < 1 mm Slightly weathered walls	Slightly rough surfaces Separation < 1 mm Highly weathered walls	Slickensided surfaces or Gouge < 5 mm thick or Separation 1-5 mm Continuous	Soft gouge >5 mm thick or Separation > 5 mm Continuous
	Rating		30	25	20	10	0
5	Ground water	Inflow per 10 m tunnel length (l/m)	None	< 10	10 - 25	25 - 125	> 125
		(Joint water press)/ (Major principal σ)	0	< 0.1	0.1, - 0.2	0.2 - 0.5	> 0.5
		General conditions	Completely dry	Damp	Wet	Dripping	Flowing
	Rating		15	10	7	4	0

B. RATING ADJUSTMENT FOR DISCONTINUITY ORIENTATIONS (See F)

Strike and dip orientations		Very favourable	Favourable	Fair	Unfavourable	Very Unfavourable
Ratings	Tunnels & mines	0	-2	-5	-10	-12
	Foundations	0	-2	-7	-15	-25
	Slopes	0	-5	-25	-50	

C. ROCK MASS CLASSES DETERMINED FROM TOTAL RATINGS

Rating	100 ← 81	80 ← 61	60 ← 41	40 ← 21	< 21
Class number	I	II	III	IV	V
Description	Very good rock	Good rock	Fair rock	Poor rock	Very poor rock

D. MEANING OF ROCK CLASSES

Class number	I	II	III	IV	V
Average stand-up time	20 yrs for 15 m span	1 year for 10 m span	1 week for 5 m span	10 hrs for 2.5 m span	30 min for 1 m span
Cohesion of rock mass (kPa)	> 400	300 - 400	200 - 300	100 - 200	< 100
Friction angle of rock mass (deg)	> 45	35 - 45	25 - 35	15 - 25	< 15

E. GUIDELINES FOR CLASSIFICATION OF DISCONTINUITY conditions

Discontinuity length (persistence)	< 1 m	1 - 3 m	3 - 10 m	10 - 20 m	> 20 m
Rating	6	4	2	1	0
Separation (aperture)	None	< 0.1 mm	0.1 - 1.0 mm	1 - 5 mm	> 5 mm
Rating	6	5	4	1	0
Roughness	Very rough	Rough	Slightly rough	Smooth	Slickensided
Rating	6	5	3	1	0
Infilling (gouge)	None	Hard filling < 5 mm	Hard filling > 5 mm	Soft filling < 5 mm	Soft filling > 5 mm
Rating	6	4	2	2	0
Weathering	Unweathered	Slightly weathered	Moderately weathered	Highly weathered	Decomposed
Ratings	6	5	3	1	0

F. EFFECT OF DISCONTINUITY STRIKE AND DIP ORIENTATION IN TUNNELLING**

Strike perpendicular to tunnel axis		Strike parallel to tunnel axis	
Drive with dip - Dip 45 - 90°	Drive with dip - Dip 20 - 45°	Dip 45 - 90°	Dip 20 - 45°
Very favourable	Favourable	Very unfavourable	Fair
Drive against dip - Dip 45-90°	Drive against dip - Dip 20-45°	Dip 0-20 - Irrespective of strike°	
Fair	Unfavourable	Fair	

`

Table A- 11: GSI Chart (Marinos, et al., 2005)

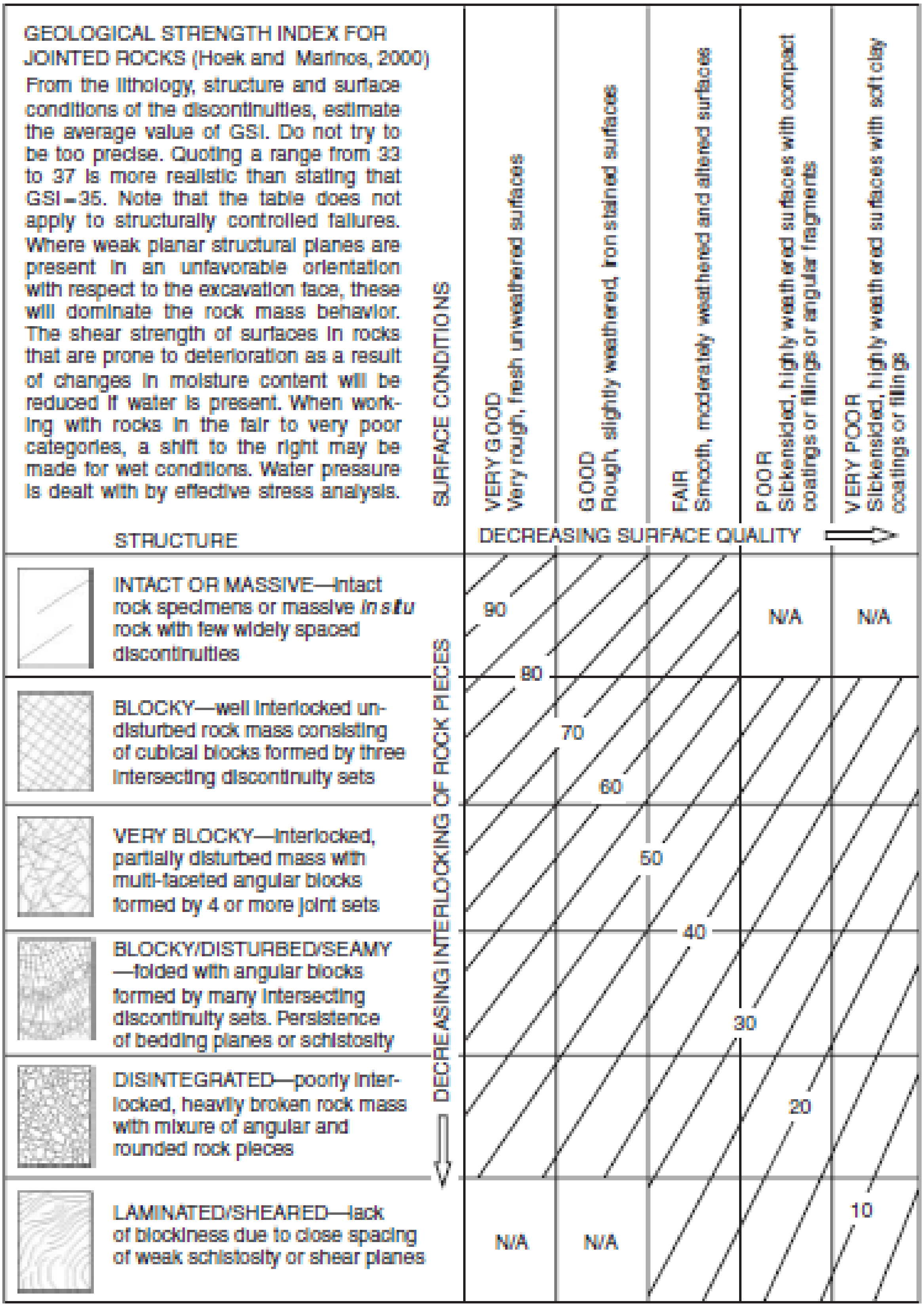

Table A- 12: GSI Chart (Rafiei & Cai, 2022)

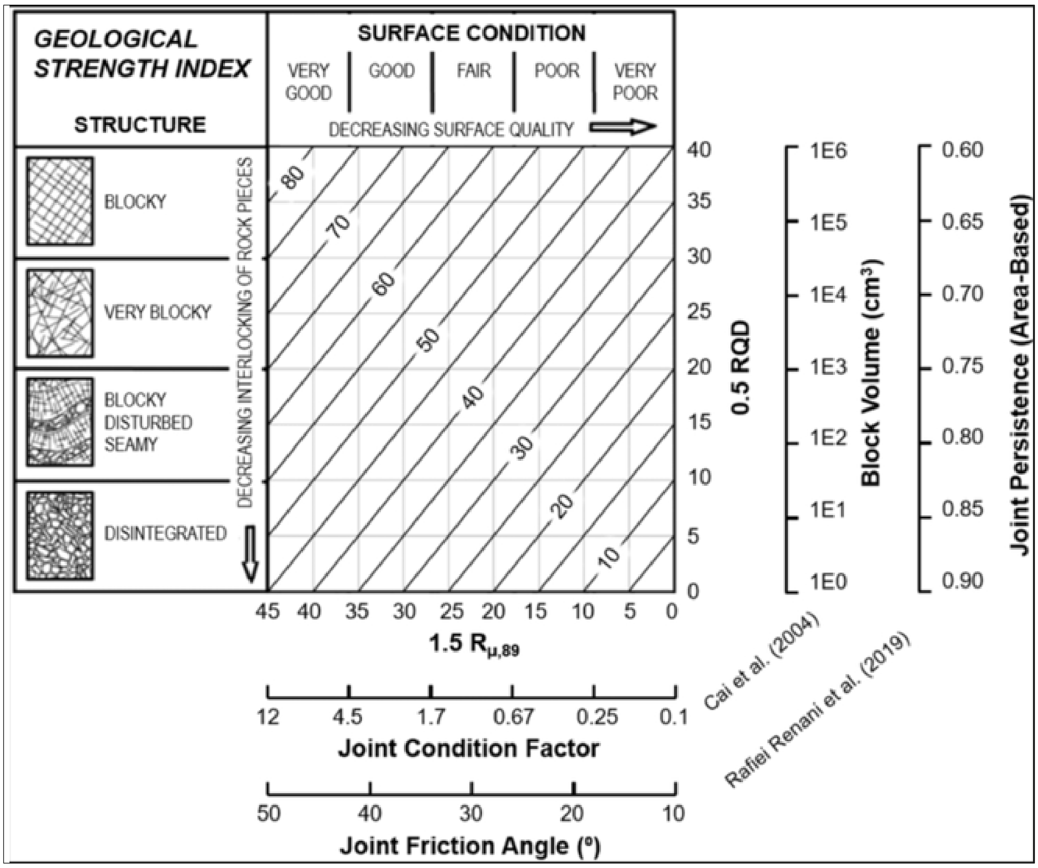

APPENDIX B. Q SYSTEM TABLES

Table B- 1: joint roughness number (Jr) (Barton, 2002)

Joint roughness number		J_r
(a) *Rock-wall contact, and (b) rock-wall contact before 10 cm sear*		
A	Discontinuous joints	4
B	Rough or irregular, undulating	3
C	Smooth, undulating	2
D	Slickensided, undulating	1.5
E	Rough or irregular, planar	1.5
F	Smooth, planar	1.0
G	Slickensided, planar	0.5
(b) *No rock-wall contact when sheared*		
H	Zone containing clay minerals thick enough to prevent rock-wall contact.	1.0
J	Sandy, gravely or crushed zone thick enough to prevent rock-wall contact	1.0

Notes: (i) Descriptions refer to small-scale features and intermediate scale features, in that order. (ii) Add 1.0 if the mean spacing of the relevant joint set is greater than 3 m. (iii) $J_r = 0.5$ can be used for planar, slickensided joints having lineations, provided the lineations are oriented for minimum strength. (iv) J_r and J_a classification is applied to the joint set or discontinuity that is least favourable for stability both from the point of view of orientation and shear resistance, τ(where $\tau \approx \sigma_n \tan^{-1}(J_r/J_a)$).

Table B- 2: Joint alteration number (Ja) (Barton, 2002)

Joint alteration number		ϕ_r approx. (deg)	J_a
(a) Rock-wall contact (no mineral fillings, only coatings)			
A	Tightly healed, hard, non-softening, impermeable filling, i.e., quartz or epidote	—	0.75
B	Unaltered joint walls, surface staining only	25–35	1.0
C	Slightly altered joint walls, non-softening mineral coatings, sandy particles, clay-free disintegrated rock, etc.	25–30	2.0
D	Silty- or sandy-clay coatings, small clay fraction (non-softening)	20–25	3.0
E	Softening or low friction clay mineral coatings, i.e., kaolinite or mica. Also chlorite, talc, gypsum, graphite, etc., and small quantities of swelling clays	8–16	4.0
(b) Rock-wall contact before 10 cm shear (thin mineral fillings)			
F	Sandy particles, clay-free disintegrated rock, etc.	25–30	4.0
G	Strongly over-consolidated non-softening clay mineral fillings (continuous, but <5 mm thickness)	16–24	6.0
H	Medium or low over-consolidation, softening, clay mineral fillings (continuous, but <5 mm thickness)	12–16	8.0
J	Swelling-clay fillings, i.e., montmorillonite (continuous, but <5 mm thickness). Value of J_a depends on per cent of swelling clay-size particles, and access to water, etc.	6–12	8–12
(c) No rock-wall contact when sheared (thick mineral fillings)			
KLM	Zones or bands of disintegrated or crushed rock and clay (see G, H, J for description of clay condition)	6–24	6, 8, or 8–12
N	Zones or bands of silty- or sandy-clay, small clay fraction (non-softening)	—	5.0
OPR	Thick, continuous zones or bands of clay (see G, H, J for description of clay condition)	6–24	10, 13, or 13–20

Table B- 3: Joint water reduction factor (Jw) (Barton, 2002)

	Joint water reduction factor	Approx. water pres. (kg/cm²)	J_w
A	Dry excavations or minor inflow, i.e., <5 l/min locally	<1	1.0
B	Medium inflow or pressure, occasional outwash of joint fillings	1–2.5	0.66
C	Large inflow or high pressure in competent rock with unfilled joints	2.5–10	0.5
D	Large inflow or high pressure, considerable outwash of joint fillings	2.5–10	0.33
E	Exceptionally high inflow or water pressure at blasting, decaying with time	>10	0.2–0.1
F	Exceptionally high inflow or water pressure continuing without noticeable decay	>10	0.1–0.05

Notes: (i) Factors C to F are crude estimates. Increase J_w if drainage measures are installed. (ii) Special problems caused by ice formation are not considered. (iii) For general characterisation of rock masses distant from excavation influences, the use of J_w = 1.0, 0.66, 0.5, 0.33, etc. as depth increases from say 0–5, 5–25, 25–250 to >250 m is recommended, assuming that RQD/J_n is low enough (e.g. 0.5–25) for good hydraulic connectivity. This will help to adjust Q for some of the effective stress and water softening effects, in combination with appropriate characterisation values of SRF. Correlations with depth-dependent static deformation modulus and seismic velocity will then follow the practice used when these were developed.

Table B- 4: Strength Reduction Factor (SRF) (Barton, 2002)

Description	UCS/σ_1	σ_t/σ_1	*SRF* Value
Low stress, near-surface	>200	>13	2.5
Medium stress	200-10	13-0.66	1.0
High stress, very tight structure (usually favourable to stability, may be unfavourable for wall stability)	10-5	0.66-0.33	0.5-2
Moderate slabbing after > 1 hour in massive rock	5-3	0.33-0.2	5-50
Slabbing and rockburst after a few minutes in massive rock	3-2	0.2-0.14	50-200
Heavy rockburst (strain burst) and immediate dynamic deformations in massive rock	<2	<0.14	200-400

Table B- 5: Excavation Parameter Category (Barton, 2002)

Excavation category		ESR
A	Temporary mine openings	**3 to 5**
B	Permanent mine openings, water tunnels for hydro power (excluding high pressure penstocks), pilot tunnels, drifts and headings for large excavations	1.6
C	Storage rooms, water treatment plants, minor road and railway tunnels, surge chambers, access tunnels.	1.3
D	Power stations, major road and railway tunnels, civil defence chambers, portal intersections.	1.0
E	Underground nuclear power stations, railway stations, sports and public facilities, factories.	0.8

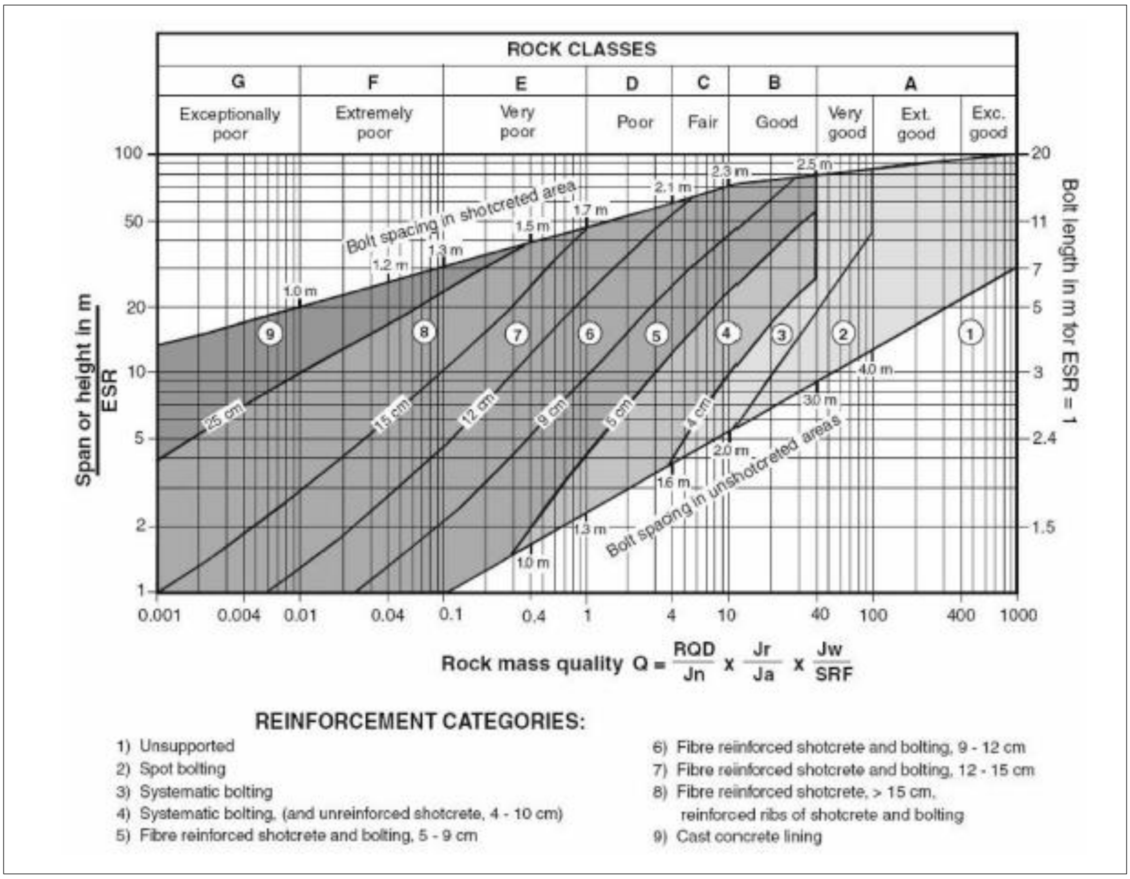

Figure B- 1: Tunnelling Quality Index estimated rock support classes (Barton, 2002)

Table B- 6: Mapping data,RQD, joint set number (Jn) ans strength reduction fator

Domain	Location	Rock formation	Discontinuity type	Joint Alteration	Ja	Water condition	Jw	Offset (mm)	Jr	RQD	Jn	SRF
1	X-6320.329 Y-16407.65	ARK	Bedding Plane	Slightly weathered	4	Dry (D)	1	6	0.9	75	3	2.5
	Z-1005.34	ARK	BD	Moderately weathered (MW)	4	Dry (D)	1	10	1.4			
		ARK	BD	MW	4	Dry (D)	1	5	0.85			
	X-6291.401	ARK	BD	MW	2	Dry (D)	1	11	1.5			
	Y-16306.34	ARK	BD	MW	2	Dry (D)	1	11	1.5			
	Z-1064.01	ARK	BD	MW	2	Dry (D)	1	13	1.6			
		ARK	BD	MW	2	Dry (D)	1	8	1.1			
		ARK	BD	MW	2	Dry (D)	1	12	1.5			
		ARK	BD	MW	2	Dry (D)	1	13	1.6			
		ARK	BD	MW	2	Dry (D)	1	11	1.5			
		ARK	BD	MW	2	Dry (D)	1	8	1.1			
		ARK	BD	MW	2	Dry (D)	1	9	1.3			
		ARK	BD	MW	2	Dry (D)	1	5	0.85			
		BAS	BD	Highly weathered (HW)	2	Dump	1	3	0.75			
		BAS	BD	MW	2	Dump	1	6	0.9			
		ARK	Face									
	X-6364.72	ARK	JN	MW	2	Dry (D)	1	8	1.1			
	Y- 16030.45	ARK	JN	MW	2	Dry (D)	1	8	1.1			
	Z- 1192.077	ARK	JN	MW	2	Dry (D)	1	6	0.9			
		ARK	JN	MW	2	Dry (D)	1	11	1.5			
	X-6384.8	ARK	JN	MW	2	Dry (D)	1	7	1			
	Y-16100.14	ARK	JN	MW	2	Dry (D)	1	13	1.6			
	Z-1187.496	ARK	JN	MW	2	Dry (D)	1	11	1.5			
		BAS	JN	MW	2	Dry (D)	1	11	1.5			
		BAS	JN	MW	2	Dry (D)	1	5	0.85			
		BAS	BD	MW	2	Dry (D)	1	9	1.3			
		BAS	BD	MW	2	Dry (D)	1	13	1.6			
		ARK	BD	MW	2	Dry (D)	1	6	0.9			
		ARK	BD	MW	2	Dry (D)	1	6	0.9			
		ARK	BD	MW	2	Dry (D)	1	12	1.5			

Table B- 7: Domain 1 rock mass rating, mine support and mining cost calculations

Area	Description	
Rock Mass Rating (Planar Domain) and Support requirements	GSI	81.4
	RQD	75
	Jn	3
	Jr	1.2
	Ja	2.2
	Jw	1
	SRF	2.5
	Excavation height (m)	182
	ESR	1.6
	De	113.75
	Q	**5.5**
	Rock mass class (Planar domain)	Fair
	Support Requirements based on Q	Fibre reignforced shotcret and bolting - 9 - 12cm
	Support Spacing (m)	2.2 by 2.2
	Support length (m)	20
Support Cost	Area requiring support	71,650
	Number of cable anchors	14,804
	total support meters	296,074
	Drlling cost/m ($)	6.6
	cost of one cable anchor ($)	344
	Grouting cost/m ($)	1.1
	Total cable anchor support cost	5,092,479
	Total Grouting cost ($)	325,681.82
	Shotcrete Thickness (m)	0.105
	Shotcrete volume (m^3)	7,523.25
	Cost of shotcrete/m^3 ($)	15.60
	Total cost of shotcrete ($)	117,362.70
	Labour cost of installation & shotcreting	553,552.39
	Total cost of support ($)	6,096,615
Mining Cost	Length of area to mine (m)	790
	Cross sectional Area to be mined(m^2)	10,215
	Volume of waste to be mined (m^3)	8,069,850
	Rock density (ton/m^3)	2.6
	waste to be mined (tons)	20,981,610
	Mining cost/ton ($)	2.8
	Total cost of mining ($)	58,748,508

APPENDIX C. GSI DATA AND STRENGTH PARAMETERS

Table C- 1: COPF/D GSI classification data and calculation of strength parameters for Domain 1 on the Footwall slope

AREA	Domain	ROCK TYPE	BENCH LEVEL		REMARKS	GSI VALUE	UCS (Mpa)	E (Gpa)	Cohesion (Kpa)	Phi (°)
			From	to						
Footwall	1	ARK	0	50	Slightly weathered blocky rock	76	260	14	22.5000	44.6
		ARK	50	100	Slightly weathered blocky rock	76	260	14	22.5000	44.6
		ARK	100	150	Slightly weathered blocky rock	77	260	14	23.0000	45.1
		ARK	150	200	Very good, Unweathered rock	89	260	14	30.7000	50.2
		ARK	200	300	Very good, Unweathered blocky rock	89	260	14	30.7000	50.2

Table C- 2: COPF/D GSI classification data and calculation of strength parameters for the Domain 2 on the Southwall slope

AREA	Domain	ROCK TYPE	BENCH LEVEL (MB)		REMARKS	GSI VALUE	UCS (Mpa)	E (Gpa)	Cohesion (Kpa)	Phi (°)
			From	to						
South wall	2	ARK	0	75	Moderately weathered with 3 joint sets	65	192	15	13.4000	39.6
		ARK	75	90	Unweathered blocky rock	85	200	15	21.2000	48.6
		ARK	90	105	Unweathered blocky rock	82	200	15	19.8000	47.3
		ARK	120	300	Very good, Unweathered blocky rock	82	200	14	19.8000	47.3
		BAS	75	90	unweathered blocky rock	85	345	16	37.0000	49.1
		BAS	90	105	Very good, Unweathered rock	90	345	16	42.3000	51.1
		BAS	120	300	Very good, Unweatheredrock	93	345	16	46.3000	52.3
		BAS,	0	75	Very poor Highly weathered and loose	15	5	16	0.1000	17.0

Table C- 3: COPF/D GSI classification data and calculation of strength parameters for the Domain 3 on the hanging wall slope

AREA	Domain	ROCK TYPE	BENCH LEVEL		REMARKS	GSI VALUE	UCS (Mpa)	E (Gpa)	Cohesion (Kpa)	Phi (°)
			From	to						
Hanging wall	3	URD	0	45	Very poor Highly weathered rock	20	5	3.3	0.1000	12.5
		URD	45	60	Poor and highly weathered	50	5	3.3	0.2000	24.3
		URD	60	75	unweathered rock with 3 joint sets	85	200	3.3	18.6000	39.6
		URD	75	90	unweathered rock with 3 joint sets	85	200	3.3	18.6000	39.6
		URD	90	105	unweathered rock with 3 joint sets	85	200	3.3	18.6000	39.6
		SWG	105	158	unweathered rock with 2 joint sets	85	180	6	16.4000	35.8
		SWG	105	158	unweathered rock with 2 joint sets	90	180	6	21.0000	37.6
		SWG	158	191	unweathered rock with 2 joint sets	90	180	6	21.0000	37.6
		SWG	158	191	unweathered rock with 2 joint sets	90	180	6	21.0000	37.6
		CDOL	191	193	Moderately weathered rock	53	100	3.8	5.4000	32.2
		CDOL	191	193	Moderately weathered rock	54	100	3.8	5.5000	32.5
		CDOL	191	193	Moderately weathered rock	54	100	3.8	5.5000	32.5
		DOLSCH	193	206	unweathered rock with 2 joint sets	90	180	4.5	20.5000	43.7
		DOLSCH	193	206	unweathered rock with 2 joint sets	90	180	4.5	20.5000	43.7
		DOLSCH	193	206	unweathered rock with 2 joint sets	86	180	4.5	17.6000	42.0
		UBS	206	221	unweathered with persistent bedding schistocity	85	130	3.8	11.9000	35.8
		UBS	206	221	unweathered with persistent bedding schistocity	82	130	3.8	10.4000	34.6
		UBS	206	221	unweathered with persistent bedding schistocity	85	130	3.8	11.9000	35.8
		TFQ	221	229	unweathered and very blocky rock.	74	180	7.9	13.7000	40.6
		TFQ	221	229	unweathered and very blocky rock.	74	180	7.9	13.7000	40.6
		TFQ	221	229	unweathered and very blocky rock.	72	180	7.9	13.1000	39.7
		BSSU	229	236	Slightly weathered with no interlocking	45	35	4.2	1.4000	26.5
		BSSU	229	236	Slightly weathered with no interlocking	40	35	4.2	1.3000	24.3
		BSSU	229	236	Slightly weathered with no interlocking	45	35	4.2	1.4000	26.5
		PQ	236	241	Unweathered rock	90	150	5.6	17.5000	47.6
		PQ	236	241	Unweathered rock	85	150	5.6	15.0000	45.5
		PQ	236	241	Unweathered rock	90	150	5.6	17.5000	47.6
		BSSL	241	248	Slightly weathered with no interlocking	40	20	3.5	0.7000	24.3
		BSSL	241	248	Slightly weathered with no interlocking	45	20	3.5	0.8000	26.5
		BSSL	241	248	Slightly weathered with no interlocking	45	20	3.5	0.8000	26.5
		LBS	248	264	unweathered with persistent bedding	85	170	2.5	15.5000	35.8
		LBS	248	264	unweathered with persistent bedding	82	170	2.5	13.6000	34.6
		LBS	248	264	unweathered with persistent bedding	85	170	2.5	15.5000	35.8
		ARK	264	300	Very good rock with atleast 3 joint sets	80	260	14	24.5000	46.4
		ARK	264	300	Very good rock with atleast 3 joint sets	85	260	14	27.6000	47.6
		ARK	264	300	Very good rock with atleast 3 joint sets	86	260	14	28.3000	49.0

APPENDIX D. UCS test result data

Table D- 1: UCS data for COPF/D

AREA	Rock Type	UCS(MPa)	Average UCS (Mpa)	Median UCS (Mpa)	Standard deviation
HANGING WALL	Weathered URD	5	184.71	200	42.6
	URD	193			
	URD	179			
	URD	200			
	URD	245			
	URD	241			
	URD	230			
	SWG	160	172	180	17.3
	SWG	160			
	SWG	180			
	SWG	180			
	SWG	180			
	CDOL	100	103	100	5.8
	CDOL	110			
	CDOL	100			
	DOLSCH	180	185	180	11.5
	DOLSCH	200			
	DOLSCH	180			
	DOLSCH	180			
	UBS	130	127.5	130	16.3
	UBS	120			
	UBS	130			
	UBS	130			
	TFQ	200	184	180	7.1
	TFQ	200			
	TFQ	160			
	TFQ	180			
	TFQ	180			
	BSSU	30	33.3	35	1.5
	BSSU	35			
	BSSU	35			
	PQ	150	166.7	150	3.1
	PQ	150			
	PQ	200			

AREA	Rock Type	UCS(MPa)	Average UCS (Mpa)	Median UCS (Mpa)	Standard deviation
HANGING WALL	BSSL	20	16.7	20	2.5
	BSSL	20			
	BSSL	10			
	LBS	180	155	170	11.5
	LBS	160			
	LBS	180			
	LBS	100			
FOOTWALL	ARK	260	261	260	44.37
	ARK	260			
	ARK	250			
	ARK	250			
	ARK	260			
	ARK	280			
	ARK	260			
	ARK	260			
	ARK	260			
	ARK	280			
	ARK	250			
SOUTHWALL	Weathered BAS	5	247	345	5
	BAS	340			
	BAS	350			
	BAS	345			
	BAS	350			
	ARK	200	225	225	27.1
	ARK	200			
	ARK	250			
	ARK	250			
	ARK	250			
	ARK	200			

APPENDIX E. COPF/D Strength parameters from mine Database

Table E- 1: COPF/D strength parameters from mine database

ROCK UNIT	COHESION (KPa)	FRICTION ANGLE (°)
URD	20.00	15.00
SWG	48.00	18.00
CDOL	30.00	18.00
DOLSCH	43.00	20.00
UBS	65.00	19.00
TFQ	78.00	28.50
BSSU	71.00	27.00
PQ	48.50	22.00
BSSL	78.00	22.00
LBS	76.00	23.50
ARK	50.00	20.00
BAS	42.00	17.00

APPENDIX F. COPF/D Rock properties

Table F- 1: COPF/D rock properties

Rock Formation	In-Situ unit weight (KN/m^3)	Modulus of Elasticity (MPa)
URD	26.8	3.3
SWG	26.8	6.0
CDOL	26.8	3.8
DOLSCH	26.8	4.5
UBS	26.8	3.8
TFQ	26.8	7.9
BSSU	26.8	4.2
PQ	26.8	5.6
BSSL	26.8	3.5
LBS	26.8	2.5
ARK	28.0	14.0
BAS	28.0	16.0

APPENDIX G. COPF/D STRUCTURAL/MAPPING DATA

Table G- 1: COPF/D structural data for Domain 1 on the footwall

Domain	Location	Rock formation	Discontinuity type	Dip (°)	Dip Direction (°)	Aperture	Infilling	Joint Alteration	Water condition	Offset
1	X-6320.329	ARK	Face	44	276					
	Y-16407.65	ARK	Bedding Plane (BD)	39	256	1	sand	Slightly weathered (SW)	Dry (D)	6
	Z-1005.34	ARK	BD	44	263	1	sand	Moderately weathered (MW)	D	10
		ARK	BD	50	259	1	sand	MW	D	5
	X-6291.401	ARK	BD	52	259	1	iron stained	MW	D	11
	Y-16306.34	ARK	BD	47	273	1	iron stained	MW	D	11
	Z-1064.01	ARK	BD	39	267	1	iron stained	MW	D	13
		ARK	BD	44	287	1	iron stained	MW	D	8
		ARK	BD	46	273	1	iron stained	MW	D	12
		ARK	BD	50	268	1	iron stained	MW	D	13
		ARK	BD	35	258	1	iron stained	MW	D	11
		ARK	BD	50	273	1	iron stained	MW	D	8
		ARK	BD	42	277	1	iron stained	MW	D	9
		ARK	BD	42	258	1	iron stained	MW	D	5
		BAS	BD	42	297	1	iron stained	Highly weathered (HW)	Dump	3
		BAS	BD	56	253	1	iron stained	MW	Dump	6
		ARK	Face	37	270					
	X-6364.72	ARK	JN	75	98	1	iron stained	MW	D	8
	Y- 16030.45	ARK	JN	70	94	1	iron stained	MW	D	8
	Z- 1192.077	ARK	JN	75	98	1	iron stained	MW	D	6
		ARK	JN	70	96	1	iron stained	MW	D	11
	X-6384.8	ARK	JN	75	3	1	iron stained	MW	D	7
	Y-16100.14	ARK	JN	75	10	1	iron stained	MW	D	13
	Z-1187.496	ARK	JN	75	4	1	iron stained	MW	D	11
		BAS	JN	90	4	1	iron stained	MW	D	11
		BAS	JN	75	16	1	iron stained	MW	D	5
		BAS	BD	40	295	1	iron stained	MW	D	9
		BAS	BD	40	254	1	iron stained	MW	D	13
		ARK	BD	45	265	1	iron stained	MW	D	6
		ARK	BD	30	260	1	iron stained	MW	D	6
		ARK	BD	40	251	1	iron stained	MW	D	12

Table G- 2: COPF/D structural data for Domain 2 on the South wall

Domain	Location	Rock forma	Discontinuity t	Dip (°)	Dip Direction (°)	Aperture	Infilling	Joint Alteration	Water condition	Offset
	X-6123.64	ARK	Face	65	347					
2	Y-15668.05	ARK	BD	40	319	1	iron stained	MW	D	18
	Z-1159	ARK	BD	44	311	1	iron stained	MW	D	7
		ARK	BD	70	315	1	iron stained	MW	D	6
	X-6150.82	ARK	BD	71	328	1	iron stained	MW	D	11
	Y-15655.33	ARK	BD	45	312	1	iron stained	MW	D	8
	Z-1159	ARK	JN	84	214	1	iron stained	MW	D	6
		ARK	JN	62	204	1	iron stained	MW	D	12
		ARK	JN	77	81	1	iron stained	MW	D	9
		ARK	BP	45	314	1	iron stained	MW	D	7
		BAS	JN	82	244	1	iron stained	MW	D	10
		BAS	BD	45	303	1	iron stained	MW	D	13

Table G- 3: COPF/D structural data for Domain 3 on the Hanging wall

Domain	Location	Rock formation	Discontinuity type	Dip (°)	Dip Direction (°)	Aperture	Infilling	Joint Alteration	Water condition	Offset
	X-6031.648	URD	Face	76	55					
	Y-15469.95	URD	JN	86	102	5	sand	Slightly Weathe	D	8
	Z-1258.667	URD	JN	81	16	3	sand	SW	D	8
		URD	JN	85	28	3	sand	SW	D	8
		URD	JN	89	8	5	sand	SW	D	7
	X-5945.908	URD	JN	90	12	5	sand	SW	D	7
	Y-15508.4	URD	JN	74	50	5	sand	SW	D	6
	Z-1267.833	URD	JN	86	359	4	sand	SW	D	8
		URD	JN	81	346	2	iron stained	SW	D	8
		URD	VIEN (VN)	75	93	50	sandstone	SW	D	8
		URD	JN	90	176	2	sand	SW	D	8
		URD	VN	74	171	2	sand	SW	D	8
		URD	JN	64	10	120	quartz	SW	D	6
		URD	VN	80	96	2	sand	SW	D	6
		URD	JN	70	113	5	sand	SW	D	6
		URD	JN	80	88	5	sand	SW	D	7
		URD	JN	84	29	2	sand	SW	D	7
		URD	JN	80	92	1	iron stained	SW	D	7
			Face	72	122					
	X-6159.204	TFQ	JN	79	143	1	iron stained	SW	D	10
	Y-16326.23	TFQ	JN	50	96	1	iron stained	SW	D	5
	Z-1093.078	TFQ	BD	46	263	1	iron stained	SW	D	5
		TFQ	VN	55	28	20	quatz	SW	D	5
		TFQ	JN	55	142	2	quatz	SW	D	5
	X-6198.181	TFQ	JN	52	103	1	iron stained	SW	D	6
	Y-16455.71	TFQ	JN	89	11	1	iron stained	SW	D	6
	Z-1107.377	TFQ	VN	50	52	43	quatz	SW	D	6
3		TFQ	JN	40	125	10	quatz	SW	D	6
		TFQ	VN	49	37	150	quatz	SW	D	7
		TFQ	BD	35	258	1	sand	SW	D	6
		TFQ	VN	74	100	45	quatz	SW	D	5
		TFQ	VN	52	92	15	quatz	SW	D	5
		TFQ	JN	75	107	1	iron stained	SW	D	5
		TFQ	JN	50	54	1	iron stained	SW	D	5
		TFQ	JN	52	148	1	iron stained	SW	D	6
		TFQ	VN	40	81	45	quatz	SW	D	5
		TFQ	JN	55	44	1	iron stained	SW	D	5
		TFQ	JN	67	140	1	iron stained	SW	D	7
		TFQ	JN	67	88	1	iron stained	SW	D	5
	X-6264.72		Face	70	20					
	Y-16007.45	TFQ	JN	65	145	1	iron stained	SW	D	6
	Z- 1192.077	TFQ	BD	46	292	1	iron stained	SW	D	6
		TFQ	JN	70	90	1	iron stained	SW	D	8
		TFQ	JN	60	152	1	iron stained	SW	D	6
	X-6284.8	TFQ	BD	45	205	1	iron stained	SW	D	6
	Y-16070.14	TFQ	JN	70	125	1	iron stained	SW	D	7
	Z-1187.496	PQ	JN	60	104	1	iron stained	Unweathered (U)	D	7
		PQ	JN	71	175	1	iron stained	U	D	6
		PQ	JN	75	202	1	iron stained	U	D	7
		BSSL	BD	50	295	2	sand	SW	Dump	4
		BSSU	JN	90	231	2	sand	SW	Dump	3
		BSSU	JN	75	55	2	sand	SW	Dump	6
		ARK	JN	80	74	1	iron stained	U	D	8
		ARK	JN	75	96	1	iron stained	U	D	6
		ARK	JN	85	26	1	iron stained	U	D	12
		ARK	BD	35	310	1	iron stained	U	D	9

APPENDIX H. COPF/D Discontinuity offset measurement data and friction angle (Phi) calculation

Table H- 1: Offset data and Phi calculation for Domain 3 on the Hangingwall

Domain	Location	Rock formation	Discontinuity type	Joint Alteration	Ja	Water condition	Jw	Offset (mm)	Jr	Phi (°)
	X-6320.329	ARK	Face							
	Y-16407.65	ARK	Bedding Plane (BP)	Slightly weathered (SW)	4	Dry (D)	1	6	0.9	12.7
	Z-1005.34	ARK	BP	Moderately weathered (MW)	4	Dry (D)	1	10	1.4	19.3
		ARK	BP	MW	4	Dry (D)	1	5	0.85	12.0
	X-6291.401	ARK	BP	MW	2	Dry (D)	1	11	1.5	36.9
	Y-16306.34	ARK	BP	MW	2	Dry (D)	1	11	1.5	36.9
	Z-1064.01	ARK	BP	MW	2	Dry (D)	1	13	1.6	38.7
		ARK	BP	MW	2	Dry (D)	1	8	1.1	28.8
		ARK	BP	MW	2	Dry (D)	1	12	1.5	36.9
		ARK	BP	MW	2	Dry (D)	1	13	1.6	38.7
		ARK	BP	MW	2	Dry (D)	1	11	1.5	36.9
		ARK	BP	MW	2	Dry (D)	1	8	1.1	28.8
		ARK	BP	MW	2	Dry (D)	1	9	1.3	33.0
		ARK	BP	MW	2	Dry (D)	1	5	0.85	23.0
1		ARK	Face							
		ARK	JN	MW	2	Dry (D)	1	8	1.1	28.8
		ARK	JN	MW	2	Dry (D)	1	8	1.1	28.8
		ARK	JN	MW	2	Dry (D)	1	6	0.9	24.2
	X-6364.72	ARK	JN	MW	2	Dry (D)	1	11	1.5	36.9
	Y- 16030.45	ARK	JN	MW	2	Dry (D)	1	7	1	26.6
	Z- 1192.077	ARK	JN	MW	2	Dry (D)	1	13	1.6	38.7
		ARK	JN	MW	2	Dry (D)	1	11	1.5	36.9
	X-6384.8	ARK	BD	MW	2	Dry (D)	1	6	0.9	24.2
	Y-16100.14	ARK	BD	MW	2	Dry (D)	1	6	0.9	24.2
	Z-1187.496	ARK	BD	MW	2	Dry (D)	1	12	1.5	36.9
		BAS	BP	Highly weathered (HW)	2	Dump	1	3	0.75	20.6
		BAS	BP	MW	2	Dump	1	6	0.9	24.2
		BAS	JN	MW	2	Dry (D)	1	11	1.5	36.9
		BAS	JN	MW	2	Dry (D)	1	5	0.85	23.0
		BAS	BD	MW	2	Dry (D)	1	9	1.3	33.0
		BAS	BD	MW	2	Dry (D)	1	13	1.6	38.7

Table H- 2: Offset data and Phi calculation for Domain 2 on the Footwall

Domain	Location	Rock formation	Discontinuity type	Joint Alteration	Ja	Water condition	Jw	Offset (mm)	Jr	Phi (°)
	X-6123.64	ARK	Face							
	Y-15668.05	ARK	BP	MW	2	Dry (D)	1	18	2.5	51.4
	Z-1159	ARK	BP	MW	2	Dry (D)	1	7	7	74.1
		ARK	BP	MW	2	Dry (D)	1	6	0.9	24.2
	X-6150.82	ARK	BP	MW	2	Dry (D)	1	11	1.5	36.9
	Y-15655.33	ARK	BP	MW	2	Dry (D)	1	8	1.1	28.8
2	Z-1159	ARK	JN	MW	2	Dry (D)	1	6	0.9	24.2
		ARK	JN	MW	2	Dry (D)	1	12	1.5	36.9
		ARK	JN	MW	2	Dry (D)	1	9	1.3	33.0
		ARK	BP	MW	2	Dry (D)	1	7	1	26.6
		BAS	JN	MW	2	moderately wet	0.66	10	1.4	24.8
		BAS	BP	MW	2	moderately wet	0.66	13	1.6	27.8

Table H- 3: Offset data and Phi calculation for Domain 3 on the Hangingwall

Domain	Location	Rock formation	Discontinuity type	Joint Alteration	Ja	Water condition	Jw	Offset (mm)	Jr	Phi (°)
	X-6031.648	URD	Face	Slightly Weathered (SW)						
	Y-15469.95	URD	JN	SW	4	Dry (D)	1	8	1.1	15.4
	Z-1258.667	URD	JN	SW	4	Dry (D)	1	8	1.1	15.4
		URD	JN	SW	4	Dry (D)	1	8	1.1	15.4
		URD	JN	SW	4	Dry (D)	1	7	1	14.0
	X-5945.908	URD	JN	SW	4	Dry (D)	1	7	1	14.0
	Y-15508.4	URD	JN	SW	4	Dry (D)	1	6	0.9	12.7
	Z-1267.833	URD	JN	SW	4	Dry (D)	1	8	1.1	15.4
		URD	JN	SW	2	Dry (D)	1	8	1.1	28.8
		URD	JN	SW	0.75	Dry (D)	1	8	1.1	55.7
		URD	JN	SW	4	Dry (D)	1	8	1.1	15.4
		URD	VN	SW	4	Dry (D)	1	8	1.1	15.4
		URD	JN	SW	0.75	Dry (D)	1	6	0.9	50.2
		URD	JN	SW	4	Dry (D)	1	6	0.9	12.7
		URD	JN	SW	4	Dry (D)	1	6	0.9	12.7
		URD	JN	SW	4	Dry (D)	1	7	1	14.0
		URD	JN	SW	4	Dry (D)	1	7	1	14.0
		URD	JN	SW	2	Dry (D)	1	7	1	26.6
	X-6159.204	TFQ	JN	SW	2	Dry (D)	1	10	1.4	35.0
	Y-16326.23	TFQ	JN	SW	2	Dry (D)	1	5	0.85	23.0
	Z-1093.078	TFQ	BD	SW	2	Dry (D)	1	5	0.85	23.0
		TFQ	VN	SW	0.75	Dry (D)	1	5	0.85	48.6
		TFQ	JN	SW	0.75	Dry (D)	1	5	0.85	48.6
	X-6198.181	TFQ	JN	SW	2	Dry (D)	1	6	0.9	24.2
	Y-16455.71	TFQ	JN	SW	2	Dry (D)	1	6	0.9	24.2
	Z-1107.377	TFQ	VN	SW	0.75	Dry (D)	1	6	0.9	50.2
3		TFQ	JN	SW	0.75	Dry (D)	1	6	0.9	50.2
		TFQ	VN	SW	0.75	Dry (D)	1	7	1	53.2
		TFQ	BD	SW	4	Dry (D)	1	6	0.9	12.7
		TFQ	VN	SW	0.75	Dry (D)	1	5	0.85	48.6
		TFQ	VN	SW	0.75	Dry (D)	1	5	0.85	48.6
		TFQ	JN	SW	2	Dry (D)	1	5	0.85	23.0
		TFQ	JN	SW	2	Dry (D)	1	5	0.85	23.0
		TFQ	JN	SW	2	Dry (D)	1	6	0.9	24.2
		TFQ	VN	SW	0.75	Dry (D)	1	5	0.85	48.6
		TFQ	JN	SW	2	Dry (D)	1	5	0.85	23.0
		TFQ	JN	SW	2	Dry (D)	1	7	1	26.6
		TFQ	JN	SW	2	Dry (D)	1	5	0.85	23.0
	X-6264.72									
	Y-16007.45	TFQ	JN	SW	2	Dry (D)	1	6	0.9	24.2
	Z- 1192.077	TFQ	BD	SW	2	Dry (D)	1	6	0.9	24.2
		TFQ	JN	SW	2	Dry (D)	1	8	1.1	28.8
		TFQ	JN	SW	2	Dry (D)	1	6	0.9	24.2
	X-6284.8	TFQ	BD	SW	2	Dry (D)	1	6	0.9	24.2
	Y-16070.14	TFQ	JN	SW	2	Dry (D)	1	7	1	26.6
	Z-1187.496	ARK	JN	Unweathered (U)	1	Dry (D)	1	8	1.1	47.8
		ARK	JN	U	1	Dry (D)	1	6	0.9	42.0
		ARK	JN	U	1	Dry (D)	1	12	1.5	56.3
		ARK	BD	SW	4	Dump	1	9	1.3	18.0
		PQ	JN	SW	4	Dump	1	7	1	14.0
		PQ	JN	SW	4	Dump	1	6	0.9	12.7
		PQ	JN	U	1	Dry (D)	1	7	1	45.0
		BSSL	BD	U	1	Dry (D)	1	4	0.7	35.0
		BSSU	JN	U	1	Dry (D)	1	3	6.5	81.3
		BSSU	JN	U	1	Dry (D)	1	6	0.9	42.0

APPENDIX I. COPF/D GROUNDWATER LEVELS

Table I - 1: COPF/D pit groundwater levels piezometer readings from the hanging wall and south wall

DATE	Southern-120mB(PZ5)	Water level change	Northern-NEW 120mB(3PZ4)	Water level change	Southern-NEW 90mB(3PZ2)	Water level change	0mB-SS7	Water level change
01.12.22	1227.05		1210.81		1201.26		1293.60	
02.12.22	1227.44	0.39	1211.22	0.41	1201.65	0.39	1293.24	-0.36
03.01.23	1227.96	0.51	1211.91	0.69	1201.25	-0.40	1292.85	-0.39
04.01.23	1228.65	0.69	1212.09	0.18	1200.94	-0.31	1292.44	-0.41
05.02.23	1228.93	0.28	1211.78	-0.31	1200.47	-0.47	1291.85	-0.58
06.02.23	1229.34	0.40	1211.58	-0.20	1201.07	0.60	1291.00	-0.85
07.02.23	1229.07	-0.27	1212.19	0.62	1200.92	-0.15	1290.42	-0.58
08.02.23	1228.71	-0.36	1211.73	-0.46	1200.52	-0.40	1290.00	-0.43
09.02.23	1228.22	-0.49	1211.36	-0.37	1200.05	-0.47	1289.68	-0.31
10.02.23	1227.91	-0.30	1210.97	-0.39	1199.57	-0.48	1290.52	0.84
27.02.23	1228.63	0.72	1211.44	0.47	1199.04	-0.53	1290.25	-0.27
02.03.23	1229.28	0.65	1211.92	0.48	1198.66	-0.38	1289.94	-0.31
13.03.23	1230.02	0.74	1212.38	0.46	1198.29	-0.37	1289.36	-0.58
20.03.23	1230.50	0.48	1211.59	-0.79	1198.81	0.51	1289.63	0.27
28.03.23	1231.19	0.69	1211.29	-0.30	1198.52	-0.29	1290.25	0.63
03.04.23	1231.45	0.26	1211.12	-0.17	1198.26	-0.26	1291.10	0.85
10.04.23	1231.98	0.53	1211.59	0.47	1198.57	0.31	1292.02	0.92
18.04.23	1232.78	0.81	1212.23	0.64	1199.10	0.53	1292.66	0.64
23.04.23	1232.69	-0.09	1212.81	0.58	1199.58	0.48	1293.41	0.75
28.04.23	1232.45	-0.24	1213.43	0.63	1198.97	-0.62	1294.47	1.06
02.05.23	1232.13	-0.32	1214.46	1.03	1200.04	1.07	1295.10	0.63
08.05.23	1232.10	-0.03	1213.51	-0.95	1201.74	1.70	1295.51	0.41
16.05.23	1231.90	-0.20	1212.25	-1.26	1202.74	1.00	1295.09	-0.43
24.05.23	1231.20	-0.70	1211.54	-0.70	1203.67	0.93	1296.04	0.95
26.05.23	1232.90	1.70	1211.15	-0.39	1204.63	0.96	1296.33	0.29
28.05.23	1232.60	-0.30	1210.57	-0.58	1206.52	1.89	1297.75	1.42
30.05.23	1232.90	0.30	1210.02	-0.55	1207.24	0.72	1299.11	1.35
01.06.23	1236.17	3.27	1211.93	1.91	1210.80	3.56	1299.49	0.38
02.06.23	1236.34	0.17	1211.85	-0.08	1210.83	0.03	1299.51	0.02
03.06.23	1236.83	0.49	1211.26	-0.59	1209.68	-1.15	1299.40	-0.11
09.06.23	1237.08	0.25	1211.15	-0.11	1209.55	-0.13	1299.38	-0.02
10.06.23	1237.52	0.44	1211.93	0.78	1210.80	1.25	1299.49	0.11
	Average water leve change	0.34		0.04		0.31		0.19

Table I - 2: Piezometer PZ5 calculation of Ru

PZ5							
Borehole Bottom elevation (m)	**Water elevation (m)**	**Height of water in borehole (m)**	**Unit weight of water(KN/m^3)**	**Pore Pressure(Kpa)**	**Unit weight of rock(KN/m^3)**	**overburdun height (h)**	**Ru**
1098.52	1227.053	128.5	9.8	1259.6	26.8	234.5	0.20
1098.52	1227.445	128.9	9.8	1263.5	26.8	234.5	0.20
1098.52	1227.959	129.4	9.8	1268.5	26.8	234.5	0.20
1098.52	1228.653	130.1	9.8	1275.3	26.8	234.5	0.20
1098.52	1228.933	130.4	9.8	1278.0	26.8	234.5	0.20
1098.52	1229.336	130.8	9.8	1282.0	26.8	234.5	0.20
1098.52	1229.067	130.5	9.8	1279.4	26.8	234.5	0.20
1098.52	1228.709	130.2	9.8	1275.9	26.8	234.5	0.20
1098.52	1228.217	129.7	9.8	1271.0	26.8	234.5	0.20
1098.52	1227.915	129.4	9.8	1268.1	26.8	234.5	0.20
1098.52	1228.631	130.1	9.8	1275.1	26.8	234.5	0.20
1098.52	1229.28	130.8	9.8	1281.4	26.8	234.5	0.20
1098.52	1230.018	131.5	9.8	1288.7	26.8	234.5	0.21
1098.52	1230.5	132.0	9.8	1293.4	26.8	234.5	0.21
1098.52	1231.193	132.7	9.8	1300.2	26.8	234.5	0.21
1098.52	1231.451	132.9	9.8	1302.7	26.8	234.5	0.21
1098.52	1231.977	133.5	9.8	1307.9	26.8	234.5	0.21
1098.52	1232.782	134.3	9.8	1315.8	26.8	234.5	0.21
1098.52	1232.69	134.2	9.8	1314.9	26.8	234.5	0.21
1098.52	1232.45	133.9	9.8	1312.5	26.8	234.5	0.21
1098.52	1232.13	133.6	9.8	1309.4	26.8	234.5	0.21
1098.52	1232.1	133.6	9.8	1309.1	26.8	234.5	0.21
1098.52	1231.9	133.4	9.8	1307.1	26.8	234.5	0.21
1098.52	1231.2	132.7	9.8	1300.3	26.8	234.5	0.21
1098.52	1232.9	134.4	9.8	1316.9	26.8	234.5	0.21
1098.52	1232.6	134.1	9.8	1314.0	26.8	234.5	0.21
1098.52	1232.9	134.4	9.8	1316.9	26.8	234.5	0.21
1098.52	1236.173	137.7	9.8	1349.0	26.8	234.5	0.21
1098.52	1236.341	137.8	9.8	1350.6	26.8	234.5	0.21
1098.52	1236.833	138.3	9.8	1355.5	26.8	234.5	0.22
1098.52	1237.079	138.6	9.8	1357.9	26.8	234.5	0.22
1098.52	1237.516	139.0	9.8	1362.2	26.8	234.5	0.22
						Maximum Ru	0.22

Table I - 3: Piezometer 3PZ4 calculation of Ru

3PZ4							
Borehole Bottom elevation (m)	**Water elevation (m)**	**Height of water in borehole (m)**	**Unit weight of water(KN/m^3)**	**Pore Pressure (Kpa)**	**Unit weight of rock(KN/m^3)**	**overburdun height (h)**	**Ru**
1015.54	1210.805	195.3	9.8	1913.6	26.8	317.5	0.22
1015.54	1211.219	195.7	9.8	1917.7	26.8	317.5	0.23
1015.54	1211.913	196.4	9.8	1924.5	26.8	317.5	0.23
1015.54	1212.092	196.6	9.8	1926.2	26.8	317.5	0.23
1015.54	1211.779	196.2	9.8	1923.1	26.8	317.5	0.23
1015.54	1211.577	196.0	9.8	1921.2	26.8	317.5	0.23
1015.54	1212.193	196.7	9.8	1927.2	26.8	317.5	0.23
1015.54	1211.734	196.2	9.8	1922.7	26.8	317.5	0.23
1015.54	1211.365	195.8	9.8	1919.1	26.8	317.5	0.23
1015.54	1210.973	195.4	9.8	1915.2	26.8	317.5	0.23
1015.54	1211.443	195.9	9.8	1919.8	26.8	317.5	0.23
1015.54	1211.924	196.4	9.8	1924.6	26.8	317.5	0.23
1015.54	1212.383	196.8	9.8	1929.1	26.8	317.5	0.23
1015.54	1211.589	196.0	9.8	1921.3	26.8	317.5	0.23
1015.54	1211.286	195.7	9.8	1918.3	26.8	317.5	0.23
1015.54	1211.119	195.6	9.8	1916.7	26.8	317.5	0.23
1015.54	1211.589	196.0	9.8	1921.3	26.8	317.5	0.23
1015.54	1212.226	196.7	9.8	1927.5	26.8	317.5	0.23
1015.54	1212.808	197.3	9.8	1933.2	26.8	317.5	0.23
1015.54	1213.435	197.9	9.8	1939.4	26.8	317.5	0.23
1015.54	1214.464	198.9	9.8	1949.5	26.8	317.5	0.23
1015.54	1213.513	198.0	9.8	1940.1	26.8	317.5	0.23
1015.54	1212.249	196.7	9.8	1927.7	26.8	317.5	0.23
1015.54	1211.544	196.0	9.8	1920.8	26.8	317.5	0.23
1015.54	1211.152	195.6	9.8	1917.0	26.8	317.5	0.23
1015.54	1210.57	195.0	9.8	1911.3	26.8	317.5	0.22
1015.54	1210.022	194.5	9.8	1905.9	26.8	317.5	0.22
1015.54	1211.93	196.4	9.8	1924.6	26.8	317.5	0.23
1015.54	1211.85	196.3	9.8	1923.8	26.8	317.5	0.23
1015.54	1211.26	195.7	9.8	1918.1	26.8	317.5	0.23
1015.54	1211.15	195.6	9.8	1917.0	26.8	317.5	0.23
1015.54	1211.93	196.4	9.8	1924.6	26.8	317.5	0.23
						Maximum Ru	0.23

Table I - 4: Piezometer 3PZ2 calculation of Ru

3PZ2							
Borehole Bottom elevation (m)	**Water elevation (m)**	**Height of water in borehole (m)**	**Unit weight of water(KN/m^3)**	**Pore Pressure (Kpa)**	**Unit weight of rock(KN/m^3)**	**overburdun height (h)**	**Ru**
1051.02	1201.26	150.2	9.8	1472.4	26.8	282.0	0.19
1051.02	1201.652	150.6	9.8	1476.2	26.8	282.0	0.20
1051.02	1201.249	150.2	9.8	1472.2	26.8	282.0	0.19
1051.02	1200.936	149.9	9.8	1469.2	26.8	282.0	0.19
1051.02	1200.466	149.4	9.8	1464.6	26.8	282.0	0.19
1051.02	1201.07	150.0	9.8	1470.5	26.8	282.0	0.19
1051.02	1200.924	149.9	9.8	1469.1	26.8	282.0	0.19
1051.02	1200.522	149.5	9.8	1465.1	26.8	282.0	0.19
1051.02	1200.052	149.0	9.8	1460.5	26.8	282.0	0.19
1051.02	1199.57	148.6	9.8	1455.8	26.8	282.0	0.19
1051.02	1199.045	148.0	9.8	1450.6	26.8	282.0	0.19
1051.02	1198.664	147.6	9.8	1446.9	26.8	282.0	0.19
1051.02	1198.295	147.3	9.8	1443.3	26.8	282.0	0.19
1051.02	1198.81	147.8	9.8	1448.3	26.8	282.0	0.19
1051.02	1198.519	147.5	9.8	1445.5	26.8	282.0	0.19
1051.02	1198.261	147.2	9.8	1443.0	26.8	282.0	0.19
1051.02	1198.575	147.6	9.8	1446.0	26.8	282.0	0.19
1051.02	1199.1	148.1	9.8	1451.2	26.8	282.0	0.19
1051.02	1199.582	148.6	9.8	1455.9	26.8	282.0	0.19
1051.02	1198.966	147.9	9.8	1449.9	26.8	282.0	0.19
1051.02	1200.04	149.0	9.8	1460.4	26.8	282.0	0.19
1051.02	1201.741	150.7	9.8	1477.1	26.8	282.0	0.20
1051.02	1202.737	151.7	9.8	1486.8	26.8	282.0	0.20
1051.02	1203.666	152.6	9.8	1495.9	26.8	282.0	0.20
1051.02	1204.628	153.6	9.8	1505.4	26.8	282.0	0.20
1051.02	1206.519	155.5	9.8	1523.9	26.8	282.0	0.20
1051.02	1207.236	156.2	9.8	1530.9	26.8	282.0	0.20
1051.02	1210.8	159.8	9.8	1565.8	26.8	282.0	0.21
1051.02	1210.83	159.8	9.8	1566.1	26.8	282.0	0.21
1051.02	1209.68	158.7	9.8	1554.9	26.8	282.0	0.21
1051.02	1209.55	158.5	9.8	1553.6	26.8	282.0	0.21
1051.02	1210.8	159.8	9.8	1565.8	26.8	282.0	0.21
						Maximum Ru	0.21

Table I - 5: Piezometer SS7 calculation of Ru

SS7							
Borehole Bottom elevation (m)	**Water elevation (m)**	**Height of water in borehole (m)**	**Unit weight of water(KN/m^3)**	**Pore Pressure (Kpa)**	**Unit weight of rock(KN/m^3)**	**overburdun height (h)**	**Ru**
1127.47	1293.6	166.1	9.8	1628.1	28	205.53	0.28
1127.47	1293.2419	165.8	9.8	1624.6	28	205.53	0.28
1127.47	1292.8503	165.4	9.8	1620.7	28	205.53	0.28
1127.47	1292.4363	165.0	9.8	1616.7	28	205.53	0.28
1127.47	1291.8544	164.4	9.8	1611.0	28	205.53	0.28
1127.47	1291.0039	163.5	9.8	1602.6	28	205.53	0.28
1127.47	1290.4221	163.0	9.8	1596.9	28	205.53	0.28
1127.47	1289.9968	162.5	9.8	1592.8	28	205.53	0.28
1127.47	1289.6835	162.2	9.8	1589.7	28	205.53	0.28
1127.47	1290.5228	163.1	9.8	1597.9	28	205.53	0.28
1127.47	1290.2542	162.8	9.8	1595.3	28	205.53	0.28
1127.47	1289.9409	162.5	9.8	1592.2	28	205.53	0.28
1127.47	1289.359	161.9	9.8	1586.5	28	205.53	0.28
1127.47	1289.6276	162.2	9.8	1589.1	28	205.53	0.28
1127.47	1290.2542	162.8	9.8	1595.3	28	205.53	0.28
1127.47	1291.1046	163.6	9.8	1603.6	28	205.53	0.28
1127.47	1292.0222	164.6	9.8	1612.6	28	205.53	0.28
1127.47	1292.6601	165.2	9.8	1618.9	28	205.53	0.28
1127.47	1293.4098	165.9	9.8	1626.2	28	205.53	0.28
1127.47	1294.4728	167.0	9.8	1636.6	28	205.53	0.28
1127.47	1295.0995	167.6	9.8	1642.8	28	205.53	0.29
1127.47	1295.5135	168.0	9.8	1646.8	28	205.53	0.29
1127.47	1295.0883	167.6	9.8	1642.7	28	205.53	0.29
1127.47	1296.0394	168.6	9.8	1652.0	28	205.53	0.29
1127.47	1296.3304	168.9	9.8	1654.8	28	205.53	0.29
1127.47	1297.7515	170.3	9.8	1668.8	28	205.53	0.29
1127.47	1299.1055	171.6	9.8	1682.0	28	205.53	0.29
1127.47	1299.49	172.0	9.8	1685.8	28	205.53	0.29
1127.47	1299.51	172.0	9.8	1686.0	28	205.53	0.29
1127.47	1299.4	171.9	9.8	1684.9	28	205.53	0.29
1127.47	1299.38	171.9	9.8	1684.7	28	205.53	0.29
1127.47	1299.49	172.0	9.8	1685.8	28	205.53	0.29
						Maximum Ru	0.29

APPENDIX J. COPF/D NUMERICAL STABILITY ANALYSIS RESULTS OF SLIDE AND RS2 SOFTWARE

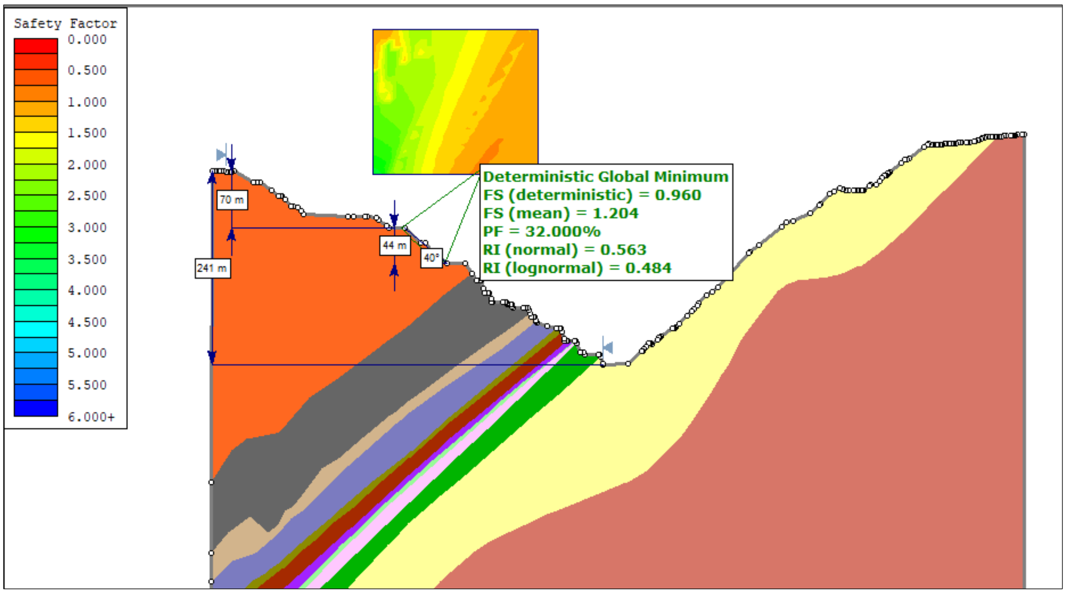

Figure J- 1: Slide2 section A-A overall slope analysis result

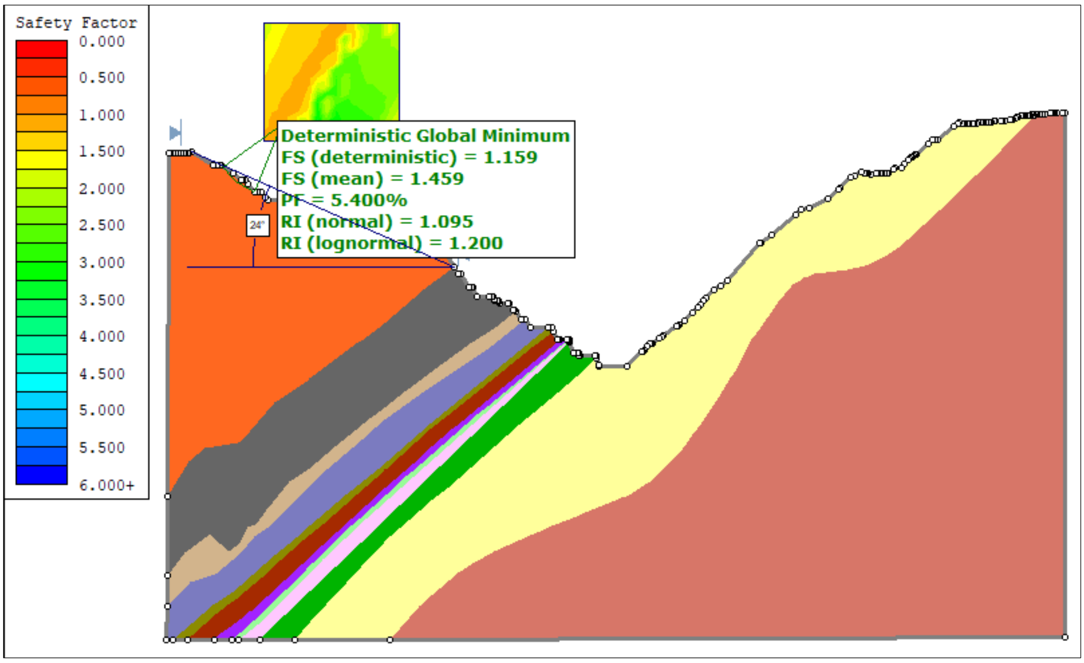

Figure J- 2: Slide2 simulated section A-A Upper stack slope analysis result

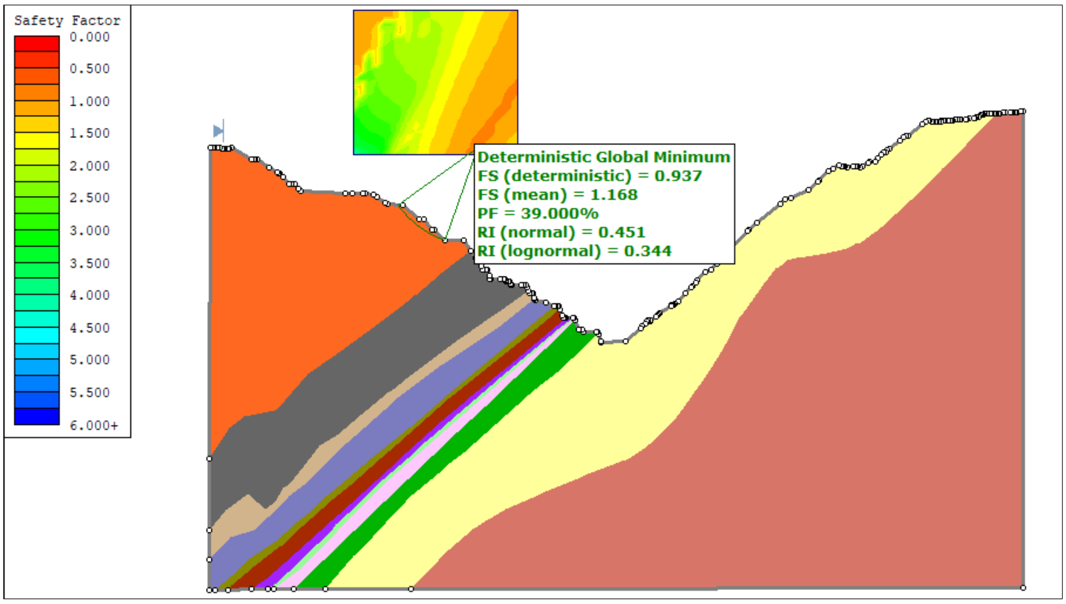

Figure J- 3: Slide2 simulated section A-A upper stack slope analysis result

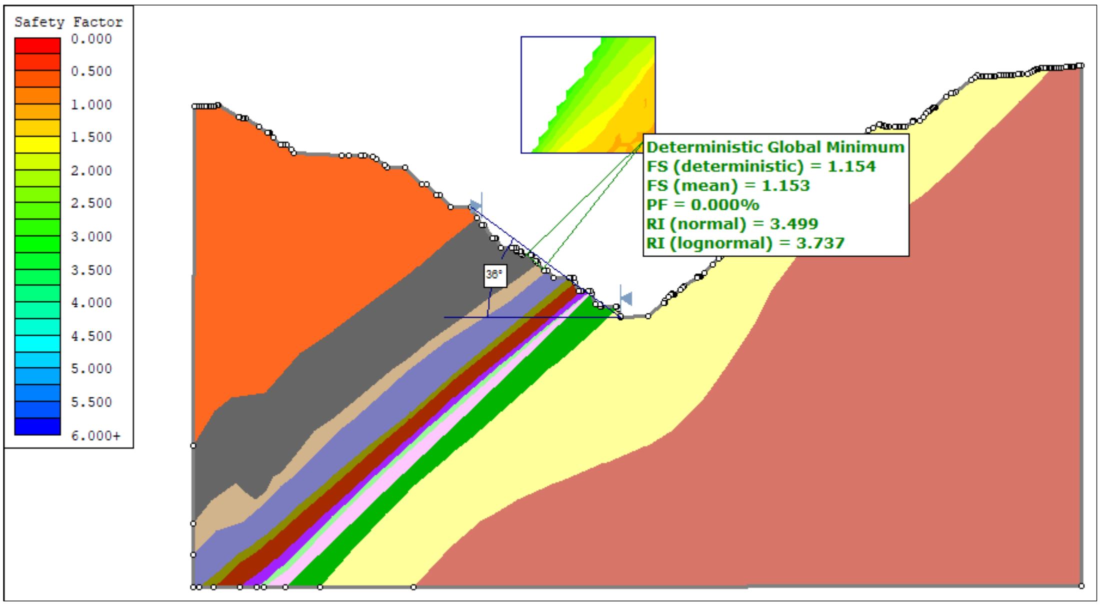

Figure J- 4: Slide2 simulated section A-A lower stack slope analysis result

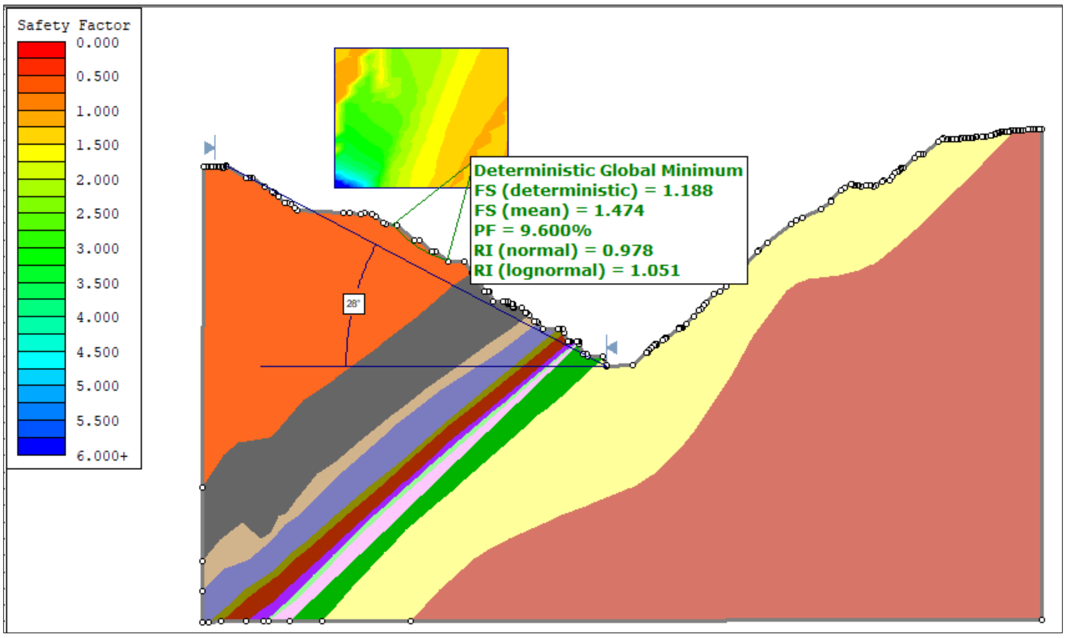

Figure J- 5: Slide2 simulated section A-A overall slope analysis result

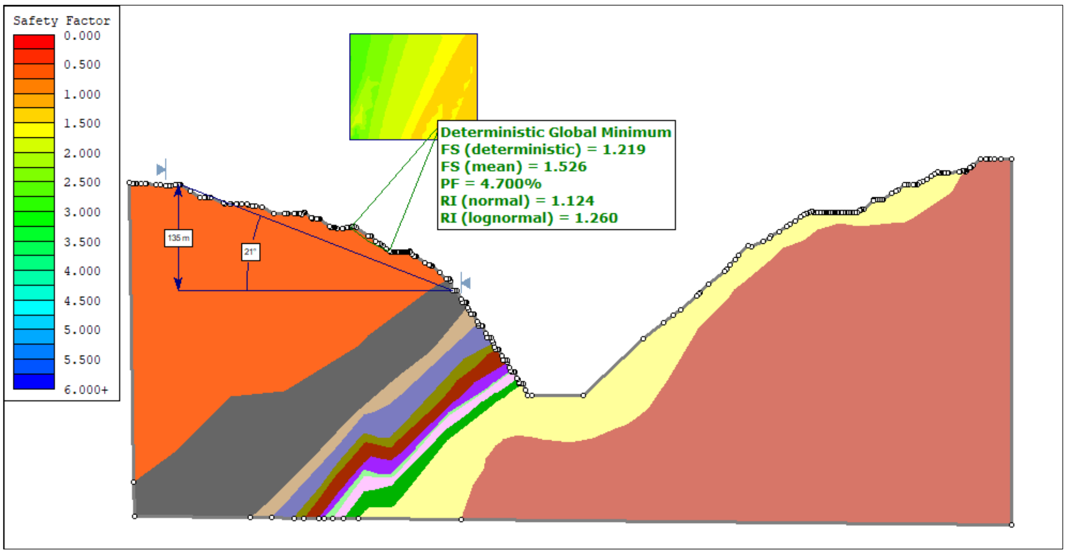

Figure J- 6: Slide2 section B-B Upper stack slope analysis result

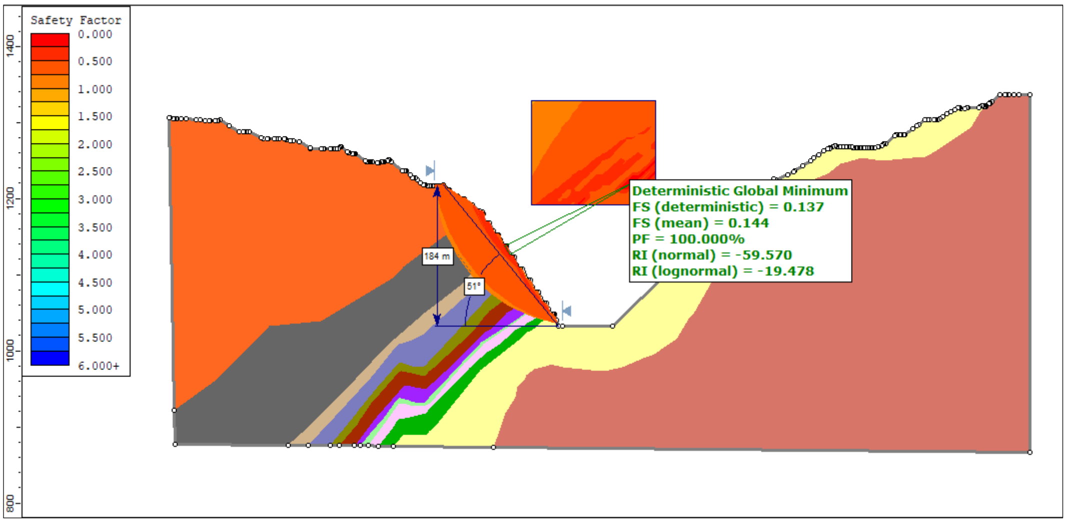

Figure J- 7: Slide2 section B-B lower stack slope analysis result

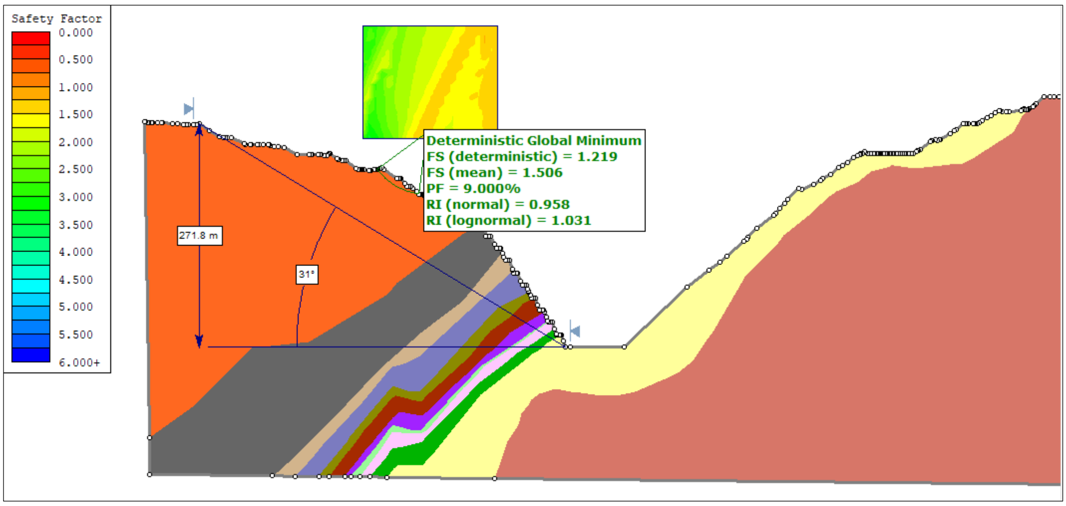

Figure J- 8: Slide2 section B-B overall slope analysis result

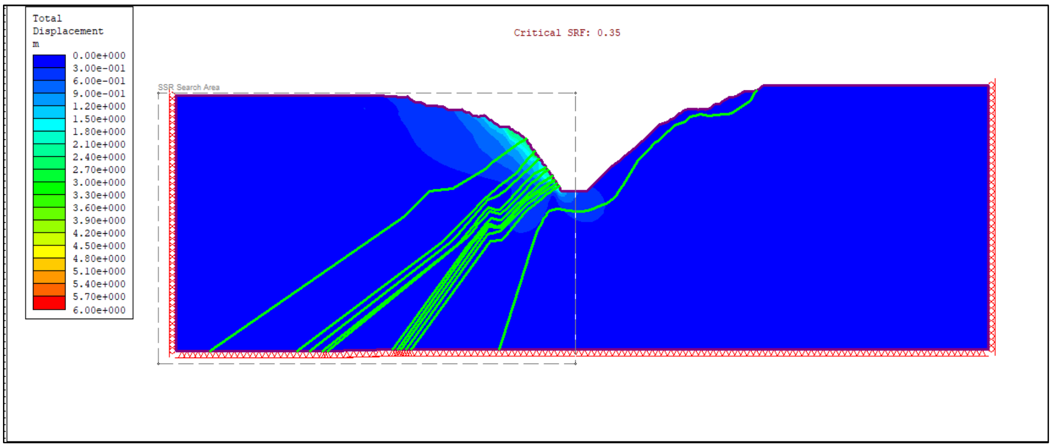

Figure J- 9: RS2 section B-B slope analysis result of Domain 3

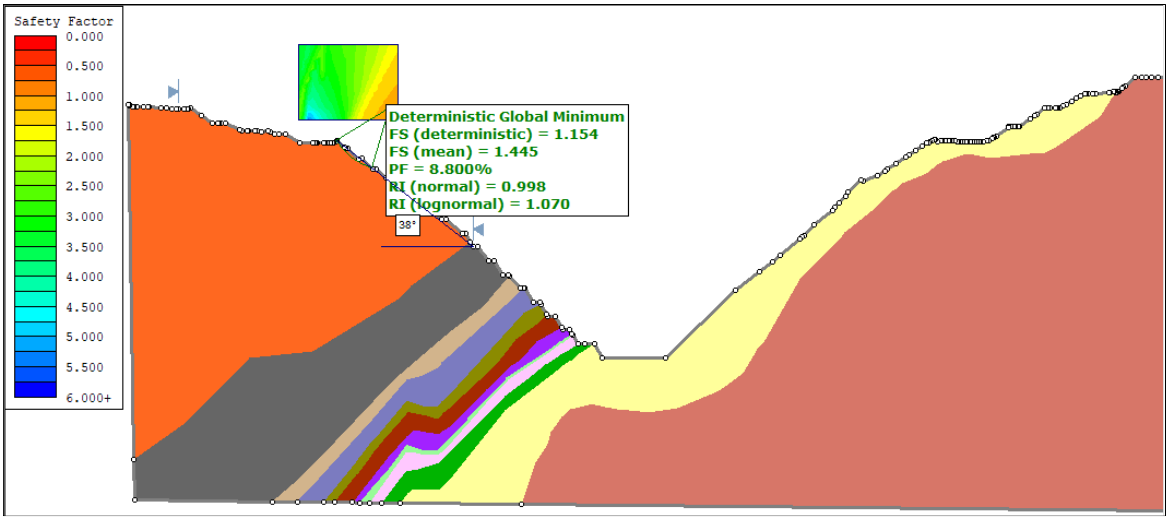

Figure J- 10: Slide2 simulated section B-B Upper stack slope analysis result

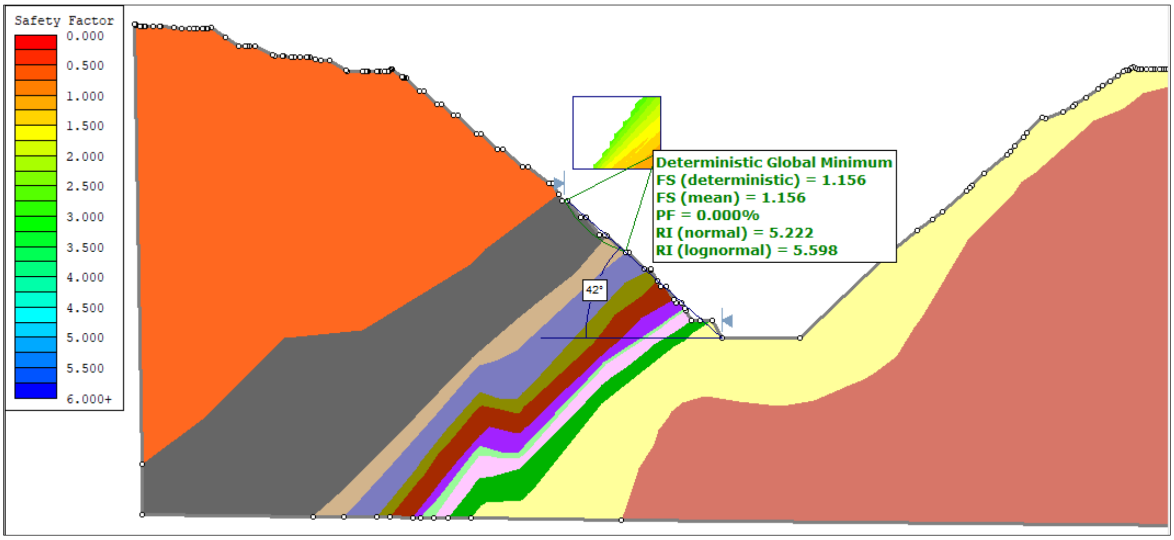

Figure J- 11: Slide2 simulated section B-B lower stack slope analysis result

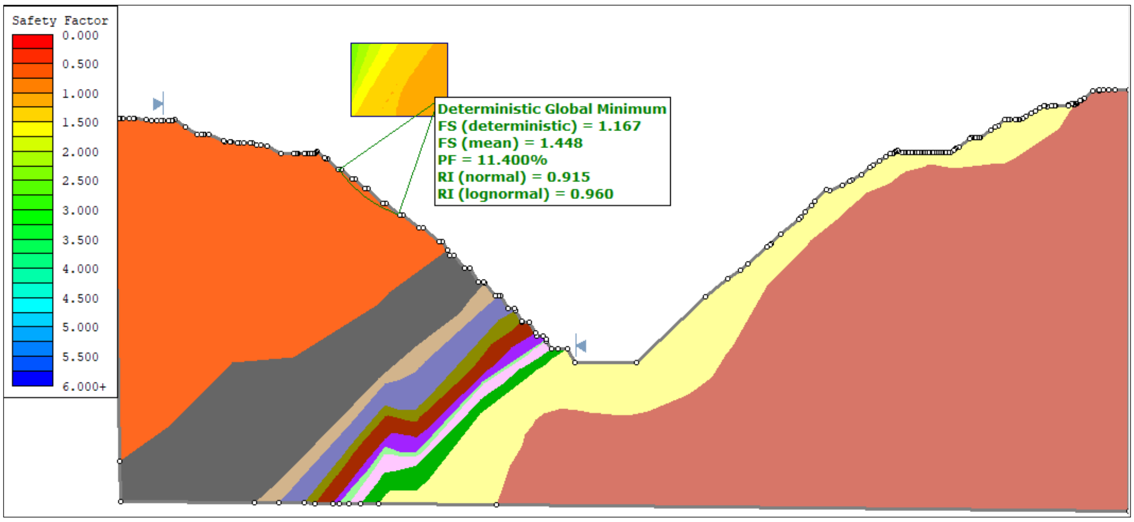

Figure J- 12: Slide2 simulated section B-B overall slope analysis result

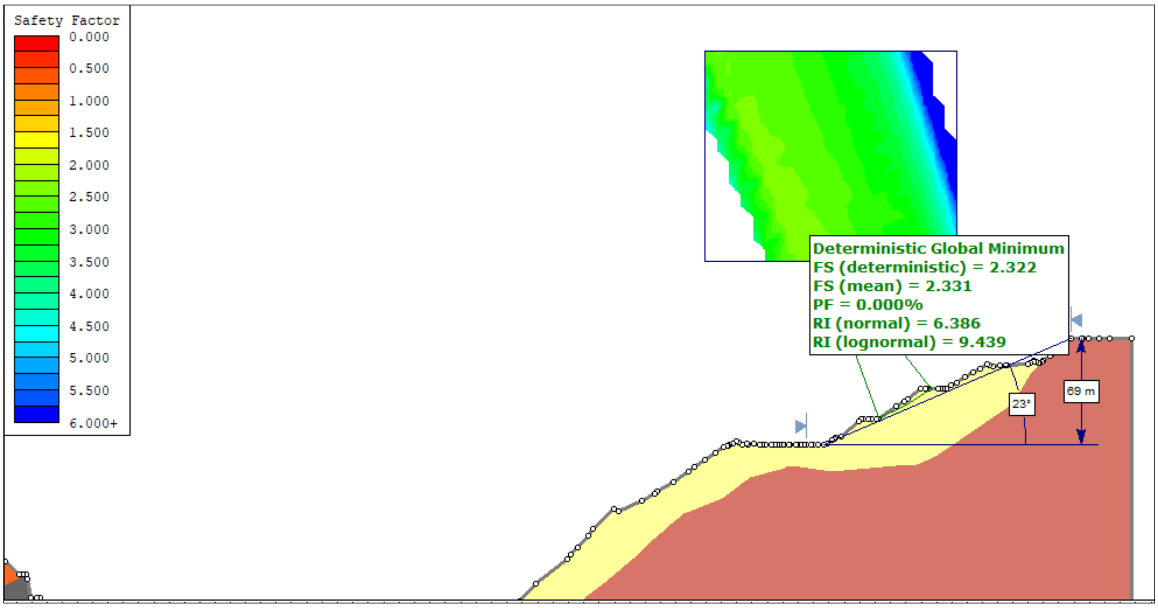

Figure J- 13: Slide2 section B-B Upper stack slope analysis result of Domain 1

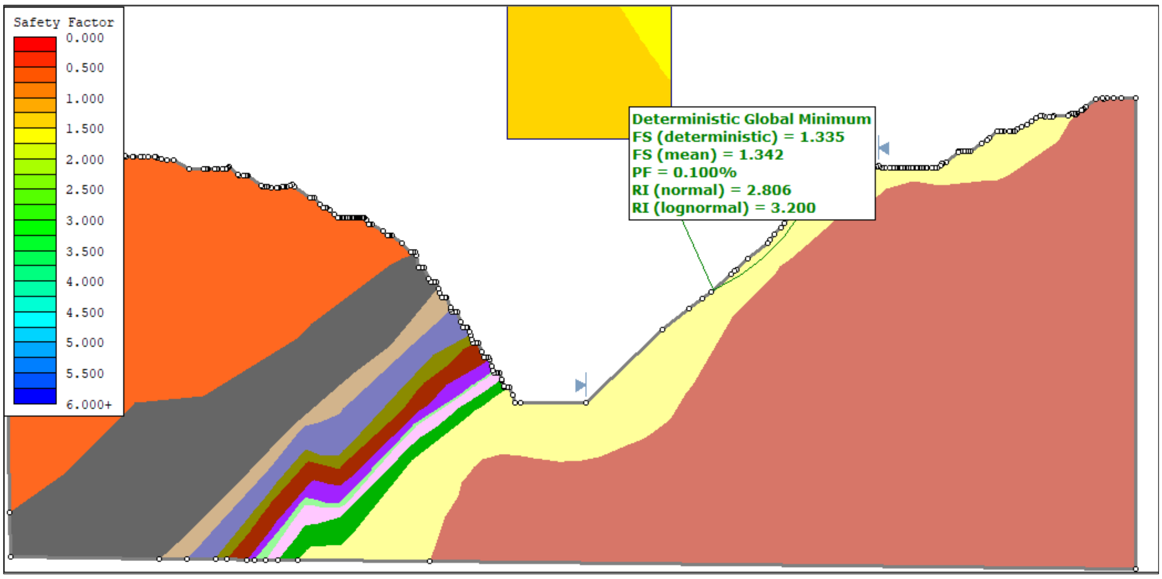

Figure J- 14: Figure J- 15: Slide2 section B-B lower stack slope analysis result of Domain 1

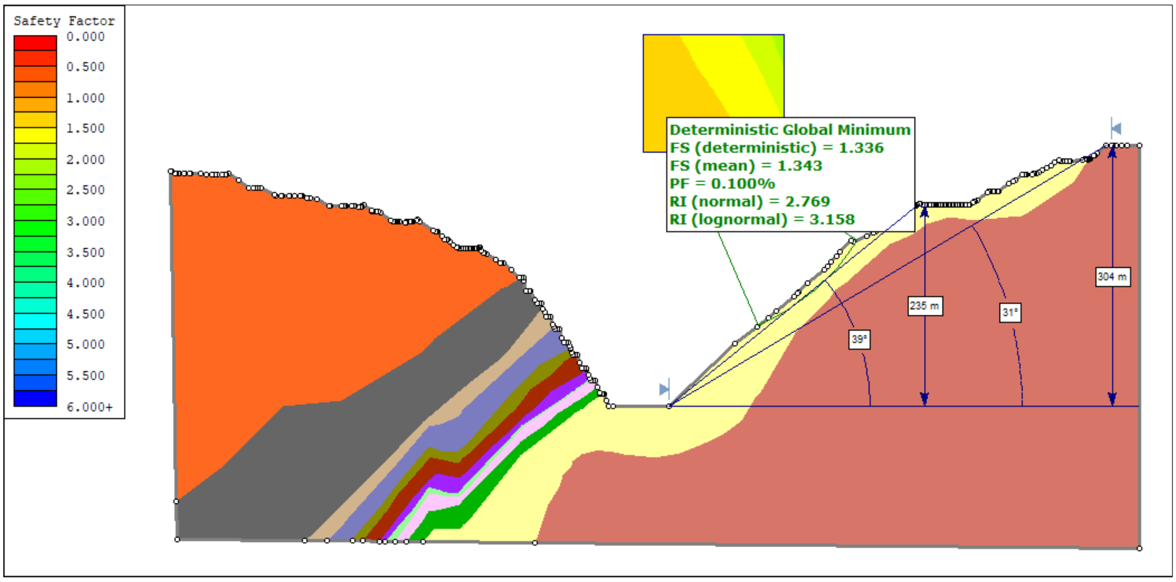

Figure J- 16: Figure J- 17: Slide2 section B-B overall slope analysis result of Domain 1

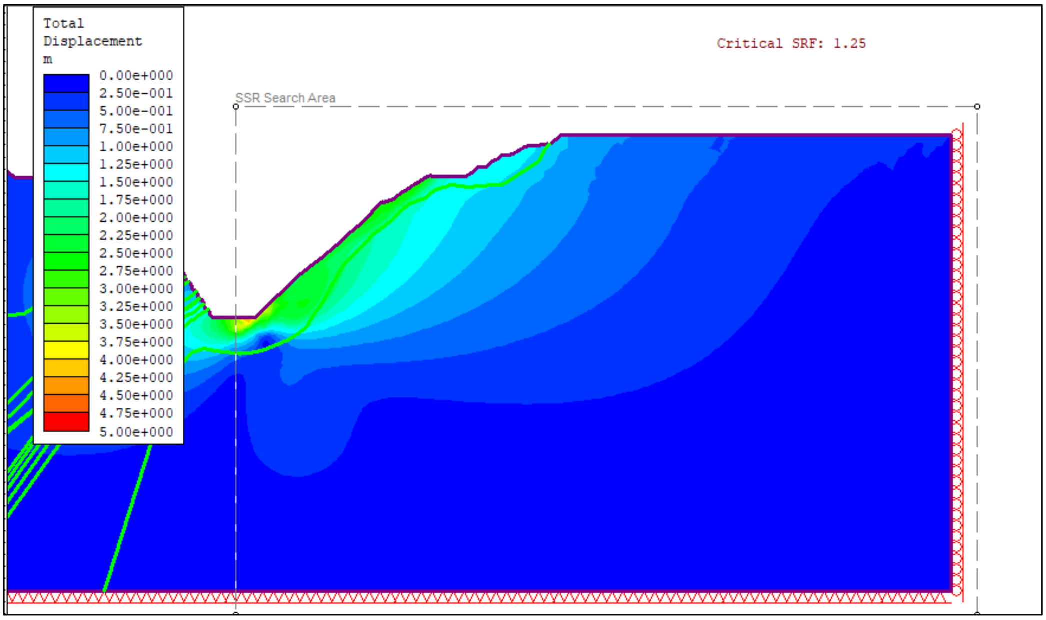

Figure J- 18: RS2 section B-B slope analysis result of Domain 1

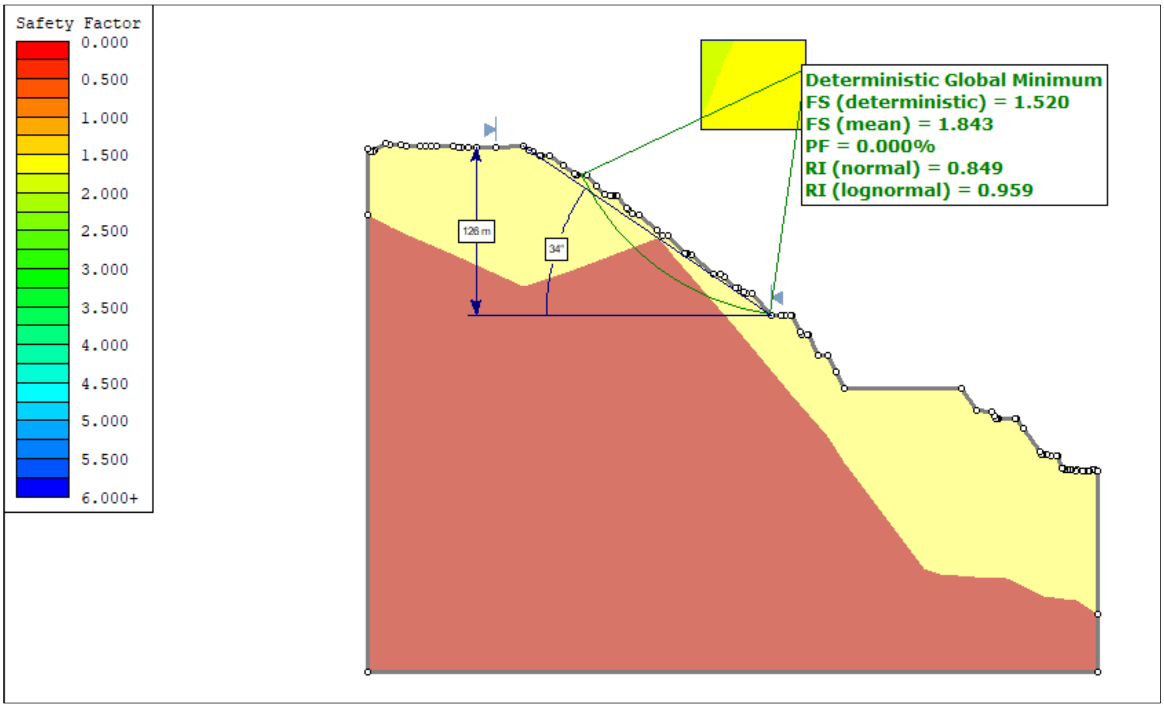

Figure J- 19: Slide2 section C-C Upper stack slope analysis result of Domain 2

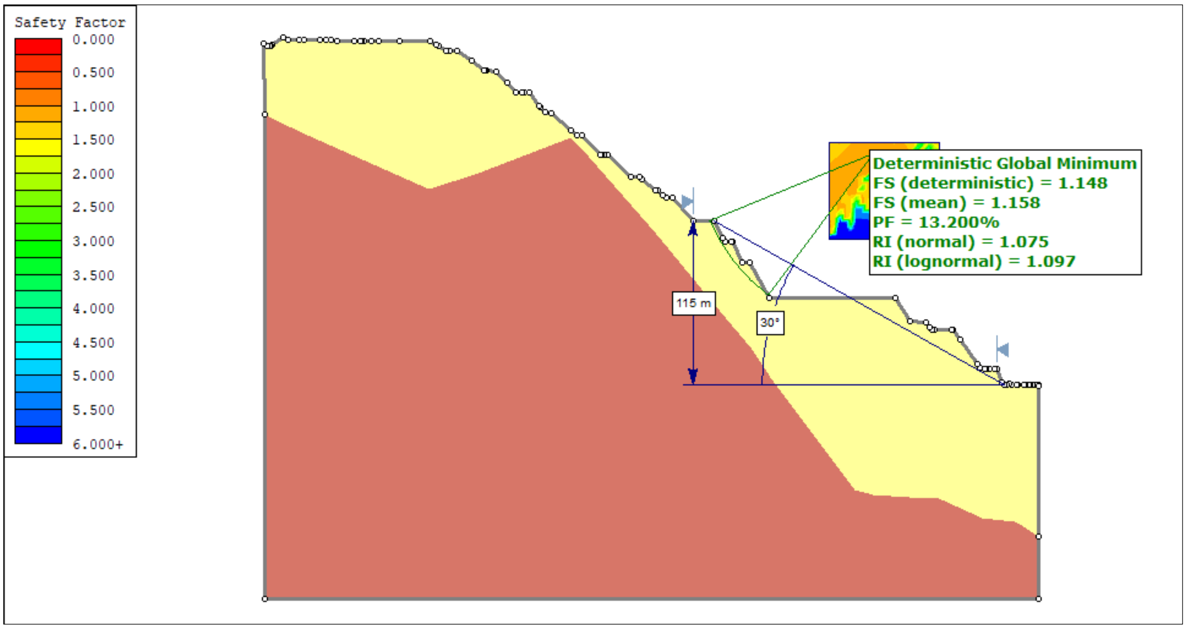

Figure J- 20: Slide2 section C-C lower stack slope analysis result of Domain 2

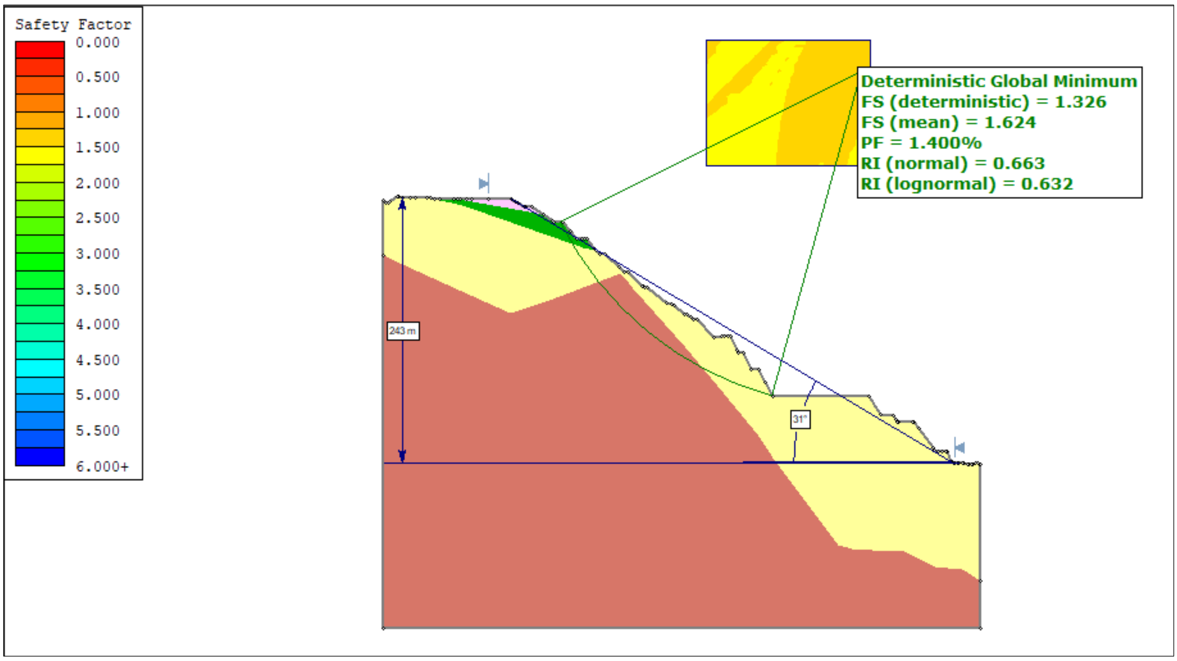

Figure J- 21: Slide2 section C-C overall slope analysis result of Domain 2

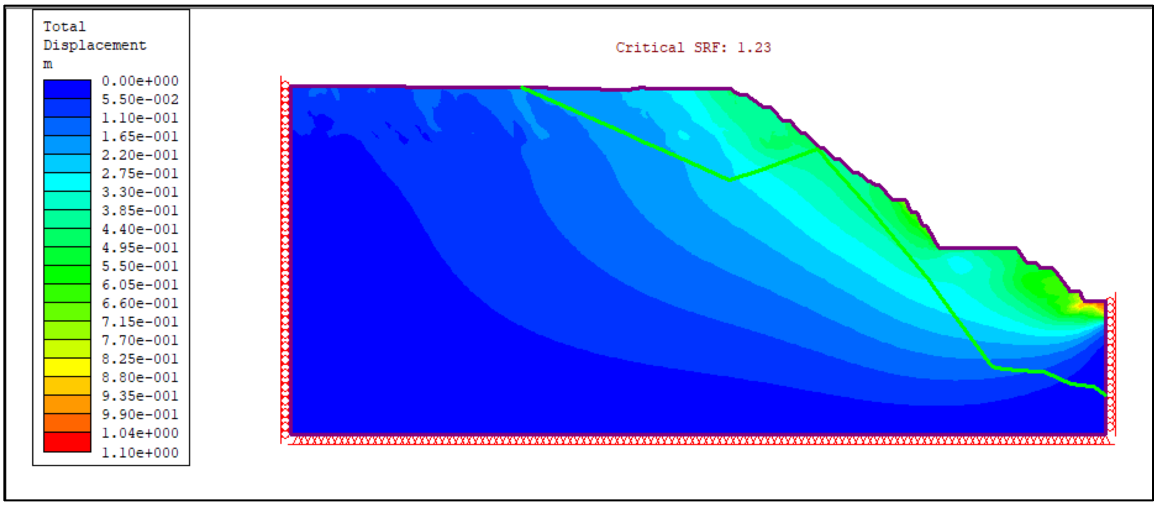

Figure J- 22: RS2 section C-C slope analysis result of Domain 2